Deltares

Modelling effect of relative sea level rise using hybrid D3D-ASMITA model

Modelling effect of relative sea level rise using hybrid D3D-ASMITA model

Client	Rijkswaterstaat Water, Verkeer en Leefomgeving-
Contact	Harry de Looff, Laura Brakenhoff
Reference	
Keywords	Wadden Sea, Sea Level Rise, Delft3D-ASMITA, Delft3D and ASMITA

Document control	
Version	1.0
Date	25-02-2025
Project nr.	11207897-002
Document ID	11207897-002-ZKS-0010
Pages	103
Classification	
Status	final

Author(s)

The allowed use of this table is limited to check the correct order-performance by Deltares. Any other client-internal-use and any external distribution is not allowed.

Doc. version	Author	Reviewer	Approver
1.0	Carola Seyfert Mónica Aguilera Chaves Zheng Bing Wang Edwin Elias Bert Jagers Ymkje Huismans	Bart Grasmeijer	Henriette Otter

Summary

In recent decades, the evolution of tidal inlet systems due to sea level rise (SLR) has been modelled using spatial and temporal aggregated models, such as ASMITA. These models facilitate the development of these systems towards a morphologic dynamic equilibrium through prescribed equilibrium equations. However, the aggregated nature of these models does not allow for inclusion of complex hydrodynamics (e.g., waves and wind), detailed resolution of morphodynamic changes, and the interaction between hydrodynamics and morphodynamics. To address these limitations, we present the development of a new model, Delft3D-ASMITA, which combines the capabilities of both process-based and aggregated models. This model is implemented in Delft3D, and utilizes a grid to resolve spatially detailed hydrodynamics and morphodynamics. Equations similar to those in ASMITA define the sediment exchange between the bed and the water column, ensuring that the modelled tidal inlet system develops towards a morphodynamic equilibrium.

The new model was applied to two different use cases based on existing Delft3D 4-only models: the Ameland tidal inlet system and the entire Dutch Wadden Sea. For the Wadden Sea model, thin dams were placed near the tidal divides to better represent the residual sediment transport in the system. Simulations with various SLR scenarios were conducted for 200 years to study the response of the individual tidal inlet systems. The model results show expected trends, qualitatively comparable to similar simulations conducted with ASMITA-only models. For example, an increasing sediment import and a faster decline of intertidal flats with higher SLR severity were observed.

Additionally, the Delft3D-ASMITA model provides the capability to output detailed spatial sedimentation/erosion patterns due to the SLR adaptation of the tidal inlet system. Despite the advantages offered by the new model compared to ASMITA, further improvements are needed. These include incorporating multiple sediment fractions with their respective sources and including processes that directly influence supratidal zones (e.g., sediment entrapment by vegetation).

For the specific case of the Wadden Sea model, detailed calibration and validation of the hydrodynamics are still necessary to accurately reproduce realistic residual sediment transport patterns without the need of placing thin dams. With Delft3D-ASMITA, it will be possible to explore more complex test cases, such as the implementation of subsidence due to gas/salt extraction, and to better connect the parameters used in ASMITA-only models to complex coastal processes.

Contents

	Summary	**4**
1	**Introduction**	**7**
1.1	Background	7
1.2	Objectives of the study	9
1.3	Set up of the report	10
1.4	Acknowledgements	10
2	**Model formulation and implementation**	**11**
2.1	Introduction	11
2.2	Implementation of the new model approach: how to get from Delft3D and ASMITA to Delft3D-ASMITA	11
2.2.1	Sediment transport in Delft3D	12
2.2.2	Sediment transport in ASMITA	13
2.2.3	Sediment transport in Delft3D-ASMITA	14
2.2.4	Hydrodynamic module	16
2.2.5	Bed level module	16
2.3	SLR implementation and model input	16
2.3.1	SLR implementation	17
2.3.2	Model input	19
2.4	Postprocessing of raw Delft3D-ASMITA output files	21
2.5	Simulation result types of interest for tidal inlet systems	22
2.5.1	Quantification of intertidal flat change	22
2.5.2	Sediment transport through the tidal inlet throat	22
2.5.3	Cumulative sedimentation/erosion maps	25
2.5.4	Water levels for specific observation stations	25
2.6	Assumptions and shared input for the test cases with the Delft3D-ASMITA model	25
2.6.1	Modelled SLR scenarios	25
2.6.2	Subsidence input	26
2.6.3	MHW and MLW	26
2.6.4	ASMITA Reference level	26
2.6.5	Equilibrium bathymetry	27
2.6.6	Sediment input	27
2.6.7	Simulation time	27
3	**Application to the Ameland Inlet**	**28**
3.1	Model setup	28
3.1.1	Grid and bathymetry	29
3.1.2	Forcing conditions	29
3.2	Results	30
3.2.1	Change in intertidal flat area, volume, and height	30
3.2.2	Hypsometric curves	32
3.2.3	Cross-throat sediment transport	33

3.2.4 Cumulative sedimentation/erosion maps 35
3.2.5 Water levels for a specific observation station 38

4 Application to the Dutch Wadden Sea 41

4.1 Model setup 41
4.1.1 Grid and bathymetry 42
4.1.2 Forcing conditions 42
4.1.3 Water level station locations 43

4.2 Testing the Delft3D-ASMITA MIS model with tidal divides 44

4.3 General model results and trends 47

4.4 MIS modelling results for the Ameland inlet system 48
4.4.1 Intertidal characteristics and hypsometric curves 48
4.4.2 Cross-throat sediment transport 49
4.4.3 Cumulative sedimentation/erosion maps 52
4.4.4 Water level analysis 54

4.5 Overview of changes in intertidal characteristics for all basins 55

4.6 Changes in channel hypsometry for all basins 58

5 Discussion, conclusions and recommendations 60

5.1 Discussion of results and current model limitations 60
5.1.1 Sediment source and supply 60
5.1.2 Residual flow pattern 60
5.1.3 Consistency between single-inlet-system (SIS) and multi-inlet-system (MIS) models 60

5.2 Comparison with ASMITA 62

5.3 Concluding evaluation of the model implementation & application 64

5.4 Recommendations 64

6 References 66

A Spin-up in morphodynamic modelling 69

A.1 Introduction 69

A.2 The problem with spin-up: does it really matter? 69

A.3 Causes of the problem 70

A.4 How can the problem be avoided / limited? 71

B Results for individual Wadden Sea basins 73

B.1 Marsdiep / Texel inlet 73

B.2 Eierland inlet 78

B.3 Vlie inlet 83

B.4 Borndiep inlet / Ameland basin 88

B.5 Pinkegat inlet 94

B.6 Zoutkamperlaag inlet 99

1 Introduction

1.1 Background

The Dutch Wadden Sea consists of six major tidal inlet systems, and an area with several smaller inlets (Groninger Wad), which connects to the Ems estuary (see Figure 1.1). Tidal inlet systems are a result of a balance between the tidal prism and the storage capacity of the back barrier basin zone (between the barrier islands and the mainland coast). The morphological development of the Wadden Sea has been influenced by sea level rise (SLR) as well as human interferences (Elias et al. 2012; Wang et al. 2018). In the last century, anthropogenic influences, such as the closure of the Lauwerszee and Zuiderzee, have dominated the morphodynamic change and sediment budget of the Wadden Sea (Elias et al. 2012). However, SLR, and in particular any acceleration in SLR, will likely become relatively more important for the morphological development in the future (Wang et al. 2018; Lodder et al. 2019).

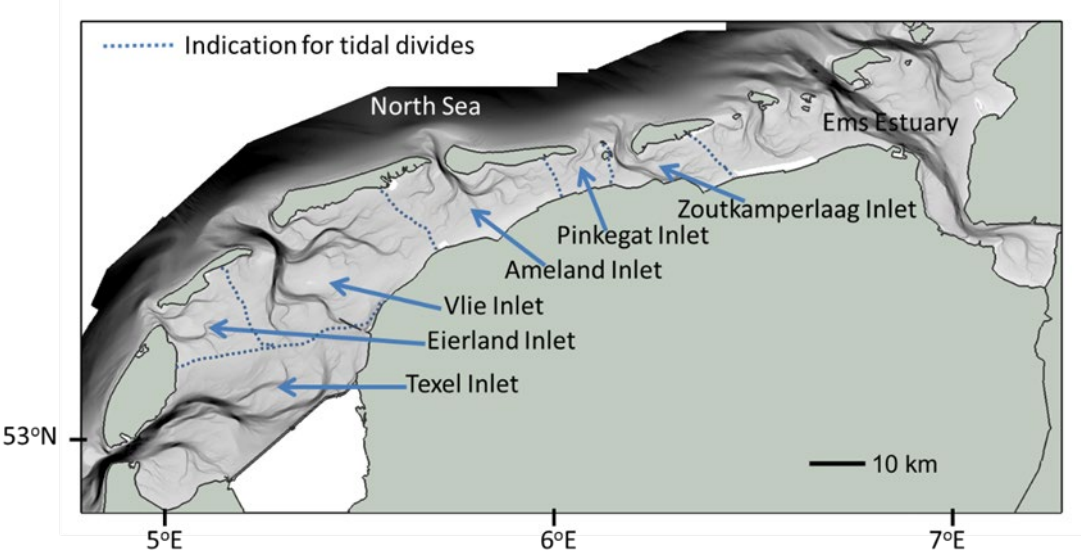

Figure 1.1. The Dutch Wadden Sea (after Lodder et al., 2019).

Understanding the future development of the Wadden Sea under the influence of SLR is important for two reasons. First, SLR can cause an increase in sediment transport from the North Sea to the Wadden Sea, and thereby result in increased coastal erosion of the Holland coast and the barrier islands. As mandated by Dutch law, coastal erosion is counterbalanced with sand nourishments to maintain a baselevel coastline (*basiskustlijn, BKL*). Therefore, an increased sediment "loss" into the Wadden Sea will also result in a need for increased nourishment volumes. Second, the intertidal flats (i.e. areas with elevation levels between mean low water (MLW) and mean high water (MHW)) in the Wadden Sea have high ecological value, providing habitat for a unique ecosystem. Provided a sufficiently high system sediment transport capacity and sediment availability, intertidal flats can grow in height and sustain themselves, within limits of SLR. If SLR rates exceed a certain threshold, the flats' sediment accretion cannot keep up anymore and the system will start to slowly drown, i.e., the intertidal flats will disappear at some point in the far future (Van Goor et al. 2003; Lodder et al. 2019).

Predicting the future morphological development of systems like the Wadden Sea relies on numerical modelling. A general challenge of modelling long-term morphological development is the discrepancy between hydrodynamic and morphodynamic timescales. While

hydrodynamic processes can usually be described well on a scale of hours, days, and months, morphodynamic development only starts to emerge after years, decades, or even centuries. Nevertheless, there have been various models successfully developed to tackle the challenge of modelling morphodynamic developments. They can be classified into several different types: process-based, idealized, and semi-empirical or aggregated.

Process-based models aim at the best possible description of the relevant processes. An example is the Delft3D package (Lesser et al., 2004), in which the mathematical equations representing the physical processes of water movement and sediment transport are solved numerically to determine the morphological changes based on a mass-balance for sediment. Such models provide a detailed presentation of the morphological changes and are useful to investigate the underlying physical processes and mechanisms responsible for the observed morphological developments. Therefore, they are commonly described as “complex” and “quasi-realistic” in literature. This type of models is particularly well suited for detailed, short-term simulations to understand the system (Elias, 2006). In recent years there has been significant progress in long-term morphodynamic modelling with process-based models (Wang et al., 1995; Hibma et al., 2003a, b, 2004, Marciano et al., 2005; Van der Wegen et al., 2008; Dastgheib et al., 2008; Dissanayake et al., 2012; Becherer et al., 2018; Hofstede et al., 2018). For practical applications however, the suitability of this type of models for long-term predictions is still limited. This is not just related to the required computing power, but also due to the limited insight into the behaviour of these models. One main problem is that a long-term simulation rarely evolves towards a morphological equilibrium (refer to Appendix A for a detailed explanation). Other problems include schematising the ever-varying driving forces realistically (tides, wind, and waves) and especially their interactions, as well as the representation of “secondary” phenomena, which determine the residual sediment transport (e.g. tidal asymmetry).

Idealized models are also process-based models, but they use simplified physical and mathematical descriptions. In contrast to the “complex” models, they do not pursue a full description of *all* processes but try to reduce it to the essential ones. Some examples of this type of models include the conceptual model of Postma (1961) on sediment transport in the Wadden Sea, explaining how tidal flow leads to sediment import, and various models for the different morphological elements within the Wadden Sea system, reviewed by De Swart and Zimmermann (2009).

Aggregated models, also known as semi-empirical models or behaviour-oriented models, make explicit use of empirical relations to define the morphological equilibrium. An important assumption is that the morphological system, after a disturbance (through natural evolution or by human interference), always tends to develop into an equilibrium state, which can be determined by a set of empirical relations. An example of this type of models is the ASMITA model (Stive et al., 1998; Stive and Wang, 2003; Townend et al., 2016a,b). It uses a schematisation in which a tidal inlet system is divided into three main morphological elements: (1) ebb-tidal delta, (2) channels and (3) inter-tidal shoals and flats (see also Figure 2.1 for a schematic of this concept). These elements exchange sediment with each other and with the outside world (surrounding offshore area, coasts, foreshores and barrier islands) to develop the morphological equilibrium as defined by the empirical relations. Simulating long-term developments with this model is computationally efficient and stable[1], making it a suitable choice to study the effects of SLR (Van Goor et al., 2003) and large-scale human interferences (Kragtwijk et al., 2004). Recently, ASMITA models have been applied for various SLR

[1] i.e. the output does not show any unexpected instabilities and/or perturbations. In contrast, process-based models running long-term morphodynamic simulations can exhibit unrealistic feedback loops based on minimal perturbations in both hydro- and morphodynamics, rendering them “unstable”, even if they reach the end of their prescribed simulation period.

scenarios to predict the sediment exchange between the Wadden Sea and North Sea, and the development of the intertidal flats in the Wadden Sea (Lodder et al., 2019, 2022; Huismans et al., 2022; Wang et al., 2024).

Up until now, SLR impact assessment in the Wadden Sea has primarily relied on aggregated morphological models, such as ASMITA (Van Goor et al., 2003). For environmental impact assessment studies of gas and salt mining, the quantitative evaluation of land subsidence is also based on ASMITA modelling (Wang & Eysink, 2005; Cleveringa & Grasmeijer, 2010; Wang et al., 2017). However, this use case is pushing the boundary of what is currently possible with this model, revealing several limitations:

1. **Lack of Spatial Distribution Information**: The model calculates morphological changes in terms of the total volume change of the morphological elements. In other words, it does not provide information on how these changes are spatially distributed. This limitation makes it impossible to conduct a detailed spatial analysis of the impact on the tidal inlet system.
2. **Inability to Include Detailed Spatial Variation of Relative SLR**: Detailed spatial variation of relative SLR (rSLR = SLR + subsidence) cannot be included. Previous impact assessment studies of gas and salt mining transferred the relative (local) subsidence to a morphological element of the model, e.g. the intertidal flats, without resolving the spatial variability.
3. **Restricted Feedback Between Morphological Development and Hydrodynamic Forcing**: The ASMITA model cannot calculate how SLR and morphodynamic change would affect tidal amplification in the tidal basin, as it does not take temporally and spatially resolved hydrodynamics into account at all.

To address the limitations and leverage the advantages of both process-based models and aggregated models, we introduce a new modelling approach in this report: the Delft3D-ASMITA model. This new model incorporates an alternative, additional formulation for sediment exchange between the bed and water column, similar to the one used in the ASMITA model, within Delft3D. The Delft3D-ASMITA model was conceptually developed for both Delft3D 4 and Delft3D FM. However, for this report, the model implementation and results are carried out in Delft3D 4 only.

1.2 Objectives of the study

The primary goal of this study is to enhance the simulation of the morphological response of the Wadden Sea to various SLR rates using the newly developed Delft3D-ASMITA model. To achieve this objective, we address the following steps within this report:

- Introduce and describe the model formulations of the Delft3D-ASMITA model
- Show how to set-up a simulation in the Delft3D-ASMITA model
- Explain the functioning and response of the Delft3D-ASMITA model
- Understand the differences between the results obtained from the Delft3D-ASMITA model compared to the original ASMITA model
- Compare the results for simulating a single tidal inlet system with results for simulating multiple inlet systems simultaneously

We conducted long-term, morphodynamic simulations for two model schematisations. The first model describes a single tidal inlet system (the Ameland inlet system), while the second encompasses the entire Dutch Wadden Sea. We simulated five different SLR scenarios based on Wang et al. (2024). All scenarios span a period of 200 years and start in the year 2000. They range from a “business as usual” scenario with a constant 2 mm SLR per year, amounting to a total SLR of 40 cm by 2200, to an extreme scenario with almost 4 m SLR by 2200, and an

accelerating SLR rate from 2020 onwards. For a more detailed description of the modelled SLR scenarios, see Section 2.6.

1.3 Set up of the report

The report is structured as follows:

- **Chapter 2**: Describes the model formulation, implementation in Delft3D, set-up, output description and assumptions.
- **Chapter 3**: Presents the model results for the single-inlet-system schematisation.
- **Chapter 4**: Details the model results on the Wadden Sea scale.
- **Chapter 5**: Discusses the results, elaborates on the learnings from this study, and outlines what will be investigated in more detail in the future.

1.4 Acknowledgements

We thank the projects which funded this work, specifically *Kennisontwikkeling Zandige Kust* financed by Rijkswaterstaat (11207897-002) and *Natuurgrens Waddenzee* financed by the Ministry of Economic Affairs (11206960-016), as well as the *WadSED* project financed by the Dutch Research Council (NWO) (11210266-010).

2 Model formulation and implementation

2.1 Introduction

In this chapter, we introduce the formulation and implementation of the new Delft3D-ASMITA model. We also describe how to set up the model, the output generated, and the assumptions made for the work presented in this report.

2.2 Implementation of the new model approach: how to get from Delft3D and ASMITA to Delft3D-ASMITA

Figure 2.1 presents conceptual schematics of a tidal inlet system, as well as of the two different model approaches (Delft3D-only and ASMITA-only). The Delft3D concept (Figure 2.1, centre panel) is a spatially resolved grid approach, where individual grid cells carry unique data (e.g. for bed and water level, but also hydrodynamic conditions) for each simulation time step. This approach results in high information density, which comes at steep computational costs but offers also the opportunity to vastly expand system understanding.

Due to the high computational costs of process-based models like Delft3D, it is not feasible to run them for the full duration of a realistic morphological development (there is a challenge regarding the time scale discrepancy between hydro- and morphodynamics, see also Chapter 1). Therefore, it is common practice to run a Delft3D model for a shorter simulation period (the hydrodynamic timescale) and then apply a morphological acceleration factor (MorFac) to upscale the morphodynamic response of the model (to morphodynamic timescale). MorFac enables upscaling of the morphodynamic behaviour by simple multiplication. The higher the MorFac, the shorter the hydrodynamic simulation period can be (i.e. saving computational cost and run time). However, a high MorFac and a short hydrodynamic simulation period can also lead to misinterpretation of complex hydrodynamic conditions or trigger an unstable model response.

The ASMITA concept (Figure 2.1, right panel) is based on spatially aggregated morphological elements, which exchange sediment (and through the ebb-tidal-delta element also with the outside world). Whether sediment is transported, and in which direction, is determined by equilibrium considerations, based on the fundamental development of tidal inlet systems behind barrier islands. These considerations are based on a balance between the tidal prism, longshore flows and available storage capacity in the back barrier basin area. The morphological elements of the ASMITA model are defined by (sediment or water) volumes and (time-constant) areas.

Note that the Delft3D model concept is based on general hydro- and morphodynamics and can be applied to a vast number of use cases (the morphological development of the Wadden Sea being one of many). In contrast, the ASMITA model concept was developed specifically for tidal inlet systems (i.e. the tidal basin with channels and flats, and the ebb-tidal delta) and is only valid in such a system and not beyond. The spatially restricted validity of the ASMITA approach has implications for the model implementation of Delft3D-ASMITA as well (see Section 2.3).

An essential difference between Delft3D and ASMITA is the formulation for the sediment exchange between the bed and the water column. In process-based models like Delft3D, the sediment exchange depends on the local instantaneous hydrodynamic condition (such as flow velocity and bed shear stress) and sediment properties (like grain size, settling velocity and

density). In aggregated models like ASMITA, the local instantaneous hydrodynamic condition is replaced by a temporally aggregated parameter, which depends on the morphological equilibrium state. In the new Delft3D-ASMITA model, we included the latter approach into the process-based Delft3D model suite as an additional sediment transport formulation, which can be selected during model setup.

In the following sections, we will first reiterate the concepts and governing equations of the two original models (Delft3D and ASMITA) for sediment transport, and then highlight the novel steps taken to develop the Delft3D-ASMITA model. For simplicity, the explanation of the implementation is limited here to the use of 2DH only, but the model approach can be implemented in both 2DH and 3D.

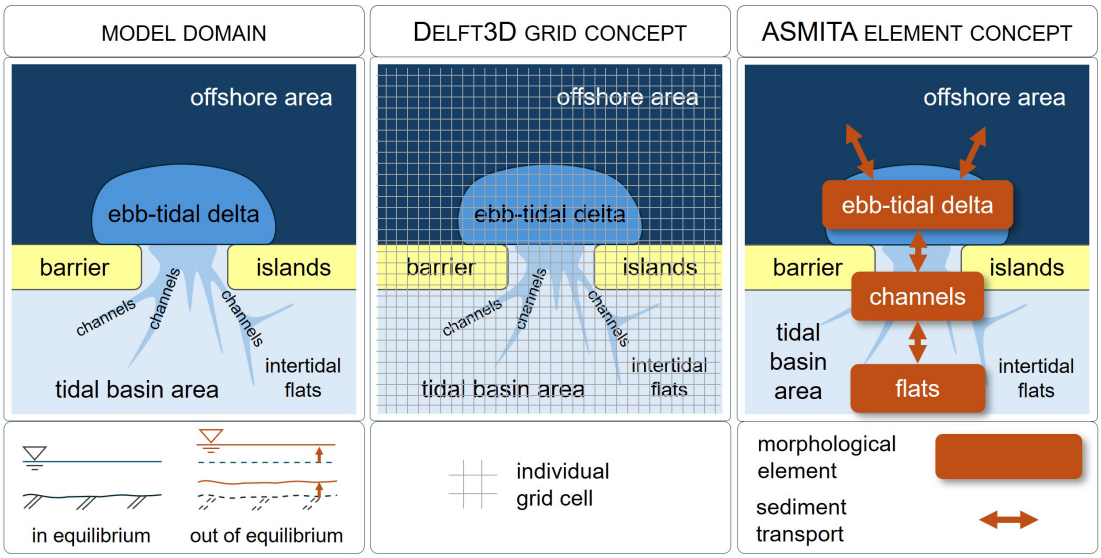

Figure 2.1 Schematic (not to scale) of the current use case of a tidal inlet system to the left, with schematics of the sediment equilibrium considerations in the lower part, and visualisations of the two model concepts: the Delft3D concept, based on a grid, in the middle, and the ASMITA concept, based on morphological elements, on the right. The legends underneath the model concepts indicate their schematization.

2.2.1 Sediment transport in Delft3D

In Delft3D, sediment can be transported as both, suspended sediment and as a bed load[2]. However, the Delft3D-ASMITA model assumes suspended load transport for the total load approximation, following the same principles as the ASMITA model. Therefore, we will focus on this transport mechanism for further explanation.

To calculate suspended sediment transport for each grid cell in the model region, Delft3D applies an advection-diffusion solver. The 2DH advection-diffusion (mass-balance) equation reads as follows:

$$\frac{\partial c(t)}{\partial t} + \frac{\partial uc}{\partial x} + \frac{\partial vc}{\partial y} - \frac{\partial}{\partial x}\left(\varepsilon_{S,x}\frac{\partial c}{\partial x}\right) - \frac{\partial}{\partial y}\left(\varepsilon_{S,y}\frac{\partial c}{\partial y}\right) = E(t), \qquad (2\text{-}1)$$

where:

c = mass concentration of sediment [kg/m^3]

[2] In Delft3D, bed load transport is based on a parametric formulation.

u, v = flow velocity components [m/s]
$\varepsilon_{s,x}, \varepsilon_{s,y}$ = eddy diffusivities of sediment [m^2/s]
$E(t)$ = sediment exchange rate (erosion rate – deposition rate) [kg/m^3/s].

The local flow velocities and eddy diffusivities are based on the results of the hydrodynamic computations in each grid cell. The sediment exchange rate $E(t)$ between the bed and the water column, based on the 1DH Galappatti model (G. Galappatti & Vreugdenhil, 1985; R. Galappatti, 1983) and extended by Wang (1989, 1992), reads as follows

$$E(t) = \gamma \frac{w_s}{h} (c_e - c_{inst}(t)), \quad (2\text{-}2)$$

where:
γ = coefficient depending on w_s/u^*, in which u^* is the bed shear stress velocity (Galappatti model formulation in 2DH models) [–]
w_s = settling velocity [m/s]
h = water depth [m]
c_e = mass sediment equilibrium concentration [kg/m^3]
c_{inst} = instantaneous mass sediment concentration [kg/m^3]. Note that this is the same time-dependent concentration as $c(t)$ in Equ. (2-1).

The sediment equilibrium concentration c_e in Eq. (2-2) is calculated by default with the Van Rijn (1984) sediment transport formula. The Delft3D model suite offers various alternative (non-cohesive) sediment transport formulations (e.g. Engelund-Hansen, Soulsby, Ashida-Michiue, Van Thiel / Van Rijn, or Wilcock-Crowe). The ASMITA formulations are added as a new, alternative sediment transport formula to obtain the Delft3D-ASMITA model. For more detailed information on the different sediment transport formulations, we refer the reader to the Delft3D 4 (FLOW) user manual (Deltares, 2024).

2.2.2 Sediment transport in ASMITA

Sediment transport in ASMITA is governed by simple equilibrium considerations: sediment volume and water volume in a tidal inlet system are balanced. If one element exhibits more sediment volume than its prescribed equilibrium, it will erode and sediment will be transported to other morphological elements to restore equilibrium. The model calculates the morphological changes of individual elements and ensures that the cumulative changes sum up (including potential sediment import from the outside world). To arrive at the morphological changes of an element, the respective equation(s) read

$$\frac{dV_{inst,element}(t)}{dt} = w_{ex,horz,element} A_{element} \left(\tilde{c}_{e,element}(t) - \tilde{c}_{inst,element}(t)\right), \quad (2\text{-}3)$$

with (per morphological element):
$V_{inst,element}$ = instantaneous volume at a given time step [m^3]
$w_{ex,horz,element}$ = horizontal exchange coefficient of the element[3] [m/s]
$A_{element}$ = area (constant in time) [m^2]
$\tilde{c}_{e,element}$ = *volume* sediment equilibrium concentration [–]
$\tilde{c}_{inst,element}$ = instantaneous *volume* sediment concentration [–]

[3] spatially and temporally aggregated representatives of the hydrodynamics

The concentrations used in ASMITA equations are the *volume* sediment concentration, in contrast to the *mass* sediment concentration used in Delft3D. Throughout this document, we distinguish the two with the tilde ($\tilde{}$) for the volume concentration.

The ASMITA concept is based on a concentration difference between the instantaneous sediment concentration and the sediment *equilibrium* concentration. Both of them change over time. To determine $\tilde{c}_e$ we take the element's *equilibrium volume* into account, which is determined by empirical equilibrium considerations. To determine whether an element is demanding sediment, or seeking to decrease its sediment volume, we calculate $\tilde{c}_e$, which is proportional to the ratio between the instantaneous volume and the equilibrium volume:

$$\tilde{c}_{e,element}(t) = \tilde{C}_E \left(\frac{V_{e,element}(t)}{V_{inst,element}(t)} \right)^n, \tag{2-4}$$

with:

$\tilde{C}_E$ = global *volume* equilibrium concentration (constant in time and space) [–]
$V_{e,element}$ = equilibrium volume defined by equilibrium considerations [m^3]
n = exponent for sediment transport equations, for suspended sediment usually set to 5 [–]

The global equilibrium concentration, $\tilde{C}_E$, is set as a constant throughout the model domain and the whole simulation period. The ratio between the equilibrium and instantaneous volumes defines the sediment concentration towards which a morphological element wants to trend at any given time step. Inserting $\tilde{c}_e$ (Equ. 2-4) into Equ. (2-3) delivers ASMITA's fundamental sediment transport formula:

$$\frac{dV_{inst,element}(t)}{dt} = w_{ex,horz} A_{element} \left(\tilde{C}_E \left(\frac{V_{e,element}(t)}{V_{inst,element}(t)} \right)^n - \tilde{c}_{inst,element}(t) \right). \tag{2-5}$$

2.2.3 Sediment transport in Delft3D-ASMITA

Combining the two model concepts above to create a successful Delft3D-ASMITA model, we use the balancing approach of ASMITA for the equilibrium concentration, and insert it into the Delft3D's sediment exchange rate:

$$E_{grid\ cell}(t) = \frac{w_s}{h} \left(c_{e,grid\ cell}(t) - c_{inst,grid\ cell}(t) \right), \tag{2-6}$$

which is Equ. (2-2) with $\gamma = 1$, and the *mass* sediment concentrations. Note the similarities between Equ.s (2-6) and (2-3), with the sediment exchange rate E per grid cell replacing the volume change of the morphological element dV/dt. With a spatially resolved grid, we can determine bed levels in grid cells directly instead of changes in the sediment volume of an entire element. Furthermore we are now taking the *mass* sediment concentration into account. This also implies that the area (of an ASMITA morphological element) is not necessary to determine the exchange rate. Hence, the equilibrium concentration takes on the form:

$$c_{e,grid\ cell} = C_E \left(\frac{d_{eq}}{d_{inst}} \right)^n, \tag{2-7}$$

with:

C_E = global *mass* equilibrium concentration (constant in time and space) [kg/m^3]
d_{eq} = ASMITA equilibrium depth in a certain grid cell [m]
d_{inst} = instantaneous ASMITA depth in a certain grid cell [m],

leading to (per grid cell):

$$E(t) = \frac{w_s}{h}\left(C_E\left(\frac{d_{eq}}{d_{inst}(t)}\right)^n - c_{inst}(t)\right), \tag{2-8}$$

as sediment exchange rate, which is then plugged back into the advection-diffusion equation (Equ. (2-1)). See also Figure 2.2 for a schematic of the different variables in a cross-section of a fictitious model domain. Note the Delft3D grid cells (thin, grey, vertical lines) spatially segregating the domain, and the ASMITA reference level determining both, the equilibrium and the instantaneous ASMITA depth. The ASMITA reference level is a model input and can be arbitrarily set at any elevation value. We recommend setting this reference level well above the model's MHW levels of the tidal forcing to prevent extreme values for the depth ratio. For more details on the best choice of elevation for the reference level, we refer the reader to Section 2.3.2 of this report. The ASMITA reference level is used within the model implementation to determine the sediment exchange only and does not affect the regular bed level determination, e.g. for cumulative sedimentation/erosion maps (see Section 2.5.3), which will remain correlated to NAP = 0 m.

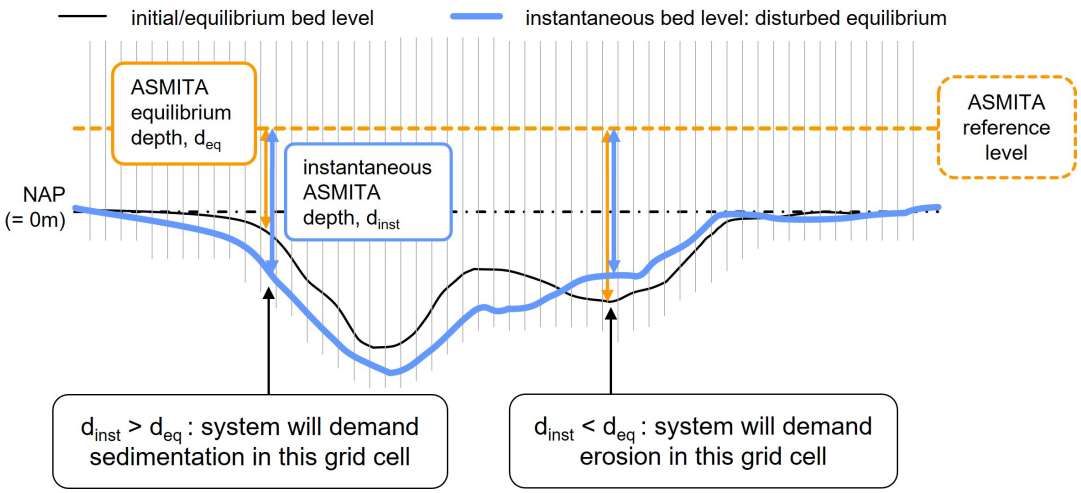

Figure 2.2. Cross-sectional schematic of a fictitious model domain (not to scale) at a random simulation time step. The thin, grey, vertical lines represent Delft3D grid lines in one dimension, and the cross-section is running along one grid line in the orthogonal dimension. The orange dashed line represents the ASMITA reference level, which is used to determine the ASMITA equilibrium depth, d_{eq}, (orange arrows) in each Delft3D grid cell; as well as the instantaneous bed level in blue, and the corresponding ASMITA depth, d_{inst} (blue arrows).

In Equ. (2-8), the ratio between equilibrium depth and instantaneous depth, d_{eq}/d_{inst}, determines the direction of sediment transport for a certain grid cell. Based on the difference in depths, a grid cell will either demand sediment ($d_{eq}/d_{inst} < 1$) and $E < 0$; or erode sediment ($d_{eq}/d_{inst} > 1$) and $E > 0$. Note that these relations only hold for d_{inst} being close to d_{eq}, i.e. slow developments without sudden large bed level changes. This limitation is met for the use cases of this report, where we present results on the influence of SLR (slow-onset development).

2.2.4 Hydrodynamic module

The hydrodynamic module of Delft3D remains unchanged. The Delft3D-ASMITA model contains all the hydrodynamic functionalities and processes which are available in Delft3D. This is a major difference to the ASMITA model, which does not take any temporally or spatially resolved hydrodynamics into account at all. The new model can handle tidal flow dynamics, as well as non-tidal processes (such as wind, waves, salinity and temperature). In this report, we present results based on tidal flow dynamics only. In future research, we plan to investigate the influence of more complex wind fields and wave dynamics.

Note that the equilibrium and instantaneous depths mentioned refer to bed levels, which must not be confused with the instantaneous water depth of the system, which is directly linked to the instantaneous water level. The water level throughout the model domain is tethered to the hydrodynamic forcing and varies spatially and temporally to reflect instantaneous hydrodynamics (e.g. tides, waves, wind, storms).

2.2.5 Bed level module

The bed level module of Delft3D remains unchanged. The bed level Z_b changes due to morphological changes (sedimentation and erosion), and can be calculated using the sediment exchange between bed and water column:

$$\frac{\partial z_b}{\partial t} = \frac{-1}{1-\varepsilon}\frac{1}{\rho_{solid}}E - \beta = \frac{1}{1-\varepsilon}w_s\left(\tilde{c} - \tilde{c}_e\right) - \beta = \frac{1}{1-\varepsilon}\frac{1}{\rho_{solid}}w_s\left(c - c_e\right) - \beta, \tag{2-9}$$

where:

ε = bed porosity [–]
ρ_{solid} = sediment density [kg/m^3]
β = subsidence rate [m/s].

Note the distinction between mass and volume sediment concentrations in this equation, and the corresponding density division where necessary. For more detailed information on the bed level module, we refer the reader to the Delft3D 4 (FLOW) user manual (Deltares, 2024).

2.3 SLR implementation and model input

The Delft3D-ASMITA model, as described above, is implemented in Delft3D as a new, alternative sediment transport formulation. Using the Delft3D-ASMITA model therefore follows the same steps as a regular Delft3D model. Given the limited applicability of the ASMITA equilibrium considerations, the Delft3D-ASMITA is specifically designed to be used in tidal inlet system domains.

In the following, we first explain the implementation of SLR in the Delft3D-ASMITA model in more detail, and clarify the general model concept implementation along the way. Then, we describe the necessary model input parameters, which are different from a regular Delft3D model setup, needed to activate and successfully run Delft3D-ASMITA. For more detailed information on a regular Delft3D setup and Delft3D default settings, we refer the reader to the Delft3D 4 (FLOW) manual (Deltares, 2024).

2.3.1 SLR implementation

In Figure 2.3, we show a schematic of the model domain, based on the schematic shown in Figure 2.1. The open domain boundaries at the offshore area are highlighted in red. In a regular Delft3D simulation, SLR can be implemented by prescribing tidal constituents at the open boundaries, and then adding a time-varying timeseries of the mean water level, representing the SLR. In this way, the water level at the open boundaries gradually rises, while still exhibiting the instantaneous hydrodynamics of tides, waves, and storms. However, this approach of SLR implementation is not suitable for the Delft3D-ASMITA model due to spatially limited applicability of the ASMITA equilibrium considerations. In Figure 2.3, we highlight the area of the system, where the ASMITA equilibrium considerations are valid with a dashed pink line ("ASMITA-governed zone"). Outside of this area, such as in the offshore area and the barrier island foreshores outside of the ebb-tidal delta, the ASMITA equilibrium equations are not a feasible approach to determine sediment transport.

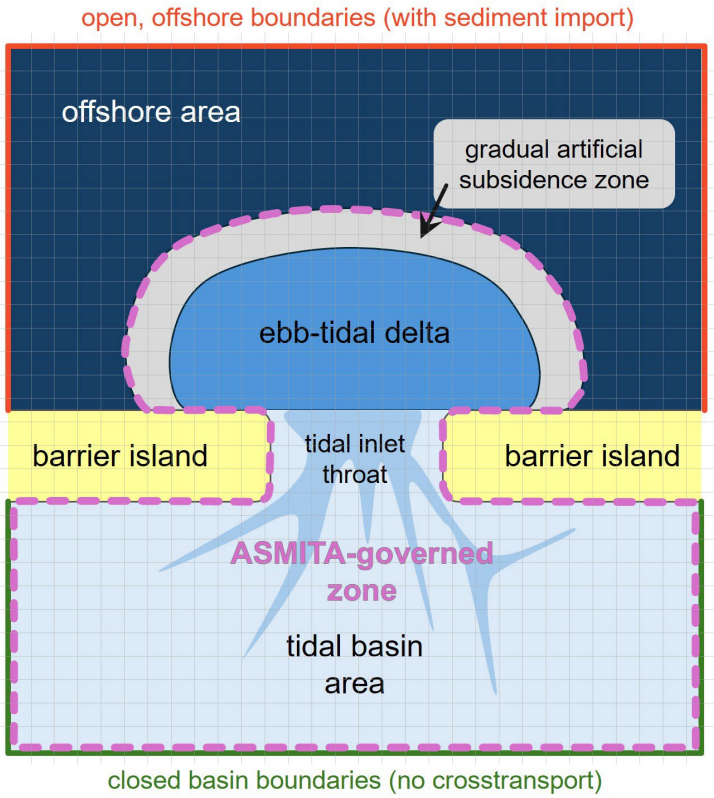

Figure 2.3 Schematic of a representative Delft3D-ASMITA model domain (not to scale), with the open and closed boundaries highlighted in red and green (respectively), and the ASMITA-governed zone indicated by the dashed, pink line. Note the gradual artificial subsidence zone surrounding the ebb-tidal delta.

The problem of implementing SLR as a water level timeseries at the open boundaries arises from the handling of sediment. The only sediment source in the model domain are the open boundaries[4]. If the water level at the open boundaries rises with a SLR timeseries forcing, the water levels throughout the domain will follow, and crucially, so will the ASMITA reference level to stay above the MHW level. Therefore, the depth ratio d_{eq}/d_{inst} will decrease everywhere. The Delft3D-ASMITA formulations cannot be applied partially to the model domain but must be imposed on the entire domain, as they are implemented as an alternative transport formulation

[4] This statement holds true if there are no nourishments implemented in the model region. In the present report, we only show results without nourishments. However, the Delft3D-ASMITA can potentially handle nourishments and sediment dumping, in line with the Delft3D capabilities.

in the regular Delft3D suite. With the entire model domain subject to the Delft3D-ASMITA sediment transport formulations, the domain will demand sediment everywhere to restore its initial equilibrium if $d_{eq}/d_{inst} < 1$. The most readily available sediment in the system is the sediment imported through the open boundaries. Hence, the freshly imported sediment will deposit where it is needed, i.e. immediately after import in the offshore region, before ever reaching the tidal inlet. But as the water levels rise throughout the domain, the tidal inlet also needs sediment to keep up with SLR. With no other sediment readily available (the imported sediment being deposited in the offshore area), erosion will occur at much higher-than-expected rate in and around the ASMITA-governed zone of the domain.

To prevent the sedimentation in the offshore area, we need to keep the mean sea level at the open boundaries constant and force the water levels there only with the tidal constituents. To implement SLR in the tidal inlet, we prescribe a localized subsidence timeseries: within the ASMITA-governed zone of the model domain, we lower the bed level artificially. This leads to an increase in water depth equivalent to the SLR effect, but only in the area of the model where the ASMITA equilibrium considerations are valid. Subsidence is implemented with the *.sdu file by specifying the total subsidence on the computational grid at certain moments in time, to correspond to SLR. Delft3D then linearly interpolates the subsidence for computational timesteps in between the specified waypoints. The increase in water depth projected for a certain SLR scenario and time step occurs in the model only in the ASMITA-governed zone (see Figure 2.3).

However, the (gradual but significant) *localized,* artificial subsidence in the ASMITA-governed zone creates a disruption in bed levels. When left unattended, the disruption at the border of the ebb-tidal delta generates instabilities in the model. We observed very high non-physical erosion appearing at the barrier island foreshores, most likely driven by the large sediment demand occurring at the ebb-tidal delta boundaries. To tackle this problem, we defined a transition zone, surrounding the ebb-tidal delta, where we apply a gradual subsidence to the grid. Figure 2.4 shows an example of the application of subsidence to achieve SLR implementation in the ASMITA-governed zone of the Ameland inlet model (for comparison, note the similarities between the visualisation of the real computational model in Figure 2.4 and the conceptual schematic in Figure 2.3). In the plot of Figure 2.4, the two barrier island shapes of Terschelling and Ameland are visible in dark blue, as well as the shape outline of the ebb-tidal delta, framed by the gradual transition zone. The colour code represents the fraction of subsidence applied in each grid cell. We define the absolute subsidence for a number of time steps to correspond to SLR. The increase in water depth projected for a certain SLR scenario and time step appears in the model as subsidence in the ASMITA-governed zone (yellow area in Figure 2.4, subsidence fraction = 1). For the transition zones surrounding the ebb-tidal deltas, the subsidence gradually decreases from 1 to 0 (yellow to dark blue).

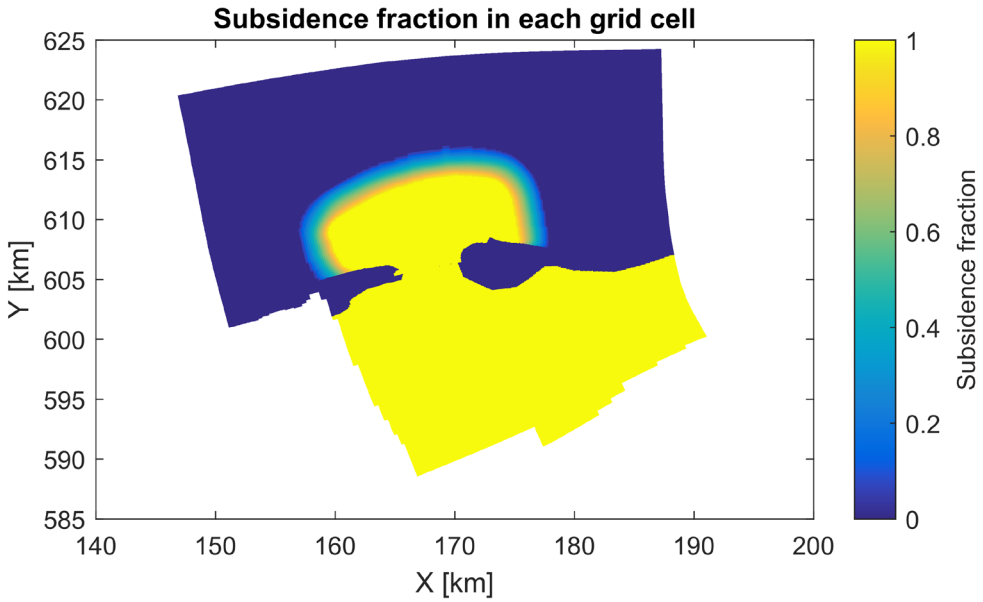

Figure 2.4. Subsidence fraction field on the computational grid of the Ameland inlet model. The subsidence at each grid cell is given by multiplying the shown subsidence fraction by the total subsidence representing the sea level at each moment in time. The dark blue colour represents the offshore area, where no subsidence is applied (i.e. subsidence fraction 0). The yellow colour represents the ASMITA-governed zone of the system, where the maximum subsidence fraction (1) is applied. Note the gradual subsidence transition zone, where the total subsidence of each time step is multiplied with a factor between 1 (in the ASMITA-governed zone of the system) to 0 (in the offshore area, where ASMITA considerations are not valid).

2.3.2 Model input

The following steps highlight specific input parameters, which need to be changed in a regular Delft3D-4 simulation, when setting up a Delft3D-ASMITA simulation.

Within the *.mdf file (Master Definition File, main input file for Delft3D 4, with * representing the file name. See screenshots in Figure 2.5):

1. define the initial (global) sediment concentration, C01. We recommend choosing the same value as for the global equilibrium concentration, C_E in Equ. (2-7). The global equilibrium concentration is also set in the *.sed file (see below).
2. set the keyword Dpsopt to #DP#, indicating that the bathymetry is specified in the water level points that correspond to the grid cell centres. This is not strictly necessary for the Delft3d-ASMITA model to run successfully. But as the equilibrium depth for the ASMITA sediment transport formulations is always defined in the cell centre, it is very useful for consistency to also use a matching bathymetry dataset.

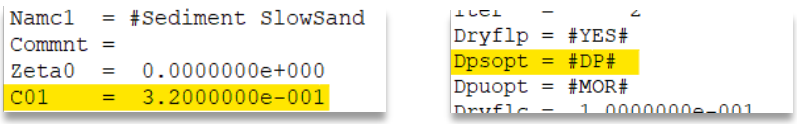

*Figure 2.5. Screenshots of parts of the *.mdf file, with the initial concentration C01 highlighted, as well as the keyword Dpsopt, which needs to be set to #DP# for the Delft3D-ASMITA model to run successfully.*

Within the *.sed file (with * representing the file name, see a screenshot in Figure 2.6):

1. ensure that the sediment type is set to “sand” (Delft3D-ASMITA currently only handles non-cohesive sediment).
2. set the transport formula, keyword TraFrm, to 22 (activating the ASMITA sediment transport formulations).
3. determine the global equilibrium concentration, CEqui (see C_E in Equ. (2-7)).
4. specify the file for the equilibrium bed level file, keyword HEqui.
5. set the exponent in the equilibrium sediment concentration equation, N (see n in Equ. (2-7)).
6. set a limit for the depth ratio d_{eq}/d_{inst}, Equ. (2-7), keyword MaxHH[5].
7. specify the reference level, keyword RefLevel, which can be changing in space and time. This reference level is shown also in Figure 2.2 as “ASMITA reference level” (dashed, orange line) and is used to calculate both, d_{eq} and d_{inst}.
8. determine the fresh water and saltwater settling velocities of the sediment (keywords WS0 and WSM.

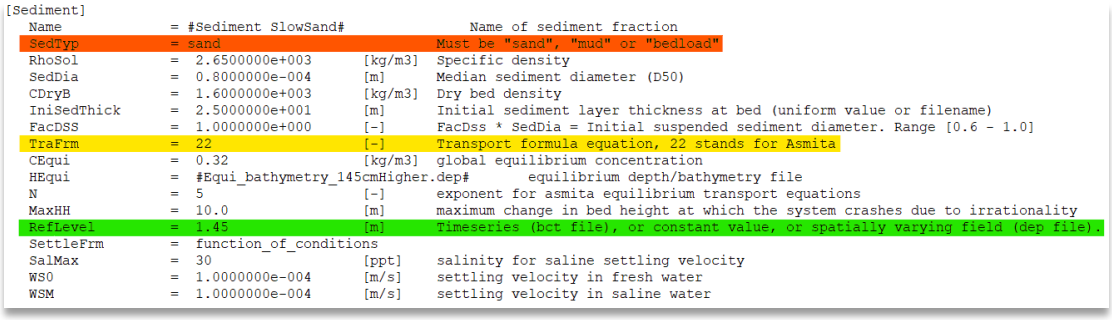

Figure 2.6. Screenshot of the .sed file. Highlighted in red is the sediment type, which has to be set to ‘sand’. Highlighted in yellow is the transport formula which is set to 22 to activate the equilibrium transport formulation of ASMITA. Highlighted in green is the definition of the reference level, which needs to be set higher than the mean high water level (MHW) of the intertidal flats (depending on the tidal range of the model).

The equilibrium bed level (HEqui) has to be defined with respect to the reference level, RefLevel. As mentioned in Section 2.2.4, the reference level should be chosen high enough to avoid negative values of the instantaneous depth at all times. We recommend setting the reference level above the MHW level of the model to avoid extreme values for the depth ratio between equilibrium depth and instantaneous depth. If the reference level is set within the tidal range (e.g. at NAP = 0 m), the depth ratio can adopt extremely large values due to a division by (near) zero. If the two depth values become very small, the equilibrium concentration (see $c_{e,grid\ cell}$ in Equ.s (2-6) and (2-7)) therefore loses its depth dependency. However, the higher the reference level is set above the bed level(s), the ratio between the equilibrium bed level and the instantaneous bed level tends to get closer and closer to 1, $d_{eq}/d_{inst} \approx 1$. If the bed level ratio is close to 1, the sediment exchange rate is directly affected (and will become smaller than for a reference level set lower above the bed level(s)). This effect can within limits be corrected by increasing the exponent N in the *.sed file (n in Equ. (2-7)). However, this measure should only be considered in extreme cases, where initial results indicate a significant decrease in depth dependency of the local equilibrium concentration.

[5] This delimiter prevents unreasonable depth ratios but should only be activated in extreme cases. Another useful adjustment to keep the depth ratio in check is to set the reference level at an appropriate elevation (see main text).

Note that the SLR implementation through artificial subsidence (see previous section) has a positive side effect regarding the reference level: this SLR implementation leads to a bed lowering, instead of a gradual continuous water level rise due to SLR. We can therefore keep the reference level constant over time, as we want to ensure it is always well above MHW, which also rises with SLR. The model implementation allows for a changing reference level, if needed, as well as a spatially varying reference level. In this report we use a spatially and temporally constant reference level (see Figure 2.5).

2.4 Postprocessing of raw Delft3D-ASMITA output files

The Delft3D-ASMITA model delivers standard Delft3D output files (a map file with high spatial resolution, and a history file with data at strategically chosen observation points and cross-sections, usually at a much higher time resolution than the map file[6]). However, the Delft3D-ASMITA output files need special postprocessing for two main reasons: (1) the bed levels need to be corrected due to the SLR implementation as subsidence in the model (see Section 2.3), and (2) specialised output is usually desired for the specific use case of the model of tidal inlet systems (e.g. the extent and morphological development of intertidal flat areas). We postprocess the Delft3D-ASMITA results with MATLAB subroutines.

The bed level correction is necessary to counteract the artificially imposed subsidence, which imitates SLR during the simulation, but also actually lowers the bed level during the simulation period. The bed levels within the ASMITA-governed zone of the simulation output need to be raised for every time step by the respective subsidence amount, taking into account the subsidence fraction especially with regards to the transition zone around the ebb-tidal delta. This postprocessing step needs to correct the bed levels with spatially (and temporally) varying values, which is the reason why this is not easily done with the QUICKPLOT toolbox from Delft3D.

A more standard postprocessing step, which is not unique to this Delft3D-ASMITA model, is the differentiation (and where necessary transformation) between the hydrodynamic and the morphodynamic timescales. Some parts of the model output are directly linked to the morphodynamic timescale, whereas the hydrodynamic variables, like the water level, are only temporally resolved on the hydrodynamic timescale. Therefore, to plot hydrodynamic variables on the morphodynamic timescale, we need to switch time scales. In this regard, this is only a multiplication of the time axis labels and has no effect on the variables' values. In contrast, the morphodynamic variables, like sediment transport or cumulative sedimentation/erosion, can be plotted against the hydrodynamic timescale or the morphodynamic timescale, with consequences for the variables' values. To plot against the morphodynamic timescale, the values of the variable will be multiplied by the MorFac (see Section 2.2). The MorFac enables upscaling of the morphodynamic response by simple multiplication. While this multiplication is partly already included in the simulation output (e.g. when it comes to sedimentation or erosion heights), it sometimes needs to be manually applied afterwards in postprocessing (e.g. for sediment transport variables). It is therefore crucial to keep in mind which output variables already include the MorFac multiplication, and which do not, as well as the variables which are not affected by the MorFac, i.e. are purely hydrodynamic variables.

[6] The resolution of both output files is a conscious choice by the modeller, but to keep computational costs as low as possible, it helps to select a higher time resolution for the history file, compared to the data-heavy map file. Nevertheless, if a specific use case requires high resolution map files, the model can be set up that way.

2.5 Simulation result types of interest for tidal inlet systems

In the following, we list the different simulation result types we obtain from our postprocessing, and which are specifically of interest for tidal inlet system use cases.

2.5.1 Quantification of intertidal flat change

To quantify the impact of SLR on the tidal flats, we derive hypsometric curves, intertidal area, intertidal (sediment) volume and mean flat height over time, for each time step of the map file, based on the subsidence-corrected bed levels. For this analysis we assume that MLW and mean high water MHW rise at the same rate as SLR. For a schematic of the variables, see also Figure 2.5. We show two fictitious hypsometric curves, one under initial conditions (in blue) and another one after SLR (red).

- To calculate hypsometric curves, the entire range of elevations is divided into bins of an equal size (note: binning happens in Figure 2.5 on the y-axis). Then, we sum up the bed level area between the lower and upper elevations for each bin and calculate the cumulative area from the elevation minimum to the elevation maximum. The hypsometric curve describes therefore the total area, which is at or below a certain elevation.

- The (total) intertidal area A_{IT} (see Figure 2.5) is defined as the area between MLW and MHW.

- The intertidal volume V_{IT} (see Figure 2.5) is computed as the total sediment volume located between MLW and MHW. We first calculate the intertidal height above MLW, h_{IT}, for each grid cell with an elevation higher than MLW, by subtracting the MLW from each grid cell's elevation. We then multiply the intertidal height h_{IT} per grid cell by the corresponding cell area. The sum of the individual grid cell volumes gives the total intertidal volume V_{IT}.

- The *mean* flat height is calculated by dividing the intertidal volume V_{IT} by the intertidal area A_{IT}.

2.5.2 Sediment transport through the tidal inlet throat

The Delft3D-ASMITA model delivers sediment transport based on cross-sections in the model. In Delft3D (and therefore also Delft3D-ASMITA), the cumulative sediment transport across a cross-section is saved in the history file at specified timesteps, with respect to the hydrodynamic timescale.

Delft3D(-ASMITA) extracts both cumulative as well as instantaneous sediment transports for the cross-sections in the domain (e.g. cross-sections over the inlet throats). We use the cumulative transport t_{sed} in our postprocessing (multiplied by the MorFac) to arrive at the estimated total amount of sediment being transported across a tidal inlet throat over the simulation period. Cross-sections in Delft3D are defined along the grid lines and depending on the grid orientation in the model, the sign of the sediment transport indicates the direction of transport. Positive sediment transport output is aligned with increasing grid cell numbers, and vice versa. For the inlet throat cross-sections, this becomes crucial to interpret correctly whether a tidal basin is importing or exporting sediment.

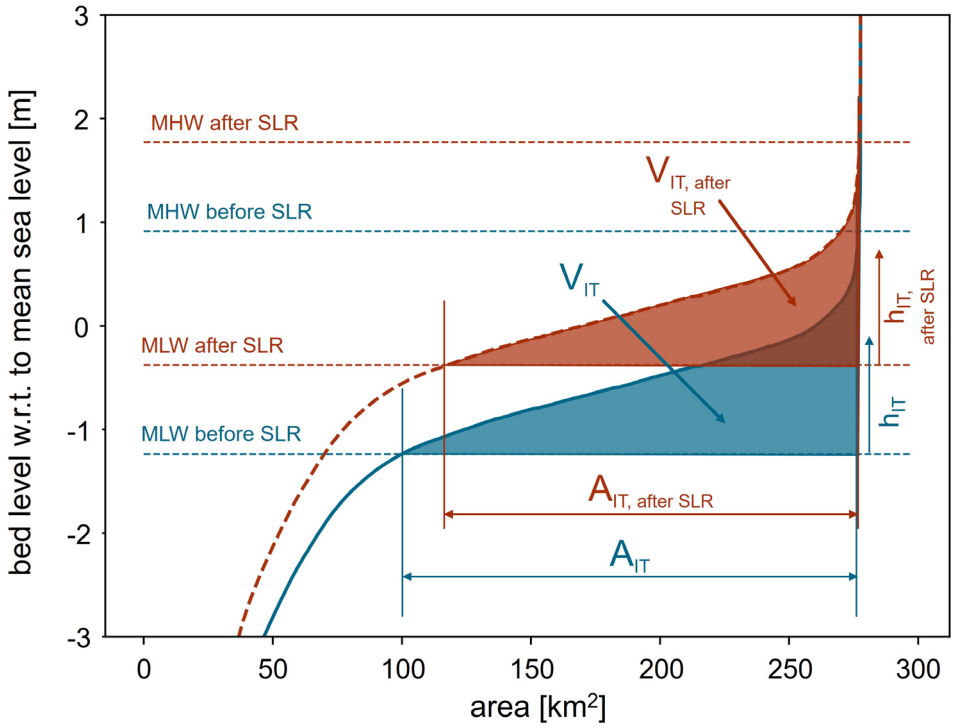

Figure 2.5. Schematization of a hypsometric curve, with the intertidal area, intertidal volume and the intertidal height indicated, before and after SLR (in blue and red, respectively). The subscript IT stands for intertidal. The upwards shift between the blue and red hypsometric curves is due to sedimentation as response to SLR. Adapted from: Huismans et al. (2022).

From the cumulative sediment transport (multiplied by the MorFac), we can also derive a sediment transport rate $\dot{t}_{sed}$ at a certain time as the gradient of the cumulative sediment transport. As mentioned above, Delft3D(-ASMITA) computes the sediment transport only on the hydrodynamic timescale, and therefore the output includes the tidal signal of the hydrodynamic forcing. This tidal forcing causes fluctuations in the sediment transport rate, with an overlying trend consistent with the consequences of the imposed SLR. To eliminate the noisy signal of the gradient due to the tidal forcing, we calculate the sediment transport gradient based on a large timestep (e.g. 10 – 20 morphodynamic years). This methodology gives a trend indication of the sediment transport rate on the timescale of morphological development responding to the imposed SLR.

From the cumulative sediment transport through a tidal inlet throat we can derive an averaged sedimentation height in the tidal basin of the inlet. If the domain boundaries around the basin are closed in the model (see Figure 2.3 for an example, closed boundaries highlighted in green), this averaged sedimentation height can be compared to the total SLR in the same period. In this case we do not take the difference in sedimentation patterns within the basin area into account. Therefore, the averaged sedimentation height $\overline{h}_{sed}$ can be calculated as:

$$\overline{h}_{sed} = \frac{t_{sed}}{A_{basin}}, \tag{2-10}$$

with:

t_{sed} = cumulative sediment transport
A_{basin} = total basin area.

Over the simulation period, a prescribed SLR rate will have amounted to a cumulative final SLR, $SLR_{cum,final}$. We can subtract the averaged sedimentation height from the cumulative SLR to arrive at the averaged water depth in the basin, Δh_{wd}:

$$\Delta h_{wd} = SLR_{cum,final} - \overline{h}_{sed}\,, \tag{2-11}$$

The value of Δh_{wd} tells us whether

1) the basin's water depth has decreased, $\Delta h_{wd} < 0$;
2) the basin has approximately maintained the initial water depth, $\Delta h_{wd} \approx 0$; or
3) the basin's water depth has increased, $\Delta h_{wd} > 0$.

However, this quantification does not yet indicate whether or not the tidal inlet system has managed to arrive at a new dynamic equilibrium over the course of the simulation period. Therefore, we take our analysis one step further, by looking at transport and sedimentation *rates*.

We derive an averaged sedimentation rate $\dot{h}_{sed}$ in a similar fashion as the averaged sedimentation height:

$$\dot{h}_{sed} = \frac{\dot{t}_{sed}}{A_{basin}}\,, \tag{2-12}$$

with:

$\dot{t}_{sed}$ = yearly sediment transport rate, based on t_{sed}, see explanation further up in this section.

Comparing the yearly $\dot{h}_{sed}$ to the yearly SLR rate $\dot{d}_{SLR}$ gives an indication, whether a dynamic equilibrium has been established:

$$\frac{\dot{h}_{sed}}{\dot{d}_{SLR}} = \begin{cases} < 1 & \text{sedimentation does not balance SLR, water depth increases} \\ \approx 1 & \text{dynamic equilibrium is established} \\ > 1 & \text{sedimentation outpaces SLR, basin fills up with sediment} \end{cases}$$

We stress again, that we take the entire basin area into account for these calculations, assuming an evenly averaged sedimentation height and rate throughout the basin area, i.e. in both intertidal flat and channel areas. This means, that the direct comparison between $\dot{h}_{sed}$ and $\dot{d}_{SLR}$ does not allow a direct interpretation of the "drowning" of intertidal flats. For such an interpretation, the analysis would have to be based on more specific areas (i.e. the intertidal area, or the channel area only), and comprise also specific sediment transports (into the intertidal flats, or into the channels, respectively). The differences in sedimentation patterns between intertidal flat and channel areas we observe in our simulations are described in more detail in Chapters 3 and 4 of this report.

For each SLR scenario considered in this report, we calculate for the end of the simulation period, the (cumulative) averaged sedimentation height for each basin $\overline{h}_{sed}$, as well as the averaged sedimentation rate $\dot{h}_{sed}$ (for the final year of the simulation). These values can then be compared to the (cumulative) increase in water depth due to SLR and the final SLR rate. These numbers are listed in tables for each model we present in the respective sections of this report.

2.5.3 Cumulative sedimentation/erosion maps

A strong advantage of the Delft3D-ASMITA model results compared to a regular ASMITA model is the grid-based spatial resolution of output variables (i.e. the Delft3D map output file). We can plot output variables like the cumulative sedimentation / erosion as a map. These maps are a quick and intuitive way of gauging the output of a simulation. To arrive at the cumulative sedimentation/erosion map, we subtract the subsidence-corrected bed level for each time step from the initial bed level.

2.5.4 Water levels for specific observation stations

In the Delft3D-ASMITA hydrodynamics and morphodynamics directly influence each other (if the user chooses to allow them to interact with each other, i.e. by allowing bed updating during the simulation period). The hydrodynamic output of the Delft3D-ASMITA model is therefore able to predict how the tidal signal will develop under SLR, as well the influence of morphological changes on the tidal signal. The water level signal at observations stations in the basin over time is a direct result of this feedback mechanism between hydro- and morphodynamics. To isolate the influence of the morphodynamics, we also carried out a purely hydrodynamic simulation for comparison, without any morphological developments.

To determine the impact of the SLR and corresponding morphological changes on the hydrodynamics, we choose to analyse an observation station located in a channel and close to the basin centre. We therefore ensure that the water level analysis takes place far from the throat and the mainland, and a continuous tidal signal (showing both flood and ebb) can be obtained. In this report, we show the location of the chosen observation stations for the water level data in Figure 3.8 and Figure 4.3.

2.6 Assumptions and shared input for the test cases with the Delft3D-ASMITA model

In the following, we explain a set of assumptions we made for the use cases we carried out with the new Delft3D-ASMITA model. Our cases are based on existing, regular Delft3D 4 models of the Ameland basin (single tidal inlet system), and of entire Dutch Wadden Sea (multiple inlet system).

2.6.1 Modelled SLR scenarios

We simulate five different SLR scenarios covering the period 2000-2200. They are based on the SLR scenarios proposed in Wang et al. (2024). We describe the scenarios here in detail and show a visual representation in Figure 2.8.

- 2 mm SLR: SLR rate constant at 2 mm/y from 2000 till 2200.
- Low SLR scenario: SLR rate constant at 2 mm/y until 2020. Then it accelerates linearly to 5 mm/y in 2055 before it remains constant at this rate.
- Moderate SLR scenario: SLR rate constant at 2 mm/y until 2020. Then it accelerates linearly to 13.8 mm/y in 2150 before it remains constant at this rate. The acceleration rate is almost the same as in the Low SLR scenario, but it continues much longer in time.
- High SLR scenario: SLR rate constant at 2 mm/y until 2020. Then it accelerates linearly to 25 mm/y in 2200, the end of the simulations.
- Extreme SLR scenario: SLR rate constant at 2 mm/y until 2020. Then it accelerates linearly to 40 mm/y in 2200, the end of the simulations.

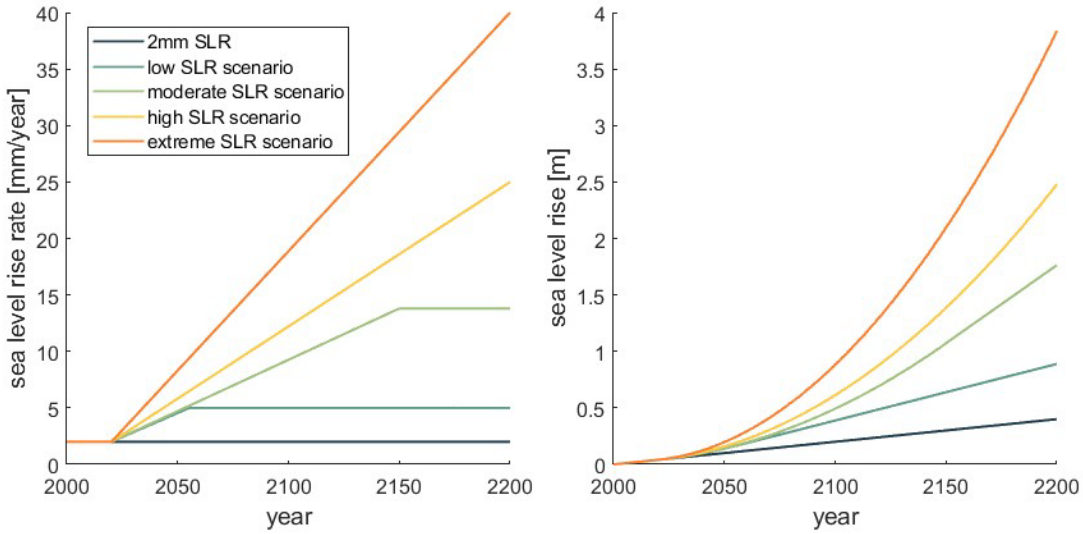

Figure 2.6. Modelled SLR scenarios. The left panel shows the used SLR rates and the right panel the sea level relative to 0 m in 2000. The same colour code is applied throughout the document.

2.6.2 Subsidence input

We prescribed subsidence within the ASMITA-governed zone at specific timesteps during the simulation period, choosing the time steps such that a linear interpolation in between would be valid. For all scenarios, we provided the subsidence values at the start and end times, i.e. the years 2000 and 2200, with no further values necessary for constant SLR rates. For all considered SLR scenarios, the SLR rate is constant at least until the year 2020. For linearly increasing SLR rates afterwards, we provided a subsidence value for each consecutive year of linear SLR rate (e.g. for the years 2021, 2022, 2023, …., 2150 for the moderate SLR scenario). Based on these provided subsidence values, Delft3D-ASMITA interpolates linearly for all computational time steps in between.

2.6.3 MHW and MLW

For this report, we assume tidal wave symmetry, i.e. MLW and MHW have the same magnitude but with opposite sign. We estimated the water level values as half the tidal range values for the Wadden Sea basins, as presented in Huismans et al. (2022). See Table 2.1 below.

Table 2.1. MHW and MLW for the tidal basins of the Dutch Wadden Sea in m with respect to NAP.

Texel	Eierland	Vlie	Ameland	Pinkegat	Zoutkamp
±0.83	±0.92	±0.95	±1.08	±1.08	±1.13

Source: Huismans et al. (2022).

2.6.4 ASMITA Reference level

We opt to use a spatially and temporally uniform value for the ASMITA reference level in our simulations, even though the Delft3D-ASMITA implementation allows for either a spatially varying field, or a time series of spatially uniform values as input for the reference level. We choose a value 1.15 times the highest MHW of all the Dutch Wadden Sea basins, which is 1.45

m NAP for the Groninger Wad[7]. The MHW for Groninger Wad was not obtained from Huismans et al. (2022),. We derived it instead based on observation stations placed in the Wadden Sea Delft3D model. For the single-inlet-system model (Ameland) we use the same reference level (1.45 m NAP) to ensure comparability.

2.6.5 Equilibrium bathymetry

As mentioned in Section 2.3.2, an equilibrium bed level position must be prescribed as part of the model input. Ideally, this would be the equilibrium bathymetry of a tidal basin if it were in dynamic equilibrium with SLR. However, we often cannot know this bathymetry because the system is out of equilibrium due to external pressures. In the case of the Dutch Wadden Sea, at least two of the tidal inlet systems are still adapting to changes due to human interventions (the construction of the Afsluitdijk and the closure of the Lauwerszee). For the results presented in this report, we assume that the input bathymetry for those Delft3D-ASMITA models is also the equilibrium bathymetry.

For the model of the Ameland inlet, the input bathymetry is from the year 2005. For the Wadden Sea model, the input bathymetry is composed of an assemblage of Vaklodingen and LIDAR surveys from the years 2002 to 2008. Specifically, the area covering the Ameland tidal system is composed of bathymetries from 2007 and 2008. Furthermore, to account for the equilibrium water depths being measured with respect to the ASMITA reference level, a constant value equal to the reference level was added to the input bathymetries.

2.6.6 Sediment input

We use a constant sediment concentration of 0.32 kg/m^3 throughout all our simulations, as global equilibrium concentration as well as open boundary concentration. This concentration value is based on previous ASMITA modelling (e.g., Wang et al., 2018, 2020; Huismans et al., 2022, Lodder et al., 2022). We define the sediment as “sand” (i.e. non-cohesive) in the .sed file, but we tune the sediment properties to match previous ASMITA calculations, where the sediment could not be described neither as a sand, nor a mud fraction, but rather as a mixture.

The median sediment diameter in our Delft3D-ASMITA model simulations is 80 µm. However, the defining parameter for sediment transport modelling is the settling velocity, which we define independently from the grain size. Hence, the model does not take the median diameter further into account. We prescribe a settling velocity of 0.1 mm/s, which is much lower than what a sand particle of 80 µm median diameter would exhibit. This approach artificially creates a slowly settling sediment, which shows non-cohesive behaviour.

Note that the Delft3D-ASMITA model can potentially handle several sediment fractions. We plan to investigate the behaviour of this model for various different sediment fractions in the future.

2.6.7 Simulation time

All SLR scenarios are simulated for a time period of 200 years (from 2000 till 2200). The hydrodynamic simulation time was 362 days, which we assume to be representative of one year. We applied a MorFac of 200, which extends this hydrodynamic year to 200 morphodynamic years.

[7] To avoid the loss of depth dependency of the equilibrium concentration, the reference level is defined based on the maximum MHW in the entire model domain. This leads to the use of the one from Groninger Wad. For more information on the reference level setting, see Section 2.3.2.

3 Application to the Ameland Inlet

In this chapter, we describe the first successful application of the Delft3D-ASMITA model. The model focuses on the Ameland tidal inlet system, with the two barrier islands Ameland and Terschelling bordering the inlet throat. We chose the Ameland tidal inlet system because it is generally considered to be close to, or even in, morphological equilibrium. As the Delft3D-ASMITA model requires an equilibrium bathymetry as input, the Ameland system is an ideal test case.

In the following, we present the set-up of the model, as well as the different results obtained from different simulations. In Chapter 4, we present results for a bigger model encompassing the entire Wadden Sea. To compare the results of the single-inlet-system model (SIS model) of this chapter to the corresponding results of the multi-inlet-system model (MIS model), we refer the reader to B.4.

3.1 Model setup

In this section, we describe only the parts of the model input not previously mentioned in Sections 2.3.2 and 2.6. We refer the reader to said sections for a wider overview of model input and baseline assumptions.

Table 3.1 presents the overview of the selected model parameters for the Ameland SIS model. For other parameters not mentioned in the table, which are part of the standard flow module in Delft3D 4, we used the default values.

Table 3.1. Overview of selected model parameters for the Ameland standalone model

Parameter	Value/setting
Hydrodynamic simulation time	362 days
Timestep	0.5 s
Morphological scale factor (morfac)	200
Morphological simulation time	200 years
Dimensions	2D
Initial concentration constituent (C01)	0.32 kg/m^3
Water density (Rhow)	1023 kg/m^3
Horizontal eddy viscosity	1 m^{2}s^{-1} (uniform)
Horizontal eddy diffusivity	1 m^{2}s^{-1} (uniform)
Chezy coefficient	63 m$^{1/2}$/s (uniform)
Dpsopt	#DP#
Cstbnd	#yes#
Sediment type	sand
Initial sediment layer thickness	25 m
Sediment transport formula	22 (ASMITA)
Settling velocity (WS0/WSM)	0.0001 m/s
Global equilibrium concentration (CEequi)	0.32 kg/m^3
Power in the ASMITA transport equation (N)	5
Maximum change in bed height (MaxHH)	10
Reference level	1.45 m

3.1.1 Grid and bathymetry

We model the Ameland inlet system based on an existing Delft3D model (de Fockert, 2008; Jiao, 2014; Chen, 2021). It has a structured curvilinear grid that covers the inlet system and an offshore region extending 16 km seaward. Overall, the model domain spans around 50 x 40 km. The grid resolution varies approximately between 30mx40m and 320x380m, with the highest resolution near the inlet throat. In total, the flow grid comprises 112752 grid cells (see Figure 3.1). The bathymetry data is an integration of Vaklodingen and LIDAR surveys from 2005 (see Figure 3.2).

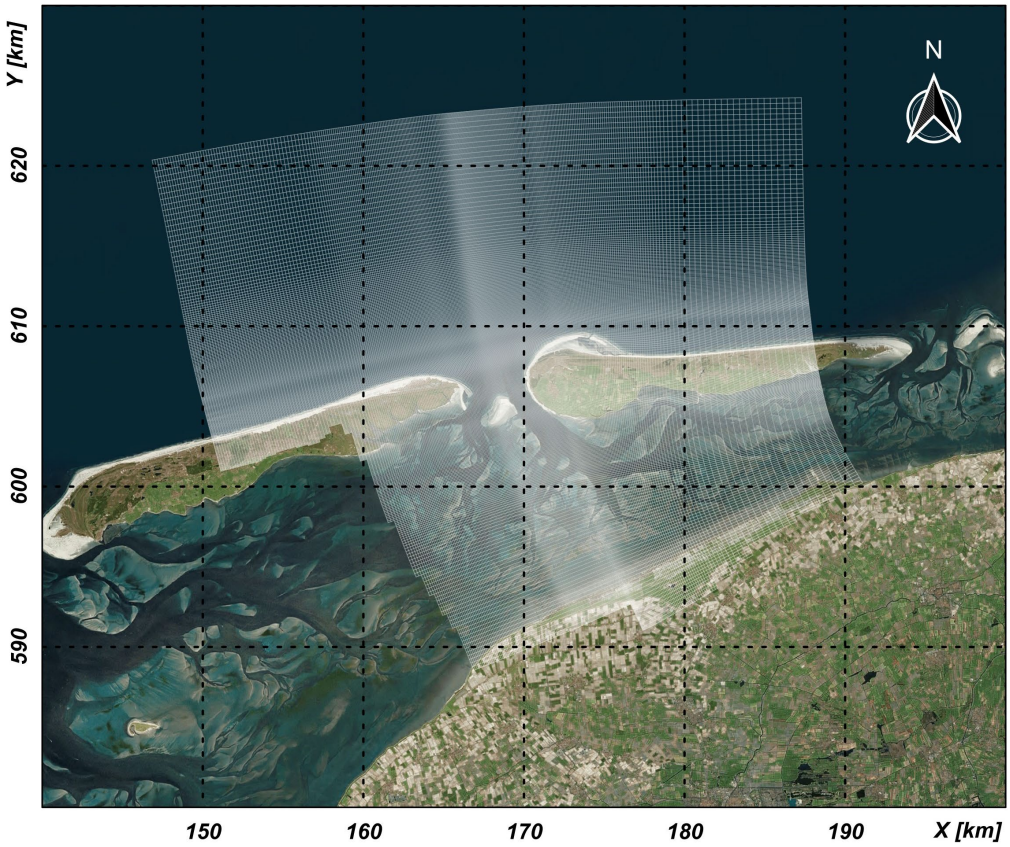

Figure 3.1. Computational grid of the Ameland inlet model.

3.1.2 Forcing conditions

We use cyclic and harmonic water level boundary conditions, which are based on nine tidal constituents. The shore-parallel open boundaries are water level boundaries (denomination “Z” in the auxiliary .bnd file), and the cross-shore open boundaries are Neumann boundaries (denomination “N” in the auxiliary .bnd file). These forcing conditions include a semidiurnal and a diurnal tidal signal, but no spring-neap signal. This is obviously a simplification which can lead to unrealistic results, which needs to be considered while interpreting the results of the model.

We implement SLR as subsidence (see Section 2.3.1), hence the mean water levels in the model domain and at the boundaries do not change over the course of the simulation.

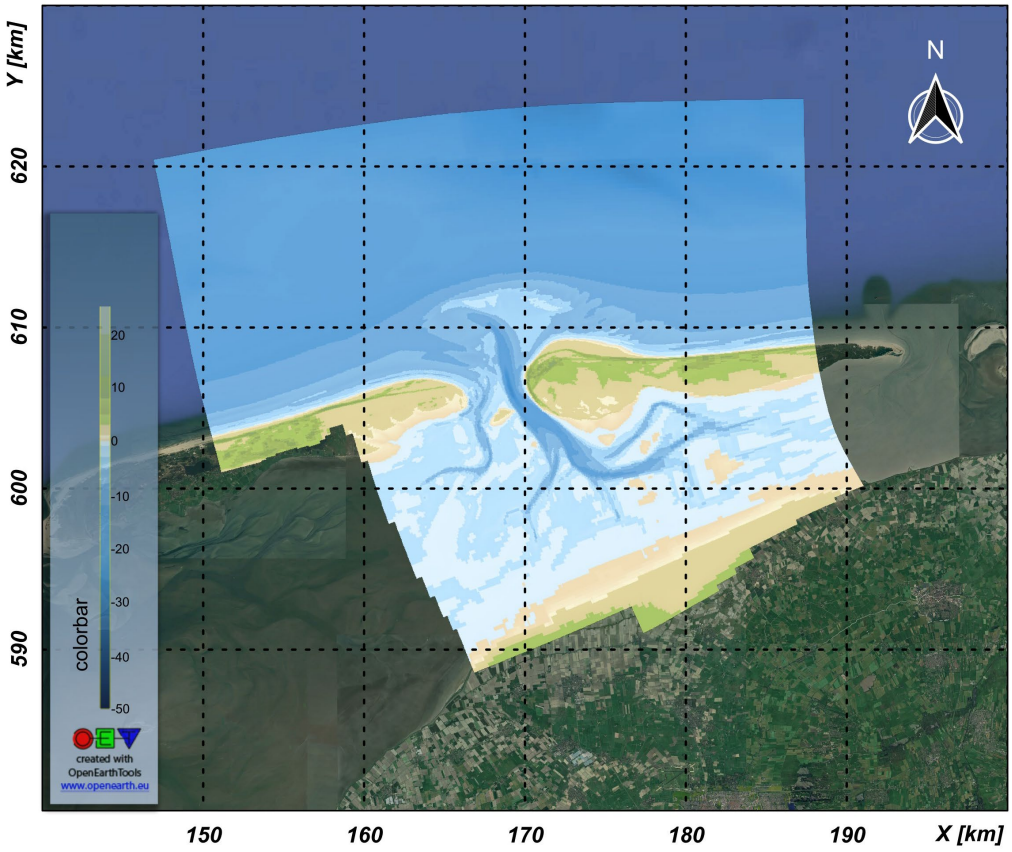

Figure 3.2. Bathymetry input for the Ameland inlet model. Note that the data is already interpolated onto the model grid.

3.2 Results

3.2.1 Change in intertidal flat area, volume, and height

In Figure 3.3, we show the change in intertidal flats over the simulation period for the Ameland basin. The results are based on the analysis of the hypsometric curves, as shown in Figure 3.4. For a detailed explanation of how we arrive at the results, we refer the reader to Section 2.5.1.

The three panels of Figure 3.3 show the intertidal area, the intertidal sediment volume and the mean flat height (intertidal characteristics). The different colours in graphs indicate the SLR scenario, as designated in the legend in the lower left corner of the left-most panel (showing the intertidal area). In all three panels, we can distinguish similar trends to varying degrees depending on the SLR scenario: initially, the intertidal flats are trending downwards at a slow but steady rate. After about 70 years of simulation, the downwards trend reverses in all three panels, and intertidal area, sediment volume and flat mean height increase for a short period. Depending on the SLR scenario, this increase picks up faster (more extreme scenarios) or slower (milder scenarios) for the intertidal flat volume and mean flat height (this trend is less clear for the intertidal area). The three higher SLR scenarios (moderate, high and extreme SLR) lead to the fastest increase in sediment volume and flat height. However, for these scenarios, the increase eventually reverses again, turning into a decrease in flat area, volume and mean height. The two milder scenarios (2 mm linear, and low SLR) lead to a quasi-steady intertidal flat behaviour, which continues throughout the entire simulation period for the 2 mm/year case. From 2100 onwards, the most extreme SLR scenario causes a rapid decline of intertidal flats, with the area decreasing in total by roughly 60%, the sediment volume by almost 80%, and the flat height by 50% at the end of the 200-year period. The less extreme scenarios

(moderate and high SLR scenarios) also show intertidal flat decline, albeit to a lesser extent. The moderate SLR scenario shows a slowing trend of intertidal flat loss at the end of the 200-year period. Even for the most extreme SLR scenario, we do not observe any “complete drowning”, i.e. disappearance of the entire intertidal flats.

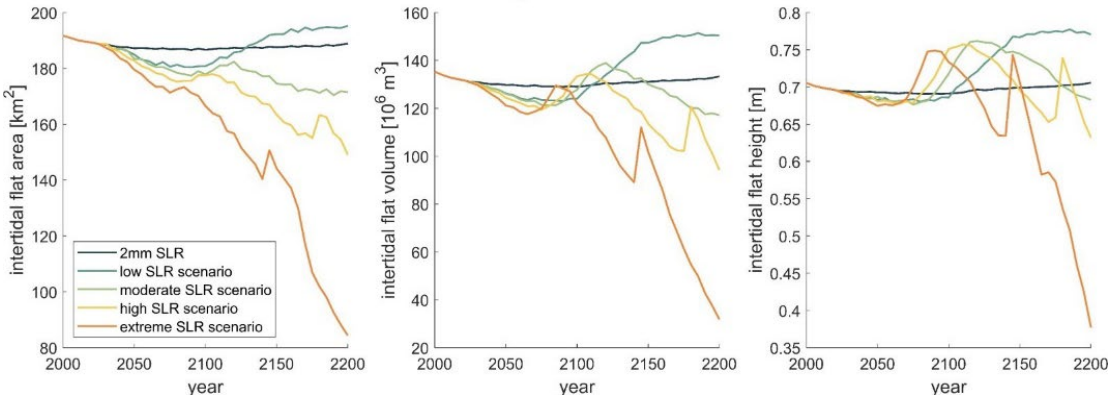

Figure 3.3. Intertidal flat area (in square kilometres), sediment volume (in million cubic metres), and height (in metres) of the Ameland basin over time for five different SLR scenarios.

The pronounced differences between the scenarios are not surprising, yet still remarkable. While for a low SLR scenario the intertidal flats even grow in area, volume and height, they suffer significant losses for the high and extreme SLR scenarios and decline for moderate SLR. The differences appear especially in the second half of the simulation period, when the more extreme scenarios deviate further and further from the milder ones (for reference of the SLR rates and absolute values, see Figure 2.6).

The rate of SLR is directly linked to the rate of decline of the intertidal flats, such that certain features of the plots for the extreme SLR scenario (orange graph) can be found later on in the simulation period for the high SLR scenario (yellow graph) (see Figure 3.3). This applies to the first reversal of the downward trend around 2070 (for the most extreme scenario), as well as the second, quite dramatic uptick in area, volume, and height around 2150 (for the most extreme scenario, about 40 years later around 2190 for the high SLR scenario). If the simulation ran for longer, we expect to see a similar spike for the moderate SLR scenario sometime in the future after 2200.

Figure 3.3 reveals an essential difference between the Delft3D-ASMITA model and the regular ASMITA model, i.e. how the supratidal area is incorporated. The regular ASMITA model works with morphological elements of a fixed horizontal area. This means that the supratidal area is excluded from the model, and the areas of the channels, the ebb-tidal delta and the tidal flats remain constant in time during the whole simulation. Therefore, under an accelerated SLR scenario the simulated intertidal characteristics show a monotonous development, which can eventually lead to relatively fast “drowning” of intertidal flats. In the Delft3D-ASMITA model the supratidal area is included through the real (i.e. measured) bathymetry and the spatial grid resolution. SLR causes gradual inundation of higher areas, and this explains why the intertidal flat area, volume and mean height can suddenly start increasing after a period of continuous decrease over time, as shown in Figure 3.3. Hence, supratidal inundation causes a delay in drowning of intertidal flats as new regions become intertidal over time. Note that sedimentation alone due to SLR cannot explain the sudden gains in intertidal characteristics, since there is always an adaptation time-lag in between the SLR and the basin’s morphological response (Lodder et al., 2019). The increase in intertidal flat characteristics due to inundation of

supratidal zones can be more easily understood when looking at the hypsometric curves (see next Section).

3.2.2 Hypsometric curves

The hypsometric curve of the Ameland basin bathymetry shows step features towards higher elevations, best visible in the upper left panel of Figure 3.4, where we show the initial hypsometry. The step features in higher elevations indicate the presence of supratidal areas (e.g. salt marshes), which are initially not flooded during the regular tidal cycle (as they are located above the MHW line), but can be flooded occasionally, e.g. during storm surges. Over time, these supratidal areas will become inundated by the rising MHW line that follows SLR (see e.g. panels on low and moderate SLR scenarios, panels in centre row of Figure 3.4). As soon as the MHW line passes over a step feature in the hypsometric curve, a relatively large area almost instantaneously turns from supratidal into intertidal area, leading to the upticks in intertidal characteristics in Figure 3.3. Furthermore, once the MHW line reaches the “end” of the hypsometric curve, it keeps moving upwards, but the hypsometric curve is almost vertical (hence, we do not gain much more area while we increase the elevation). Therefore, the intertidal area, sediment volume and flat height decrease rapidly, because the MLW line still rises along the more horizontally oriented part of the hypsometric curve.

The different panels in Figure 3.4 show a trend with increasing severity of SLR scenarios: the steps in hypsometry are being smoothed out by sedimentation. For the extreme SLR scenario (lower right panel, orange graph), the final hypsometric curve is almost monotonously rising through all elevation levels without significant step features. The initial hypsometric curve (also plotted for comparison as a thin, grey line in the same panel) shows the original step features. This smoothening of the hypsometric curve over time is consistent with the transformation of supratidal regions into intertidal regions. Supratidal zones like salt marshes are generally inundated only occasionally during storm surges, and therefore do not exhibit a regular sedimentation period. Their height and extent remain relatively unperturbed, except during extraordinary events. In contrast, intertidal regions are constantly exposed to tidal flows and submergence, which leads to a regular sedimentation period during the tidal signal. Furthermore, the increase in instantaneous depth compared to the equilibrium depth (see Equ. (2-7)) is relatively larger in shallow areas (i.e. former supratidal regions) than in deeper areas (e.g. channels). This leads to a higher sediment demand in the newly inundated areas and to a higher sedimentation rate there as well, further assisting the smoothening of the hypsometric curve.

The inundation of supratidal areas in the Delft3D-ASMITA model is an interesting simulation result, which we want to investigate further in the future. It is yet unclear how significant the role of supratidal inundation is for morphological tidal inlet system development under SLR. With accelerating SLR, it seems inevitable that supratidal areas will eventually become submerged; however it is still not clear how the whole tidal inlet system will react and what the basin’s morphological response will look like. The Delft3D-ASMITA model could potentially provide some insight if modelling of supratidal regions was improved. For better implementation, the tidal forcing modelling needs to be realistic (e.g., with the inclusion of the spring-neap variation), and additional hydrodynamic processes, like waves and storms should be added. Furthermore, the inclusion of different sediment fractions, as well as a proper representation of the vegetation in supratidal areas, is necessary to correctly simulate their development under SLR. We plan on investigating how to implement these factors in the future and hence, improve the capability of the Delft3D-ASMITA model to reproduce salt marsh development due to SLR.

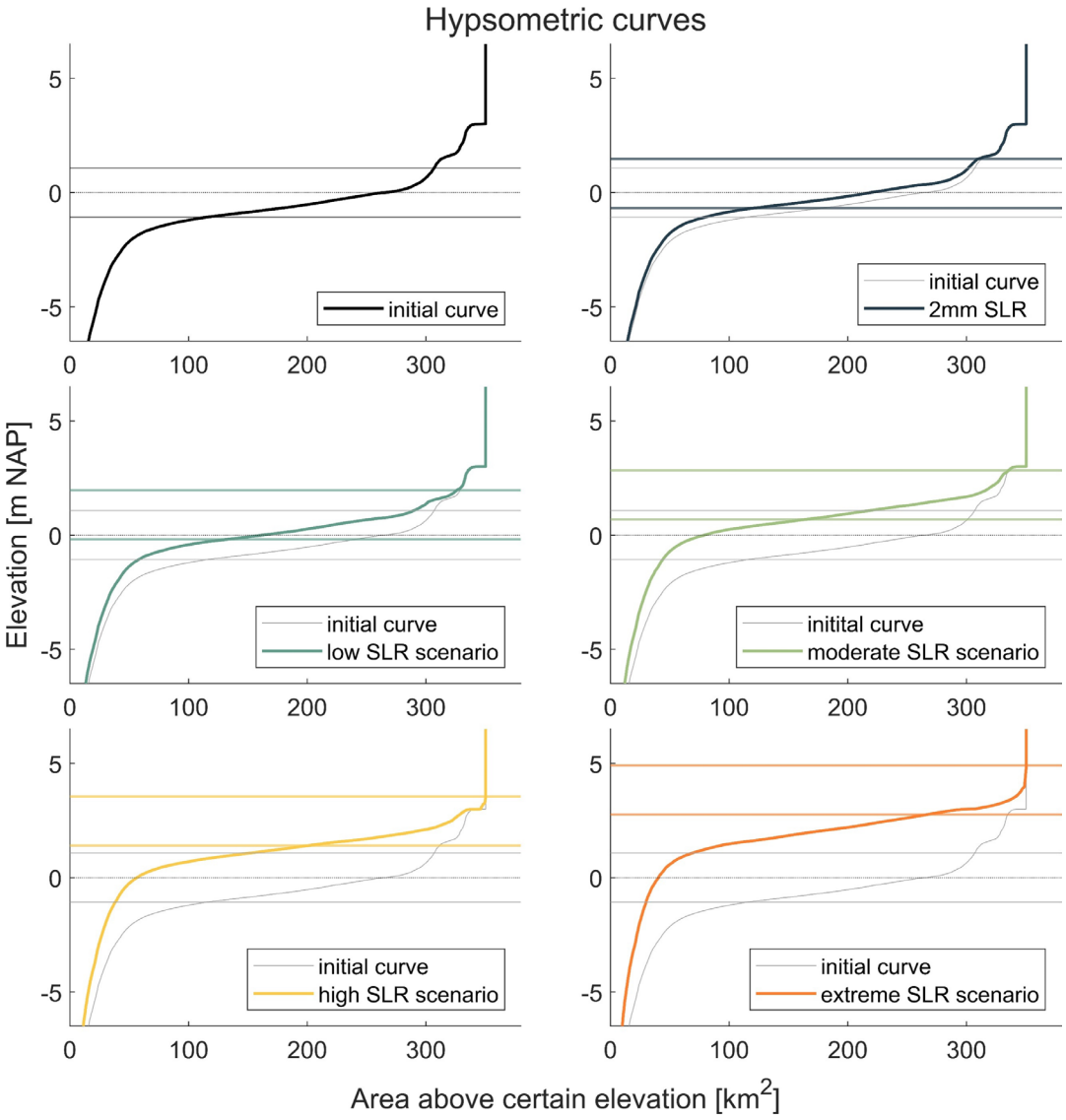

Figure 3.4. Hypsometric curves for the Ameland basin, for different SLR scenarios. In the top left panel we show the initial curve, calculated from the input bathymetry. The two horizontal lines indicate the mean low and highwater levels. In all other panels, we plot the initial hypsometric curve, together with the respective water levels, as gray, thin lines for comparison. The mean low and highwater levels shift upwards with SLR, as indicated by the coloured horizontal lines in each panel. The legends in each panel specify the considered SLR scenario. The colour scheme for the SLR scenarios follows the rest of this report.

3.2.3 Cross-throat sediment transport

In the left panel of Figure 3.5, we show the cumulative cross-throat sediment, measured along a cross-section placed between the barrier islands of Terschelling and Ameland. The plot shows the cumulative sediment transport for the five different SLR scenarios over the simulation period of 200 years, in million cubic meters. In the right panel of Figure 3.5, we show the yearly sediment transport rate, derived directly from the cumulative sediment transport shown in the left panel.

Due to the grid orientation and the cross-section definition, positive sediment transport values indicate a cumulative sediment import into the basin (and negative values would represent a cumulative sediment export). With increasing SLR severity, the sediment transport likewise

increases, from a final value after 200 years of approximately 70 million m^3 (2 mm linear SLR) to approximately 520 million m^3 (extreme SLR scenario), see also Table 3.2.

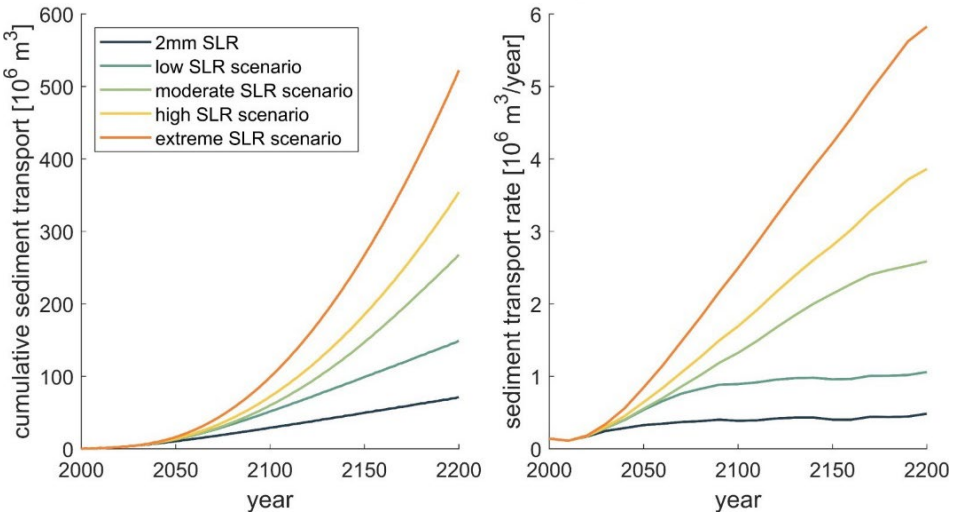

Figure 3.5. Cumulative sediment transport in million cubic metres, and yearly sediment transport rate in million cubic metres per year, through the inlet throat over time for five different SLR scenarios (colours indicated in legend in left panel).

Based on the values shown in Figure 3.5, we calculate the averaged sedimentation height and averaged sedimentation rate in the entire basin at the end of the simulation period after 200 years (refer to Section 2.5.2 for the methodology on the calculation of these values). We compare the averaged sedimentation height with the corresponding increase in water depth (i.e. the final value of SLR for each scenario), and the averaged sedimentation rate with the corresponding SLR rate. These comparisons, i.e. Δh_{wd} and $\dot{h}_{sed}/\dot{d}_{SLR}$, give an indication of overall basin development. For the results as shown in Table 3.2, we observe that the basin is closest to a dynamic equilibrium for the two mildest SLR scenarios, but the water depth increases for both cases by about half of the cumulative SLR. For the higher SLR scenarios, the sedimentation height is much smaller than the projected total SLR, and the basin does not approach a dynamic equilibrium within the simulation period.

The yearly sediment import rate for the two mildest SLR scenarios reaches a quasi-constant value over the simulation period (see right panel in Figure 3.5). The plot therefore indicates that a dynamic equilibrium has been reached. Nevertheless, the ratio of the averaged sedimentation rate with the respective final SLR rate delivers values significantly smaller than 1, namely 0.7 (2 mm SLR per year) and 0.6 (low SLR scenario). The discrepancy between the plot and the calculated values is likely due to the averaging of our methodology to arrive at the sedimentation heights and rates. We account for the total basin area to arrive at the averaged values. As we elaborate on in the next section of this report, sedimentation is expected to be higher in the shallower intertidal flat areas, and significantly lower in the deeper channel zones. This means, that intertidal flat areas can maintain a dynamic equilibrium for the milder scenarios, even though the averaged sedimentation is lower than the imposed SLR rate. This is also supported by the plots in Figure 3.3, showing no significant decline of intertidal characteristics for the milder SLR scenarios.

Table 3.2 Indication of drowning effect in the Ameland basin for different SLR scenarios. The basin area is 350.4 km² (derived from hypsometric curve).

SLR scenario	2 mm linear	low SLR	moderate SLR	high SLR	extreme SLR
$SLR_{cum,final}$ [m]	0.40	0.89	1.76	2.48	3.84
$\dot{d}_{SLR}$ [mm/year]	2	5	13.8	25	40
$t_{sed,final}$ [10^6 m^3]	71.5	146.2	267.9	354.2	522.4
$\dot{t}_{sed,final}$ [10^6 m^3/year]	0.48	1.06	2.59	3.86	5.83
$\overline{h}_{sed}$ [m]	0.20	0.43	0.76	1.01	1.49
$\dot{h}_{sed}$ [mm/year]	1.4	3.0	7.4	11.0	16.6
$\Delta h_{wd} = (SLR_{cum,final} - \overline{h}_{sed})$ [m]	0.2	0.46	1.0	1.47	2.35
$\frac{\dot{h}_{sed}}{\dot{d}_{SLR}}$	0.70	0.60	0.54	0.44	0.42

3.2.4 Cumulative sedimentation/erosion maps

In Figure 3.6, we show six different cumulative sedimentation/erosion maps from three simulations for increasingly severe SLR scenarios. For each scenario, we show the timestep halfway through the simulation (after 100 years) and at the end of the simulation period (after 200 years). The figure provides an overview of how different SLR scenarios can lead to similar results at different timesteps, as they reach certain inundation levels at different times.

We also show one of the six maps of Figure 3.6 in more detail in Figure 3.7, specifically the map of the moderate SLR scenario after 200 years (centre right panel in Figure 3.6). In Figure 3.7, the sedimentation pattern within the basin is visible in more detail. While the intertidal areas show high sedimentation, especially close to the inlet, the channels exhibit much less sedimentation. The intertidal areas closer to the tidal divides and the mainland, i.e. far away from the inlet, show lower sedimentation heights than the intertidal areas closer to the throat given their longer distance with respect to the sediment source (the open boundaries). However, all intertidal areas, and even the channels, are accreting sediment to grow in height. Their growth is however slower than the projected SLR (see Table 3.2).

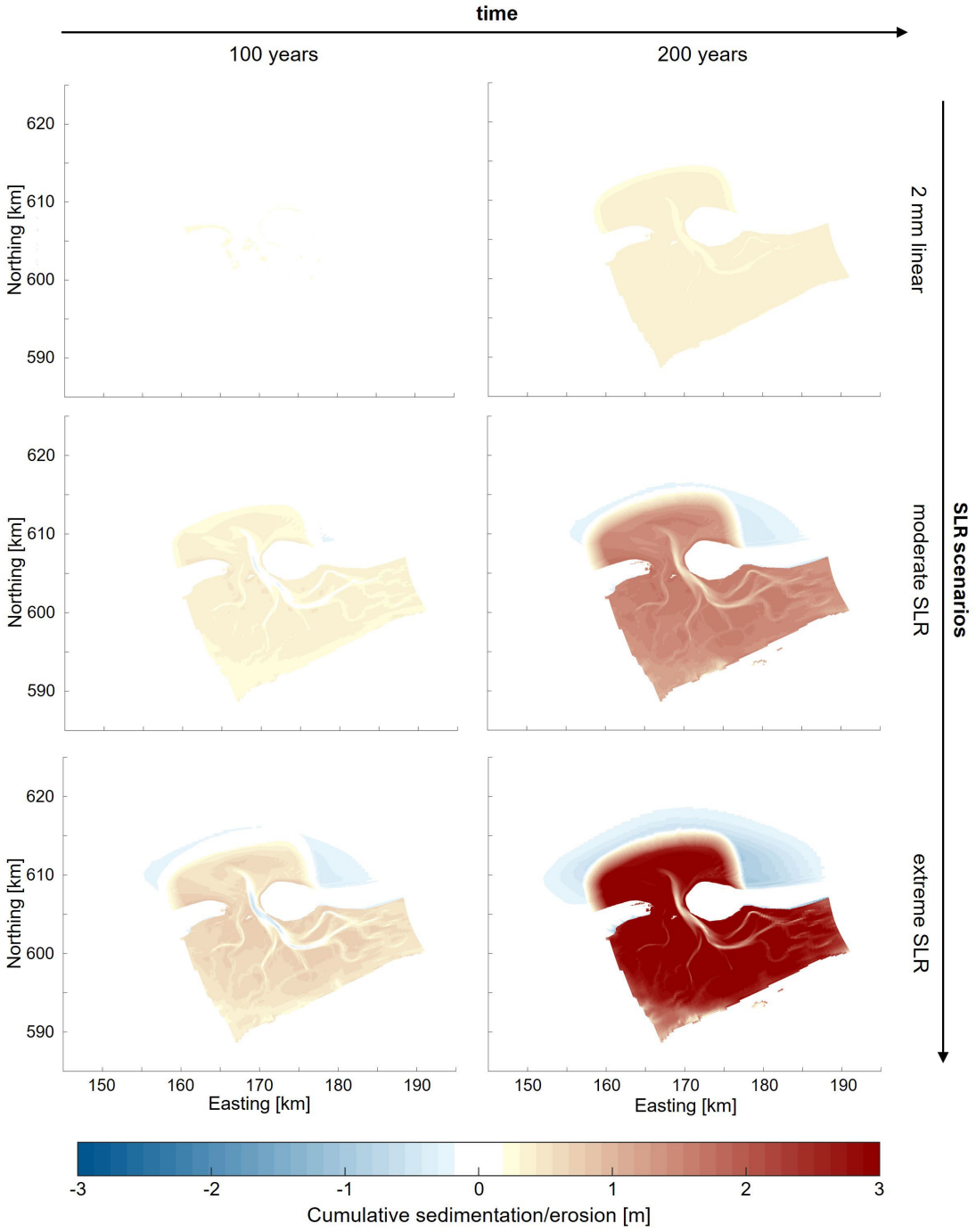

Figure 3.6. Maps of the cumulative sedimentation / erosion patterns (see colourbar at the bottom of the figure, valid for all panels), for different SLR scenarios in the vertical spread, and two different time steps of 100 and 200 years, respectively, in the horizontal spread.

Two factors determine the sedimentation in the basin: sediment demand and sediment supply. The latter is exclusively governed by the prescribed equilibrium sediment concentration at the open boundaries of the model (only sediment source in the model domain). Sediment transport (from the open boundaries, through the model) is achieved by both advection and diffusion. The sediment demand in each grid cell of the domain is determined by the ratio of the equilibrium depth (d_e) over the instantaneous depth (d_{inst}). While the equilibrium depth is space-varying (determined as a model input), the instantaneous depth increases with a constant value of SLR within the ASMITA-governed tidal inlet system area. Therefore, the ratio

of d_e/d_{inst} will be smaller in shallower areas of the basin than in deeper areas[8]. As the model attempts to regain an equilibrium and therefore achieve a ratio of 1, sediment demand will be larger in shallower areas, than in deeper areas.

This direct consequence of the ASMITA equilibrium considerations causes the Delft3D-ASMITA model results to agree with previous studies of process-based models (Becherer et al, 2018; Hofstede et al., 2018). The physical mechanism behind a lower sedimentation rate in the channels than on the intertidal flats is that SLR leads to an increase in tidal prism. Due to the larger prism, higher flow velocities in the channel can eventually even lead to erosion and channel deepening, although this is not observed in this model. We do see however that the sedimentation is higher in the flats, than in the channels (see Figure 3.7).

The cumulative sedimentation / erosion maps reveal some model artefacts. Especially in the corners of the model, the sedimentation cannot be simulated realistically, due to hindered sediment transport mechanisms. Within the model, sediment is transported by advection and diffusion, with advection being dominant throughout. However, in the corners of the model domain where the domain boundaries are closed, furthest away from the inlet throat, advection vanishes, which is partly a model artefact. This leads to a drop in sediment availability in the corners, and hence less sedimentation.

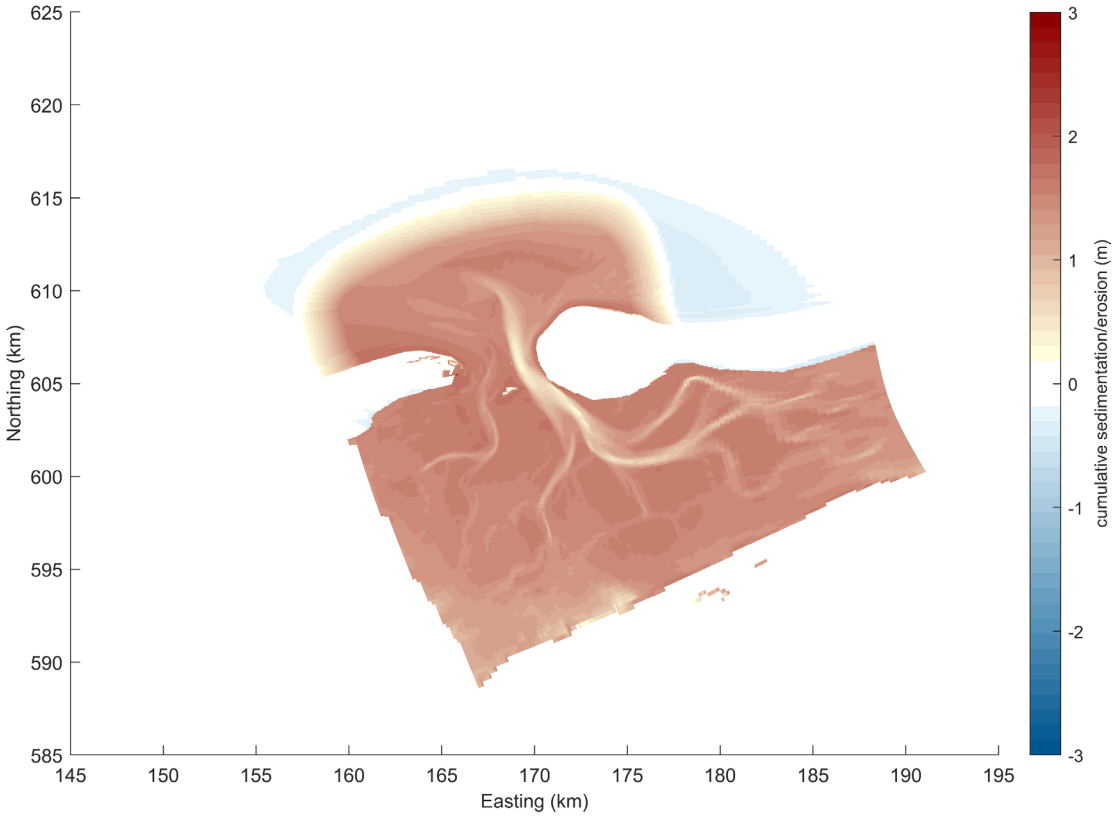

Figure 3.7. Cumulative sedimentation/erosion map for the moderate SLR scenario at the end of the simulation period (2200). The same map is also shown in Fig. 3.6, in the panel in the right column, centre row. We show it here larger again to highlight further details.

[8] with ratios in both areas being smaller than 1.

3.2.5 Water levels for a specific observation station

Figure 3.8 presents the observation station placed in one of the channels of the Ameland basin to analyse the effect of SLR and changing morphodynamics on the tidal range (for more details on the methodology, we refer the reader to Section 2.5.4). Figure 3.9 shows the water levels at the observation station for the five considered SLR scenarios during the last week of the hydrodynamic simulation period. Note that the water level is an output variable which is independent of the MorFac and is therefore better plotted against the hydrodynamic timescale. Nevertheless, we also provide an indication of the morphodynamic timescale on the x-axis of the plot, to put this result into context with the other (morphodynamically relevant) figures. The lower panel of Figure 3.9 shows a zoom-in on the last two tidal cycles of the simulation period. The reason for focussing the water level analysis on the final timesteps of the simulation is that the effect of the accelerated SLR (and associated morphodynamic changes) on the hydrodynamics becomes more evident at the end of the simulation. However, it is a gradual process throughout the simulation period. To highlight the effect, we plot the water levels for the different SLR scenarios against a water level output of a purely hydrodynamic simulation (gray line, mostly covered by the coloured SLR scenario lines plotted on top). For the colour code of this figure, we refer the reader to the legend plotted in the lower left corner of the upper panel.

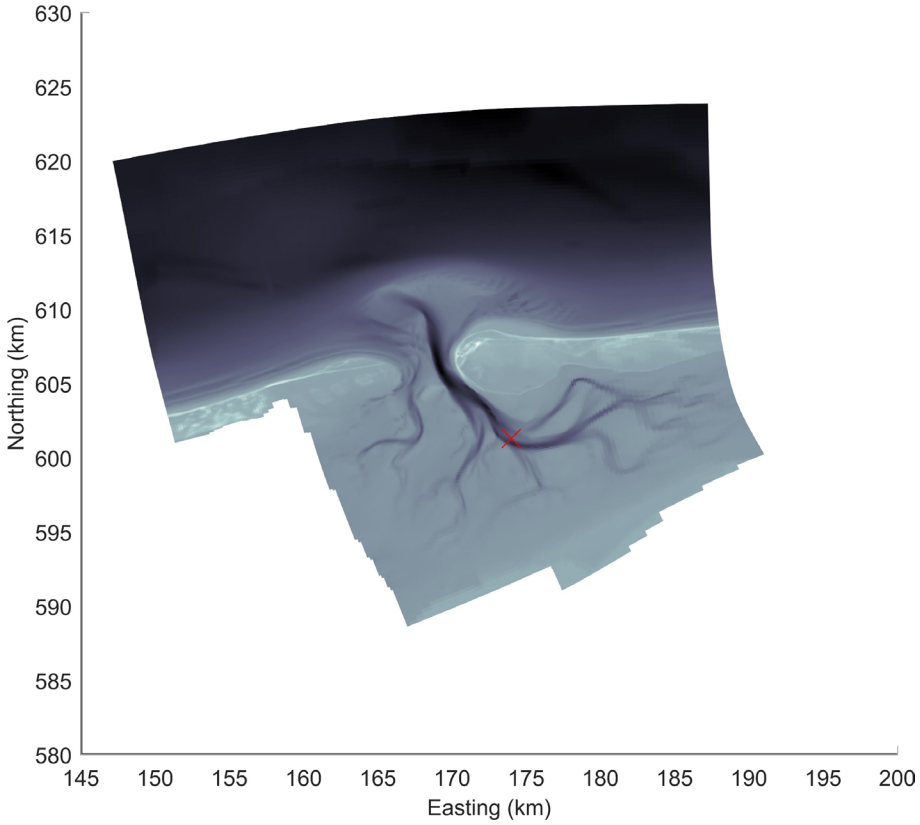

Figure 3.8 The red cross marks the location of the specific observation station. Note that while the station is located close to the centre of the basin, it is also in a channel, which ensures that the grid cell will be flooded throughout the simulation period.

In the water level output, we can see the cyclic nature of the hydrodynamic boundary conditions, which include a semidiurnal and a diurnal tidal signal, but no spring-neap signal. This is a simplification which can lead to unrealistic results, not only for the water level output, but also for the intertidal characteristics (i.e. above sections 3.2.1 and 3.2.2).

Apart from the nature of the boundary conditions, we want to remark on two features of the plots in Figure 3.9. First, the shape of the tidal signal slightly changes with accelerated SLR. During flood, the purely hydrodynamic simulation models the rising of the water levels faster at first and then slower towards the flood peak. For increasing SLR severity, the water level rise becomes more linear (compare the orange graph during flood with the grey and/or dark green graph). Second, accelerated SLR causes a dampening of the tidal signal in the basin, i.e. the tidal range decreases with an increase in SLR severity (compare the differences between the curves' minimum and maximum). While the high-water levels stay relatively stable for all six simulations, the low-water level shifts gradually upwards from the purely hydrodynamic simulation, over the mild, to the extreme SLR scenarios.

The trend of the low-water levels shifting upwards with SLR in the water level signal is surprising. With accelerated SLR, the tidal prism will increase. Tidal amplification depends on two factors: the flow carrying capacity of the channels and the tidal storage of the basin. A more significant increase in flow carrying capacity of the channels would result in an increasing tidal range, whereas a more significant increase in tidal storage would cause a decrease in tidal range. From model results, we observe accretion in the channels, albeit less than in the tidal flats. Sedimentation in the channels, together with the dampening of tidal amplification, resulting in a decreased tidal range, hints at the option that the increase in tidal storage, through supratidal inundation, is relatively more significant than the increase in flow carrying capacity.

The results for the water level development under accelerated SLR strongly indicate that the model parameters need to be evaluated further. A more accurate implementation of the supratidal areas and their gradual inundation is crucial for better predictions of intertidal characteristics, both morphodynamic and hydrodynamic.

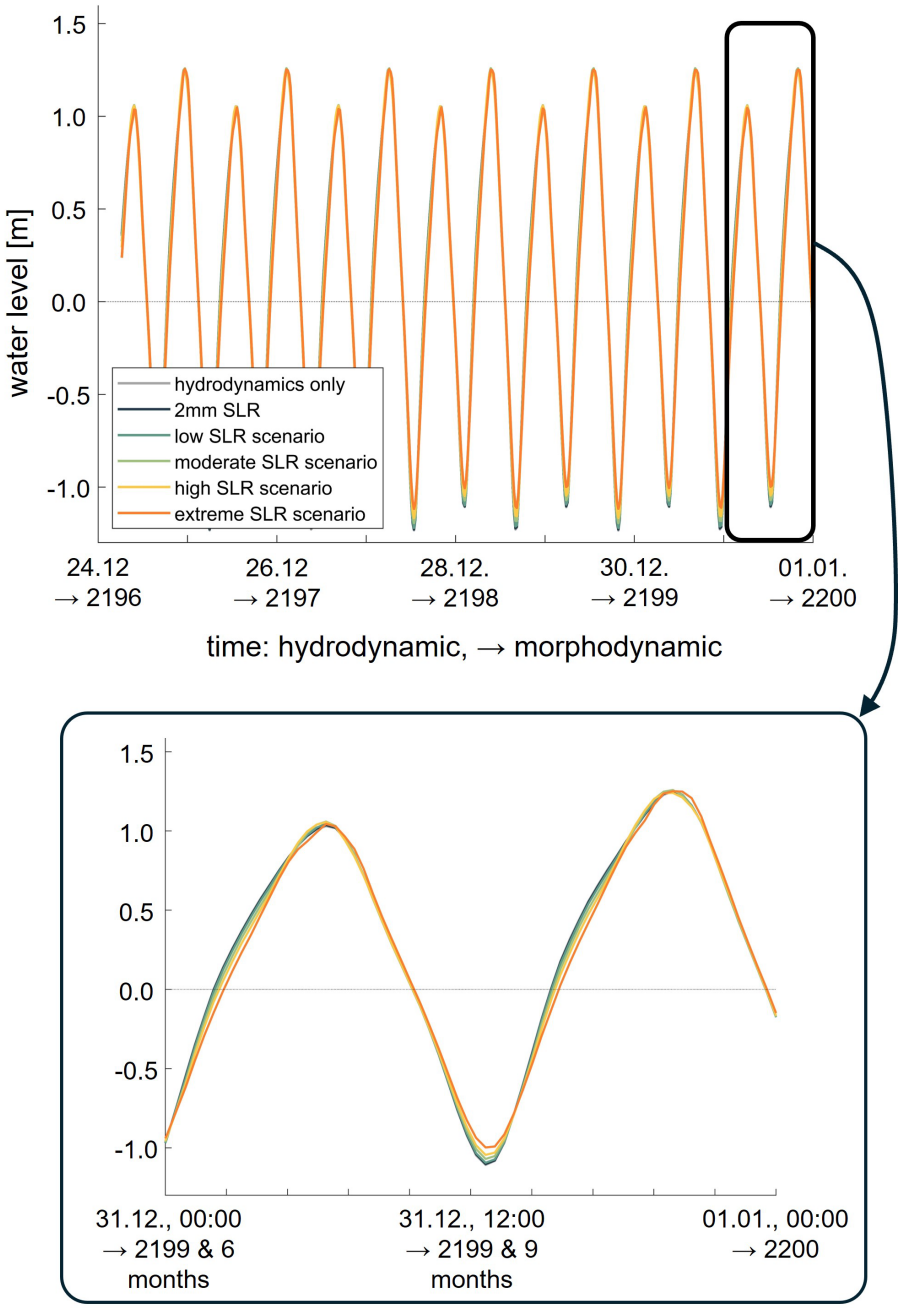

Figure 3.9 Water levels for different SLR scenarios at a water level station in the basin (for the location of the station, see Figure 3.6), plotted for the last week of the hydrodynamic simulation time, i.e. the last four years for the morphodynamic simulation period, where the changes in water level due to the imposed SLR will be most noticeable. As base line, we plot the water levels of a purely hydrodynamic simulation as a grey line, see the legend in the upper panel. The lower panel is a zoom-in on the last two tidal cycles.

4 Application to the Dutch Wadden Sea

Besides SIS modelling, as described in the previous chapter, the Delft3D-ASMITA model can also simulate morphological development in multi-inlet systems, such as the Dutch Wadden Sea. Modelling several tidal inlet systems together allows investigating sediment exchange between neighbouring tidal inlet systems, as well as on a larger scale. Ideally, the Delft3D-ASMITA model of a multi-inlet system simulates sediment transport across tidal divides between basins and longshore sediment transport between ebb-tidal deltas and the coastal zone. However, reproducing realistic sediment exchange between the different morphological features of the Wadden Sea relies on a correct and detailed hydrodynamics implementation. We elaborate more on this issue in Section 4.2.

In Section 4.3, we provide an overview of the general results, followed by Section 4.4, where we present detailed results for the Ameland inlet system, based on the MIS Wadden Sea model. For detailed results on other individual basins, we refer the reader to Appendix B. In Section 4.5 we discuss an overview of changes in intertidal characteristics as projected by the MIS model. Finally, in Section 4.6, we present results focusing on the erosion/sedimentation patterns in the basin *channels*, analysing hypsometric curves.

4.1 Model setup

In this section, we describe only the parts of the model input not previously mentioned in Sections 2.6 and 2.6. We refer the reader to said sections for a wider overview of model input and baseline assumptions.

Table 4.1 presents an overview of the selected parameters for the Delft3D-ASMITA Wadden Sea model. For other parameters not mentioned in the table, which are part of the standard flow module in Delft3D 4, we used the default values.

Table 4.1. Overview of selected model parameters for the Wadden Sea model

Parameter	Value/setting
Hydrodynamic simulation time	362 days
Timestep	1 s
Morphological scale factor (morfac)	200
Morphological simulation time	200 years
Dimensions	2D
Initial concentration constituent (C01)	0.32 kg/m^3
Water density (Rhow)	1023 kg/m^3
Horizontal eddy viscosity	1 m^{2}s^{-1} (uniform)
Horizontal eddy diffusivity	1 m^{2}s^{-1} (uniform)
Manning field	0.022 s/m$^{1/3}$ within the system, and 0.024 s/m$^{1/3}$ offshore
Dpsopt	#DP#
Cstbnd	#yes#
Sediment type	sand
Initial sediment layer thickness	25 m
Sediment transport formula	22 (ASMITA)
Settling velocity (WS0/WSM)	0.0001 m/s
Global equilibrium concentration (CEequi)	0.32 kg/m^3
Power in the ASMITA transport equation (N)	5
Maximum change in bed height (MaxHH)	10

Reference level	1.45 m

4.1.1 Grid and bathymetry

To model the Wadden Sea with the Delft3D-ASMITA model, we used an existing Delft3D model (the WadSea 2009 model by Graaff, 2009). It covers all the tidal inlet systems of the Dutch Wadden Sea (from Texel to Groninger Wad), and it extends up to 58 km in the offshore region with respect to the coastal zone. The longshore distance between the SW offshore boundary and the Texel inlet is 53 km, and the one in between the NE offshore boundary and the Groninger Wad inlet is 14 km. The computational grid is structured and curvilinear, but coarser than the one used for the Ameland standalone model (see Figure 4.1, as well as *Figure 5.1* for a comparison of the grids). The grid cell sizes range from 160 x 270 m to 3100x1500 m. The finer cells are located around the tidal inlets, and the coarser ones near the offshore boundary regions. There are 83538 grid cells in total. The input bathymetry is a combination of Vaklodingen and LIDAR surveys from the years 2002 to 2008 (see Figure 4.2). Particularly, the area covering the Ameland tidal inlet system is composed of bathymetries from 2007 and 2008.

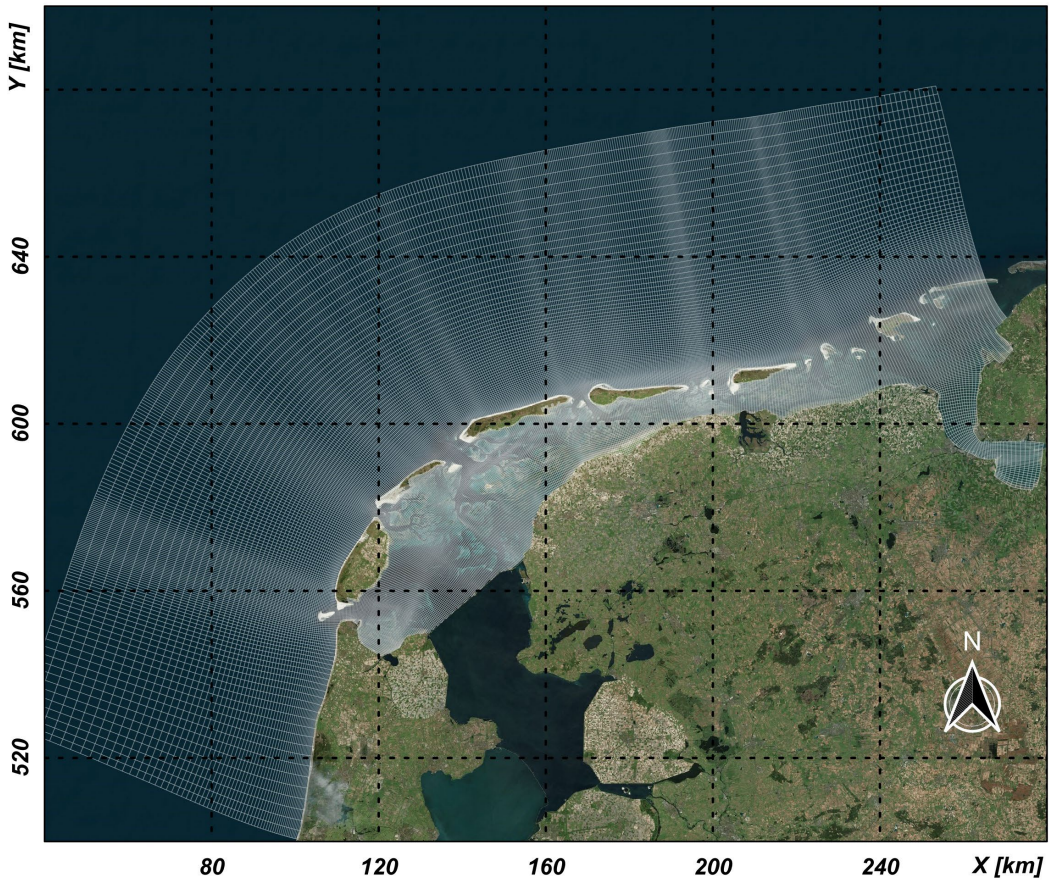

Figure 4.1. Computational grid of the Wadden Sea model.

4.1.2 Forcing conditions

The model is forced by water level boundary conditions (denomination “Z” in the auxiliary .bnd file). There are 8 sections along the southern boundary, 15 along the deepwater boundary, and 11 along the eastern boundary. We prescribed astronomical boundary conditions with a total of 72 tidal components (denomination “A” in the auxiliary .bnd file). Note that, in contrast to the

Ameland standalone model described in Chapter 3, these forcing conditions deliver a more realistic spring-neap tidal cycle.

We implement SLR as subsidence (see Section 2.3.1), hence the mean water levels in the model domain and at the boundaries do not change over the course of the simulation.

4.1.3 Water level station locations

Figure 4.3 presents the observation stations that were placed in the channels of each of the tidal inlet systems of the Dutch Wadden Sea, to analyse the effect of SLR and changing morphodynamics on the tidal range (for the methodology refer to Section 2.5.4).

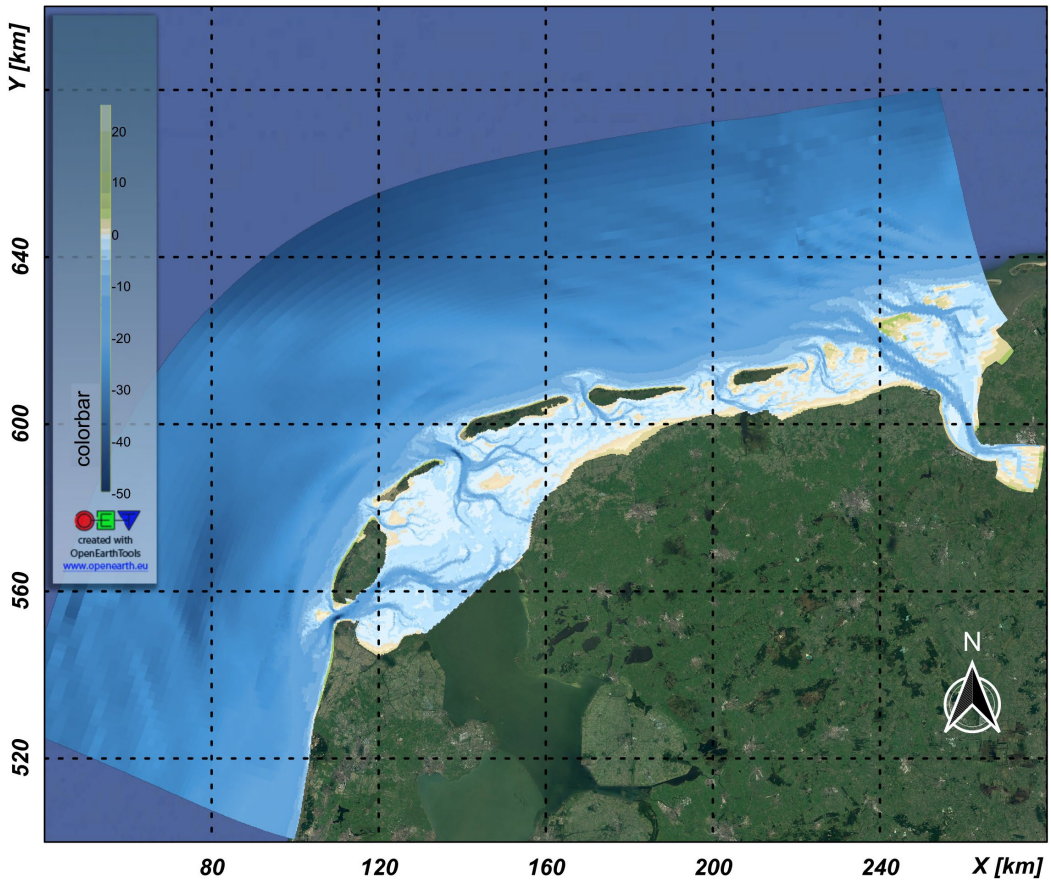

Figure 4.2. Bathymetry used for the Wadden Sea model. Notice that it is already interpolated in the model grid.

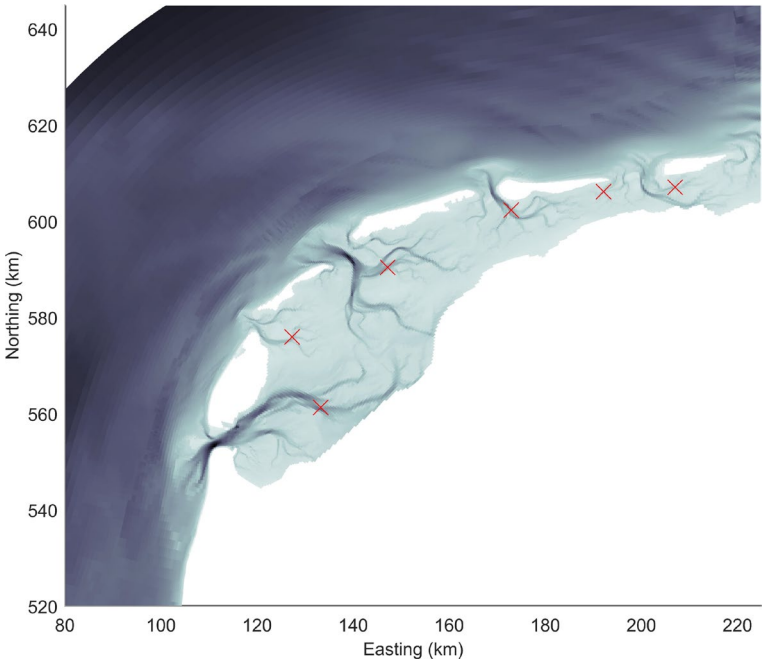

Figure 4.3 Location of specific observation stations in each basin, used for plotting water levels over time (for methodology refer to Section 2.5.4).

4.2 Testing the Delft3D-ASMITA MIS model with tidal divides

We first test the Delft3D-ASMITA MIS model on a previously used Wadden Sea Delft3D model with its original configuration (with the Delft3D-ASMITA formulations chosen as sediment transport formula). We choose the 2 mm SLR scenario, which represents the current trend, but extended for a prolonged period of 200 years. The final results in terms of cumulative sediment transport through the tidal inlet throats, and the cumulative sedimentation/erosion map are presented in Table 4.2 and Figure 4.4, respectively. In the cumulative sedimentation/erosion map, we see mostly sedimentation in the shallower part of the basins (e.g., intertidal flats), which is the expected response to SLR.

*Table 4.2. Cumulative cross-throat sediment transport in million cubic metres for each tidal inlet system, for the regular Delft3D-ASMITA model configuration with open tidal divides and tidal hydrodynamic forcing only. The values come from a simulation with the 2 mm SLR scenario. Highlighted in red are the values indicating sediment **export** from the basin.*

Inlet throat	Marsdiep / Texel	Eierland	Vlie	Borndiep / Ameland	Pinkegat	Zoutkampe r-laag
regular Delft3D configuration	- 801.3	2.3	852.1	164.5	- 55.5	105.8

Regarding the cumulative cross-throat sediment transport the model predicts a large import into the Vlie basin (more than 850 million m^3), but a similarly sized export to the North Sea from the Texel basin. Note that the intertidal flats in the basin undergo sedimentation, as visible in the cumulative sedimentation/erosion map, even though the cumulative cross-throat sediment transport is exporting sediment from the basin towards the North Sea. Intertidal sedimentation however requires an overall sediment surplus in the basin, which means there is likely sediment being imported from the Vlie basin into the Texel basin across the tidal divide.

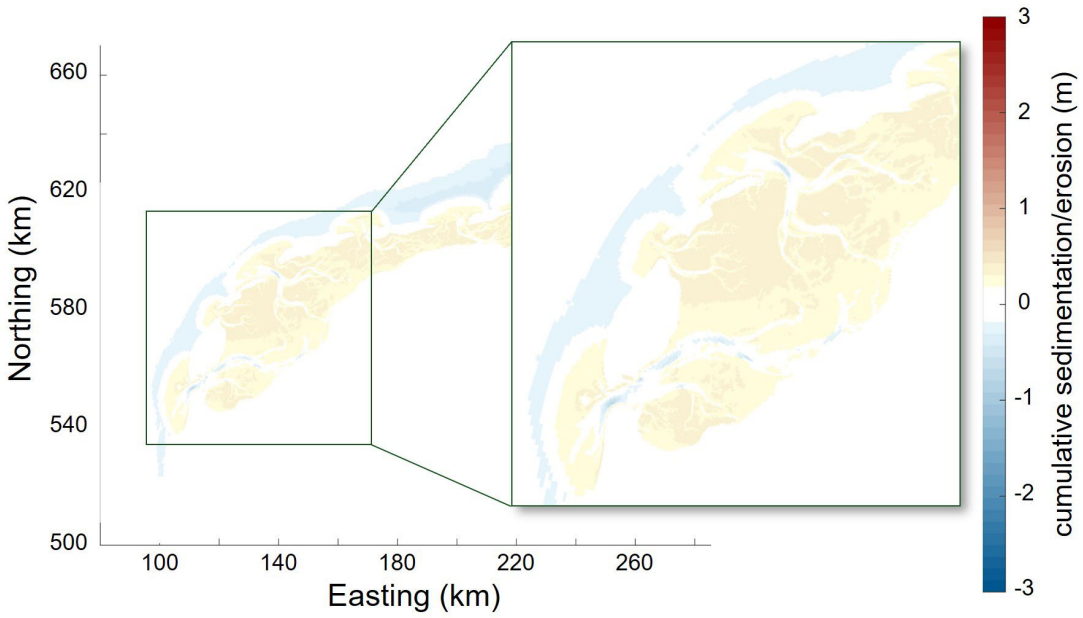

Figure 4.4. Cumulative sedimentation / erosion map of the Wadden Sea, and a zoom-in on the Western Wadden Sea specifically, at the end of a 200-year simulation of 2 mm SLR per year. The map shows results from the same simulation as presented in Table 4.2. Note that the colourbar of this figure was kept consistent with the rest of the sedimentation / erosion map figures in this report.

Sediment exchange between the Vlie and Texel basins is the result of a residual flow developing across the tidal divide. Such a circular flow pattern, with import through the Vlie inlet and export through the Texel inlet, has been reported before for the long-term average tidal flow (Duran-Matute et al., 2014). This holds true if the tidal flow is the only considered hydrodynamic forcing. However, reality is more complex and other physical processes, such as waves and wind, also influence the hydrodynamics. The combined effect of all hydrodynamic forcings can in reality lead to a reversal of residual flow direction for the Texel inlet, and to a residual sediment import into the basin through the Texel throat (Elias, 2006). Studies on the sediment budget in the Wadden Sea have shown that import through the inlets (including Texel) is the major contributor to sedimentation in the basins in response to SLR and adaptation to human interventions in the past (Elias et al., 2012).

In an attempt to reproduce more realistic hydrodynamics and potentially achieve sediment import through the Texel inlet throat, we applied a spatially uniform wind field of 7 m/s coming from the southwest. We present the cumulative cross-throat sediment transport in Table 4.3. Compared to the results of the original case without the uniform wind field (Table 4.2), the sediment export through the Texel inlet throat is smaller. However, for a realistic representation of cross-throat sediment transports, we aim for sediment *import* through all six inlet system throats. Moreover, after applying the uniform wind field, the model predicts sediment export also for the Ameland basin, which is importing sediment in the original model configuration.

Therefore, adding a spatially uniform wind field is not enough to reproduce realistic hydrodynamics. Note that the expected wind set-up and set-down in water levels cannot be properly modelled without altering the offshore boundary conditions. These alterations however would need additional calibration and sensitivity analyses to achieve a faithful reproduction of the average long-term hydrodynamics in the model, especially of the residual flow.

*Table 4.3. Cumulative cross-throat sediment transport in million cubic metres for each tidal inlet system, for a Delft3D-ASMITA model configuration with open tidal divides, tidal hydrodynamic forcing and a spatially uniform wind field of 7 m/s from the southwest. The values come from a simulation with the 2 mm SLR scenario. Highlighted in red are the values indicating sediment **export** from the basin.*

Inlet throat	Marsdiep / Texel	Eierland	Vlie	Borndiep / Ameland	Pinkegat	Zoutkampe r-laag
uniform wind field	- 214.6	113.3	598.5	- 105.7	- 120.5	140.7

With the hydrodynamics (in particular the residual flow) still requiring further calibration, the best way to achieve feasible results with the current Delft3D-ASMITA model is to eliminate the residual flow and associated sediment exchange between neighbouring tidal basins. To achieve hydrodynamically separated tidal inlet basins, we place thin dams as close as possible to the locations of the tidal divides in the Wadden Sea model. We then run the 200-year 2 mm SLR scenario test case without the uniform wind field. The associated cumulative cross-throat sediment transport at the end of the 200-year period is presented in Table 4.4. All transports through the individual throats are importing sediment into the basins. Additionally, the model predicts much lower individual values of cross-throat sediment transport per inlet system, once the thin dams stop sediment exchange across the tidal divides. Note that the overall import of sediment into the Wadden Sea area (all basins combined) is of the same order of magnitude in all three presented test cases because the large sediment export through the Marsdiep throat is reversed, and the import at the Vlie inlet decreased.

Table 4.4. Cumulative cross-throat sediment transport in million cubic metres for each tidal inlet system, for a Delft3D-ASMITA model configuration with closed tidal divides and tidal hydrodynamic forcing only. The values come from a simulation with the 2 mm SLR scenario.

Inlet throat	Marsdiep / Texel	Eierland	Vlie	Borndiep / Ameland	Pinkegat	Zoutkamper-laag
thin dam configuration	65.7	25.4	110.4	50.0	14.4	23.5

Eliminating residual flow (and hence, sediment exchange) across the tidal divides is of course not realistic. Moreover, the interacting tidal inlet systems within *one* model are a strong advantage of the Delft3D-ASMITA approach (compared to a regular ASMITA approach). However, the various hydrodynamic forcings needed for a realistic schematization have not yet been implemented / validated for the Delft3D-ASMITA model, which so far has been validated for tidal flow only (and, to a limited degree, uniform wind influence). To realistically model sediment transport in the multi-inlet Wadden Sea system, the Delft3D-ASMITA model needs to reproduce more of the relevant hydrodynamic processes, leading in turn to sediment import through the throats as main sedimentation driver in the basins (including Texel). In the meantime, the model configuration with closed tidal divides delivers sediment transport results closest to reality, since the sediment import through the throats is the main sediment source for sedimentation in the basins. Therefore, we use this model configuration with thin dams for the final simulations of the different SLR scenarios in the Wadden Sea model.

4.3 General model results and trends

Following the results presented in Section 4.2, all results we present in this section are from simulations carried out with thin dams placed on the tidal divides between the individual basins, and without wind or wave dynamics. This model configuration, without further calibration, best reproduces the patterns observed in reality, where sediment import through the inlet throats is responsible for the sedimentation observed in all the basins. In this section we explain our general model results, applicable for either the (Dutch) Wadden Sea area as a whole or to all individual basins alike. For detailed results of individual basins, we refer the reader to Appendix B.

In general, all the basins show similar trends, summarized below:

- **Extreme SLR Scenarios**: For the three most extreme SLR scenarios, we observe a strong decline in intertidal area and volume directly linked to SLR severity. Nevertheless, the intertidal flats never completely drown, even for the most extreme SLR scenario. For the milder SLR scenarios, there is either a mild decrease of intertidal area and volume, or they maintain quasi-constant values, indicating the basin is approaching dynamic morphological equilibrium.
- **Intertidal Height**: A decrease in mean intertidal height indicates that the loss of intertidal volume occurs at a higher rate than the loss of intertidal area. This is the most commonly observed response to SLR in the basins of the Wadden Sea.
- **Sediment Transport Rate**: The sediment transport rate increases with SLR severity, following the increasing demand due to the creation of accommodation space in the basin with SLR. Especially for the two mildest SLR scenarios, the sediment transport rate plateaus towards the end of the simulation period. Such behaviour indicates sedimentation balancing SLR, meaning the basin is reaching dynamic morphological equilibrium. For some of the basins and the most extreme SLR scenario, the sediment transport rate first increases rapidly before its growth starts to slow down. Eventually, the sediment transport rate becomes quasi-constant for the extreme SLR scenario. Given the extreme projected SLR of several metres at that point, sedimentation cannot balance SLR. Therefore, a plateauing sediment transport rate indicates that the critical SLR rate has been surpassed and the transport capacity through the throat has been reached. Under these circumstances, the drowning of the basin is inevitable, as the limited sediment supply renders a balance between sedimentation and SLR impossible. We assume that our simulations did not span the period during which complete drowning is projected to occur.
- **Sedimentation Patterns**: Under the influence of SLR, shallower areas experience higher sedimentation than deeper areas. This is in line with the model concept, given that the ratio between equilibrium and instantaneous depth deviates further from 1 in shallower areas than in deeper areas. This leads to higher sedimentation in intertidal flats than channels in the basin. Furthermore, intertidal flats closer to the inlet throat experience higher sedimentation than flats further away from the throat. We assume that the proximity to the sediment source is the defining parameter for this behaviour, with the only sediment source being the open offshore model boundaries.
- **Channel Erosion**: Some basins show channel erosion, which increases with SLR severity. This happens especially in the largest basins: Texel, Vlie and Ameland. As the basins struggle to adjust to SLR, and sediment input (through the inlet) and distribution over the whole basin lag behind, eroding channels provide sediment to the intertidal flats.
- **Tidal Range**: We observe an increase in tidal range that follows SLR severity. In general, the high-water levels rise, and the low-water levels fall. However, the low-water levels change less than the high-water levels. The increase in tidal amplification is due to the relatively higher gain in channel conveyance (through channel erosion)

than basin storage (supratidal area becoming intertidal). The gain in basin storage could be underpredicted in our simulations, as the grid is too coarse to properly capture the supratidal areas. Note for example, the difference in hypsometric curves for the Ameland basin between the SIS model (Chapter 3, see Figure 3.4) and the MIS model (Figure 4.6). The initial hypsometry for the MIS model does not show the same step-like features at higher elevations as the more detailed SIS model.

4.4 MIS modelling results for the Ameland inlet system

In this section, we describe in detail the results of the MIS Wadden Sea model, focussing on the Ameland basin. This allows for a direct comparison between the MIS and the SIS approach as described in Chapter 3. Note that the general interpretation of the results is very similar to Chapter 3 and holds for the other individual basins of the MIS Wadden Sea model as well. The results of the other individual inlet systems can be found in Appendix B.

4.4.1 Intertidal characteristics and hypsometric curves

The panels of Figure 4.5 present, from left to right, the intertidal area, volume and mean flat height for the five different SLR scenarios over the simulation period of 200 years. For the three most extreme SLR scenarios, we observe an acceleration in intertidal flat deterioration, which is linked directly to the SLR rate, from approximately 2080 onwards. In the case of the extreme SLR scenario, the intertidal flats are close to drowning at the end of the 200-year period (the intertidal area and volume are very close to zero). Given the shape of the hypsometric curves (see Figure 4.6), presented for the five SLR scenarios at the beginning and end of the simulation), the decrease in intertidal area is mostly due to the upward shift of the MLW. The gain of intertidal area due to inundation of supratidal areas, a crucial feature of the SIS model output, leading to significant upticks in intertidal characteristics during the simulation period, is minimal for the MIS model. Note the difference in initial hypsometric curves (Figures 3.4 and 4.6), where the SIS model exhibits distinct step features in the higher elevations, and the MIS model's hypsometric curve is much smoother.

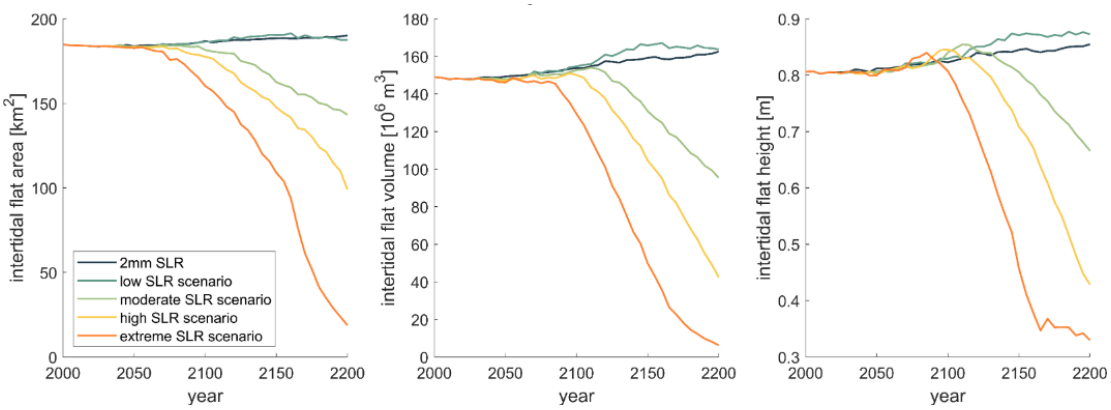

Figure 4.5. Intertidal area, volume, and mean flat height over time for five different SLR scenarios for the Ameland basin, derived from the MIS Wadden Sea model output.

For the milder SLR scenarios, all intertidal characteristics maintain the initial value or grow throughout the simulation period. The overall increase in intertidal area is due to the conversion of supratidal to intertidal zone, although this is much less pronounced in the curves compared to the SIS model results. As mentioned in Section 4.3, we explain this difference with the lower resolution of the input bathymetry of the MIS model.

One remarkable feature of all three panels in Figure 4.5 is that none of the characteristics change significantly during the first 50 to 80 years of the simulation period, independent of the

SLR scenario. The relative stability indicates that the basin is indeed in a morphological equilibrium at the beginning of the simulation, and therefore also able to adapt reasonably well to the two milder SLR scenarios over the whole simulation period. Only for the more extreme SLR scenarios, the basin is eventually pushed beyond its limits of balancing sedimentation and SLR.

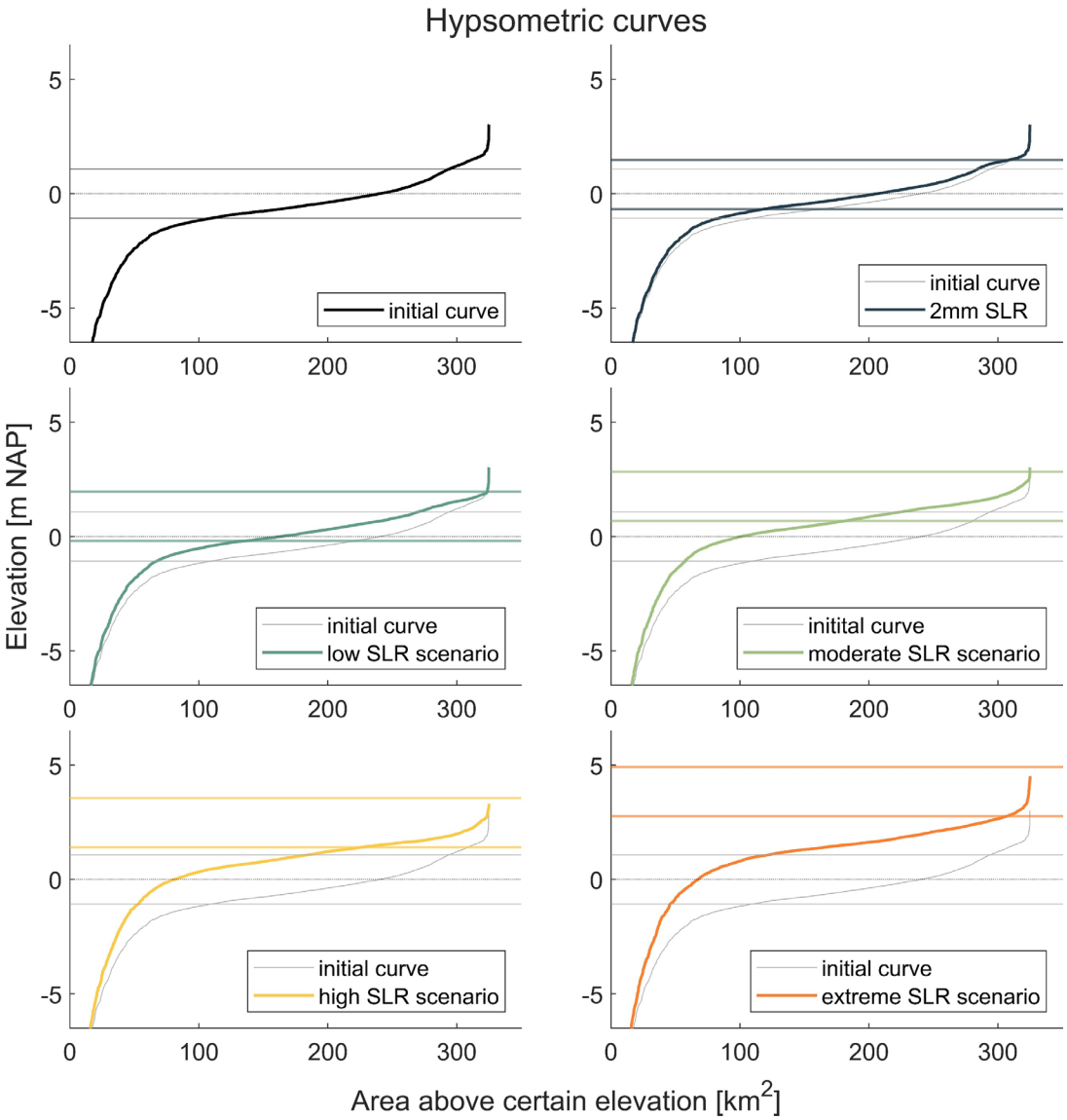

Figure 4.6. Hypsometric curves for the Ameland basin, for different SLR scenarios, derived from the MIS Wadden Sea model output. In the top left panel we show the initial curve, calculated from the input bathymetry. The two horizontal lines indicate the MLW and MHW levels. In all other panels, we plot the initial hypsometric curve, together with the respective water levels, as grey, thin lines for comparison. The MLW and MHW levels shift upwards with SLR, as indicated by the coloured horizontal lines in each panel. The legends in each panel specify the considered SLR scenario. The colour scheme for the SLR scenarios follows the rest of this report.

4.4.2 Cross-throat sediment transport

Figure 4.7 shows the cumulative cross-throat sediment transport and sediment transport rate for the five SLR scenarios over the 200-year simulation period. The basin is importing sediment for all SLR scenarios, and the cumulative transport (left panel in Figure 4.7) increases with the

severity of SLR, as accommodation space is created faster for higher SLR rates. This is also directly reflected in the increasing sediment transport rates (right panel of Figure 4.7), indicating that the basin is attempting to establish a dynamic equilibrium by balancing its accretion rate with the SLR rate. We observe an interesting trend in the sediment transport rate for the more extreme SLR scenarios, where the slope of the graphs starts to decrease from 2150 onwards, most noticeably for the most extreme SLR scenario (orange graph). One reason for the sediment transport rate increase to slow down could be that the sediment transport capacity has been exhausted. Regardless of the severity of SLR, there is a limit to how much sediment can enter the basin through the inlet throat. In previous studies (e.g. Wang et al., 2018), a limit in the sediment transport capacity has also been reported for the western inlets of the Wadden Sea (Marsdiep / Texel, Eierlandse Gat, and Vlie). For the milder SLR scenarios, the sediment transport rate shows a different behaviour. We do not observe a strong increase followed by a slowdown, but rather a less monotonous behaviour of the sediment transport rate. At the end of the simulation period, the rate still appears to trend upwards, instead of reaching a plateau.

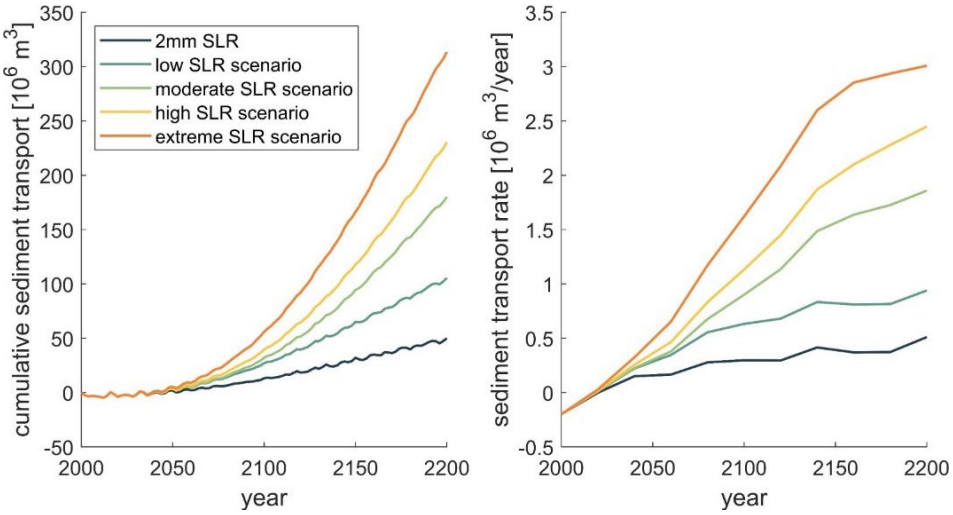

Figure 4.7. Cumulative cross-throat sediment transport and yearly sediment transport rate over time for five different SLR scenarios for the Ameland basin, derived from the MIS Wadden Sea model output.

These MIS results show similar overarching trends as the SIS results (e.g. sediment import for all SLR scenarios, and a clear dependency of the sediment import rate on the SLR severity). However, in the details the results deviate from each other. The SIS model does not predict the plateauing of the sediment transport rate for the extreme SLR scenarios, indicating that the sediment transport capacity might not be exhausted in the SIS. Furthermore, the sediment transport rate for the milder SLR scenarios shows a more stable, quasi-constant behaviour towards the end of the simulation period in the SIS model.

Following the methodology described in Section 2.5.2 to arrive at the averaged sedimentation height and rate, we present the values in Table 4.5. Our simulation results show that Δh_{wd}, the difference between final cumulative SLR and averaged cumulative sedimentation height, is quite dramatic for the Ameland basin, with values ranging from 25 cm in the 2 mm SLR/year scenario (with a cumulative SLR of 40 cm) to almost 3 m in the most extreme scenario (with a cumulative SLR of 3.84 m). Additionally, the ratio between the averaged sedimentation rate and the imposed SLR rate, $\dot{h}_{sed}/\dot{d}_{SLR}$, delivers values as low as 0.23 for the most extreme scenario, indicating that the basin is far from reaching a dynamic morphological equilibrium. Even for the mildest SLR scenario of 2 mm constant SLR per year, $\dot{h}_{sed}/\dot{d}_{SLR}$ is about 0.8. However, the intertidal characteristics curves showed that area, volume, and mean flat height all maintain initial values or even increase over the simulation period for this SLR scenario.

These MIS results correspond very well to the SIS results (see Table 3.2), where we observe a similar discrepancy between intertidal characteristics and sedimentation height over SLR comparison.

Table 4.5. Indication of drowning effect in the Ameland basin for different SLR scenarios. The basin area is 324.8 km^2 (derived from hypsometric curve).

SLR scenario	2 mm linear	low SLR	moderate SLR	high SLR	extreme SLR
$SLR_{cum,final}$ [m]	0.40	0.89	1.76	2.48	3.84
$\dot{d}_{SLR}$ [mm/year]	2	5	13.8	25	40
$t_{sed,final}$ [10^6 m^3]	50.0	105.4	180.1	230.4	313.5
$\dot{t}_{sed,final}$ [10^6 m^3/year]	0.51	0.94	1.86	2.45	3.01
$\overline{h}_{sed}$ [m]	0.15	0.32	0.55	0.71	0.97
$\dot{h}_{sed}$ [mm/year]	1.57	2.89	5.73	7.54	9.27
$\Delta h_{wd} = (SLR_{cum,final} - \overline{h}_{sed})$ [m]	0.25	0.57	1.21	1.77	2.87
$\frac{\dot{h}_{sed}}{\dot{d}_{SLR}}$	0.79	0.58	0.42	0.30	0.23

4.4.3 Cumulative sedimentation/erosion maps

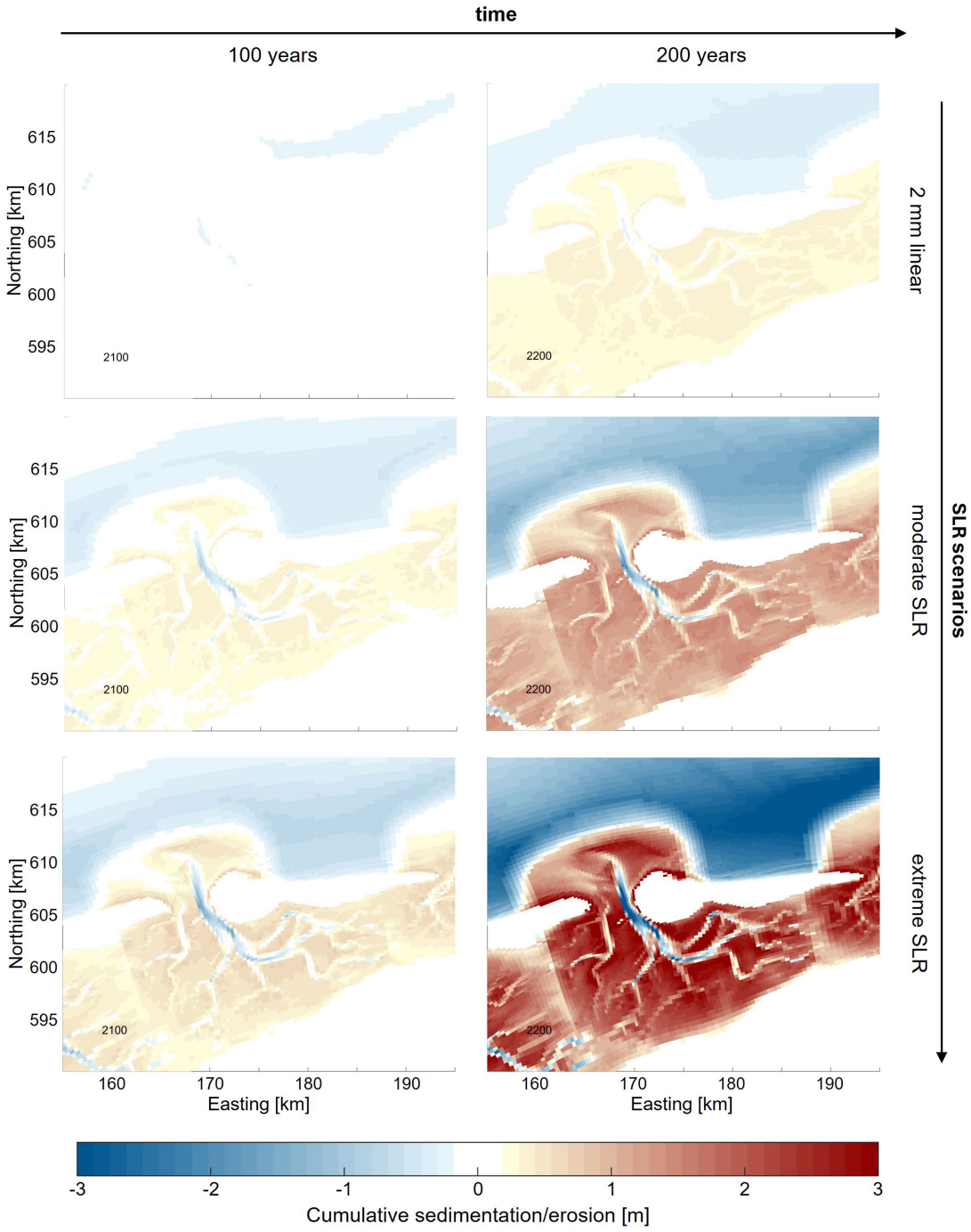

Figure 4.8. Cumulative sedimentation / erosion patterns in the Ameland basin for two timesteps (after 100 years, left column, and 200 years, right column), as well as for three different SLR scenarios (respective rows). These maps are zoom-ins of the MIS Wadden Sea model results. The years of the simulation period are printed as small, black numbers in the lower left corners of the maps. The colourbar shown at the bottom is valid for all panels. Note that the thin dams on the tidal divides between the basins cause disruptions in the pattern.

Figure 4.8 shows cumulative sedimentation/erosion maps after half of the 200-year simulation period and at the end, for three SLR scenarios (2 mm/year, moderate, and extreme). Overall, we observe high sedimentation in the intertidal flats. Close to the inlet, there is more sedimentation in the intertidal flats than farther from the inlet, due to the proximity to the sediment source (see darker yellow and red colours in the figure). Shallower areas demand more sediment given that the ratio d_{eq}/d_{inst} deviates relatively farther from 1 than in deeper areas. The model does predict erosion in the channels, which increases with the imposed SLR severity. The maps in Figure 4.8 highlight the spatially varying sedimentation in the basin, further strengthening the need for a more detailed comparison of sedimentation height and SLR in the future, instead of using the average sedimentation height.

The cumulative sedimentation/erosion maps, as shown in more detail also in Figure 4.9, show clear differences between the SIS and MIS modelling. The main channel Borndiep in the inlet throat is accreting in the SIS model (see Figure 3.7), while it experiences moderate erosion in the MIS model. While the difference in between SIS and MIS modelling is worth exploring further, we also emphasize that this result is consistent with the other MIS results presented above. The sediment transport rate for the moderate SLR scenario shows signs of trending towards a plateau in Figure 4.7, hinting at the sediment transport limitation through the throat. To satisfy the (higher) sediment demand in the shallow intertidal flats, the deeper channels will start to erode.

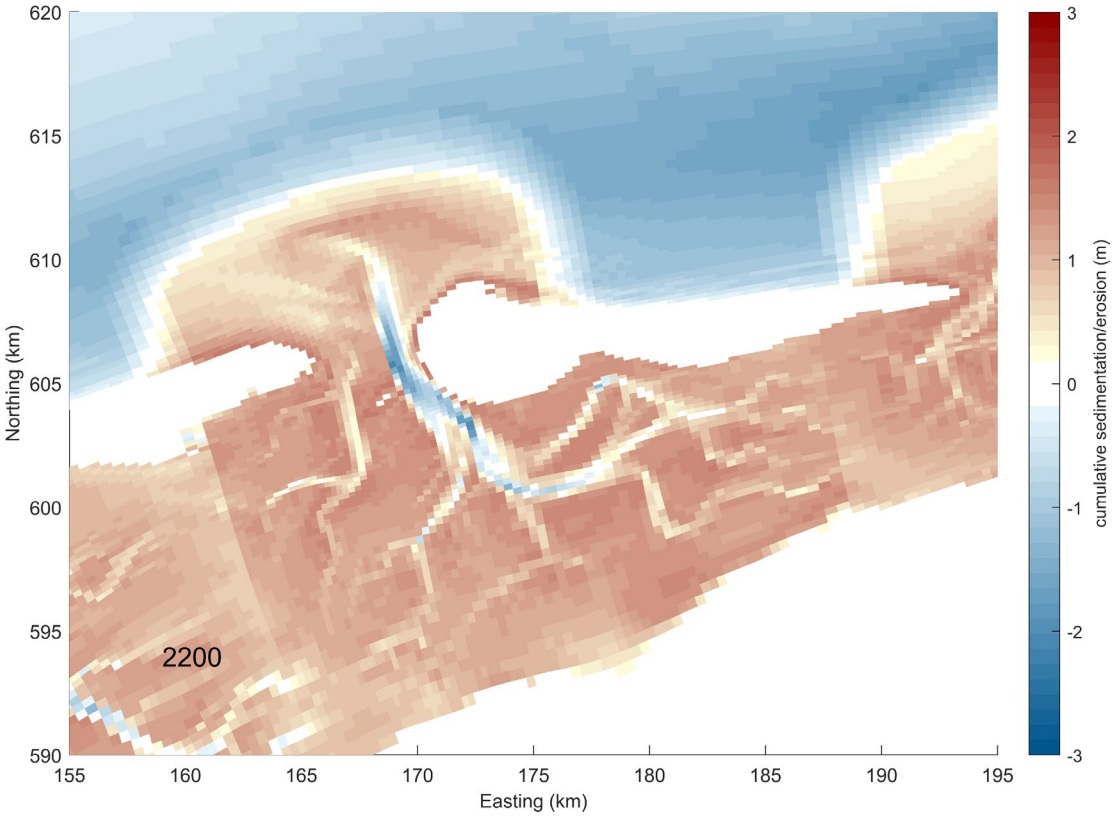

Figure 4.9. Cumulative sedimentation/erosion map for a moderate SLR scenario at the end of the simulation period (2200, as indicated by the small number in the lower left corner of the plot). This map of the Ameland basin is a zoom-in of the MIS Wadden Sea model results. Note that the thin dams on the tidal divides cause disruptions in the pattern between the individual basins. The same figure is also presented in Figure 4.8, in the centre right panel.

One reason for the difference in cumulative sedimentation/erosion patterns between the SIS and the MIS model results can be the sediment supply limitation (*not* the transport limitation

through the inlet throat, but the overall supply limitation in the model domain). The only sediment sources are the open offshore boundaries, which are located closer to the Ameland inlet system in the SIS model, and much farther away in the MIS model. More crucial than the distance is the existence of other inlet systems in the MIS model domain, which also demand sediment to keep up with the SLR. We set the same global equilibrium sediment concentrations in the two models at the open boundaries and can therefore assume that, on balance, a similar amount of sediment is entering the two systems (relative to the offshore boundary length). With the tidal flow imposing a general southwest-northeast residual longshore flow, the sediment is transported along the Wadden Sea barrier islands and passes three inlet systems before it reaches the Ameland inlet system. Assuming that the other inlet systems "syphon off" sediment from the residual longshore flow, the sediment supply limitation in the MIS model can lead to less overall sedimentation in the Ameland basin than in the SIS model.

4.4.4 Water level analysis

Figure 4.10 shows the effect of SLR and morphodynamic changes on the water levels in the Ameland basin. We extract the data from an observation station placed in the channel close to the basin centre (location shown in Figure 4.3). We plot water levels for the five considered SLR scenarios and for the last week of the hydrodynamic simulation period (the associated morphodynamic period is also indicated on the horizontal axis, below the hydrodynamic period). A zoom-in to the last two tidal cycles is shown in the lower panel.

The overall shape of the plots in the upper panel of Figure 4.10 shows the variance in hydrodynamic forcing due to the astonomic boundary conditions implemented in the MIS model. We can see the semidiurnal and diurnal tidal components, as well as the schematization of the spring-neap tidal cycle.

The influence of SLR and its corresponding morphological changes are most noticeable in the lower panel of Figure 4.10. First, the tidal range increases with SLR severity. The high-water levels rise and the low-water levels fall (though much less significantly than the high-water levels). The most extreme scenario stands out by inducing a pronounced increase in tidal range. With the larger tidal prism induced by SLR, the gain in channel flow-carrying capacity is higher than the gain in basin storage. The channel erosion observed in the cumulative sedimentation/erosion maps, which becomes more pronounced with SLR severity, is directly linked to the increase in flow-carrying capacity. Consequently, there is a growing increase in tidal amplification with increasing SLR severity. Second, the shape of the tidal signal changes subtly. The signal of the purely hydrodynamic simulation shows a mild bulge in the flood period, with the water level increasing faster at first, and then slowing down towards the high-water peak. This bulge is straightened out with increasing SLR severity, reaching an almost linear slope between low-water and high-water for the most extreme SLR scenario. This change in shape also leads to a slight shift forward in time of the high-water peak. The average water depth in the basin increases with SLR, and the tide can therefore propagate faster in the basin, leading to the water level signal rising more linearly during flood and reaching the high-water peak earlier.

These MIS results deviate significantly from the SIS results (see Figure 3.9), which is not surprising considering the fundamentally different hydrodynamic forcing conditions of the two models (cyclic and harmonic with 9 tidal constituents in the SIS model vs. astronomical with 72 tidal constituents in the MIS model). While the MIS model does not reproduce the realistic hydrodynamics (see e.g. Section 4.2), it still implements a more varied schematization than the SIS model. These differences between the results do not directly link to the larger model domain size, i.e. the existance of other inlet systems in the domain should not influence the hydrodynamics in an individual basin. This of course only holds true in this particular case, where the model configuration with thin dams on the tidal divides prohibits residual flow patterns from developing between the basins.

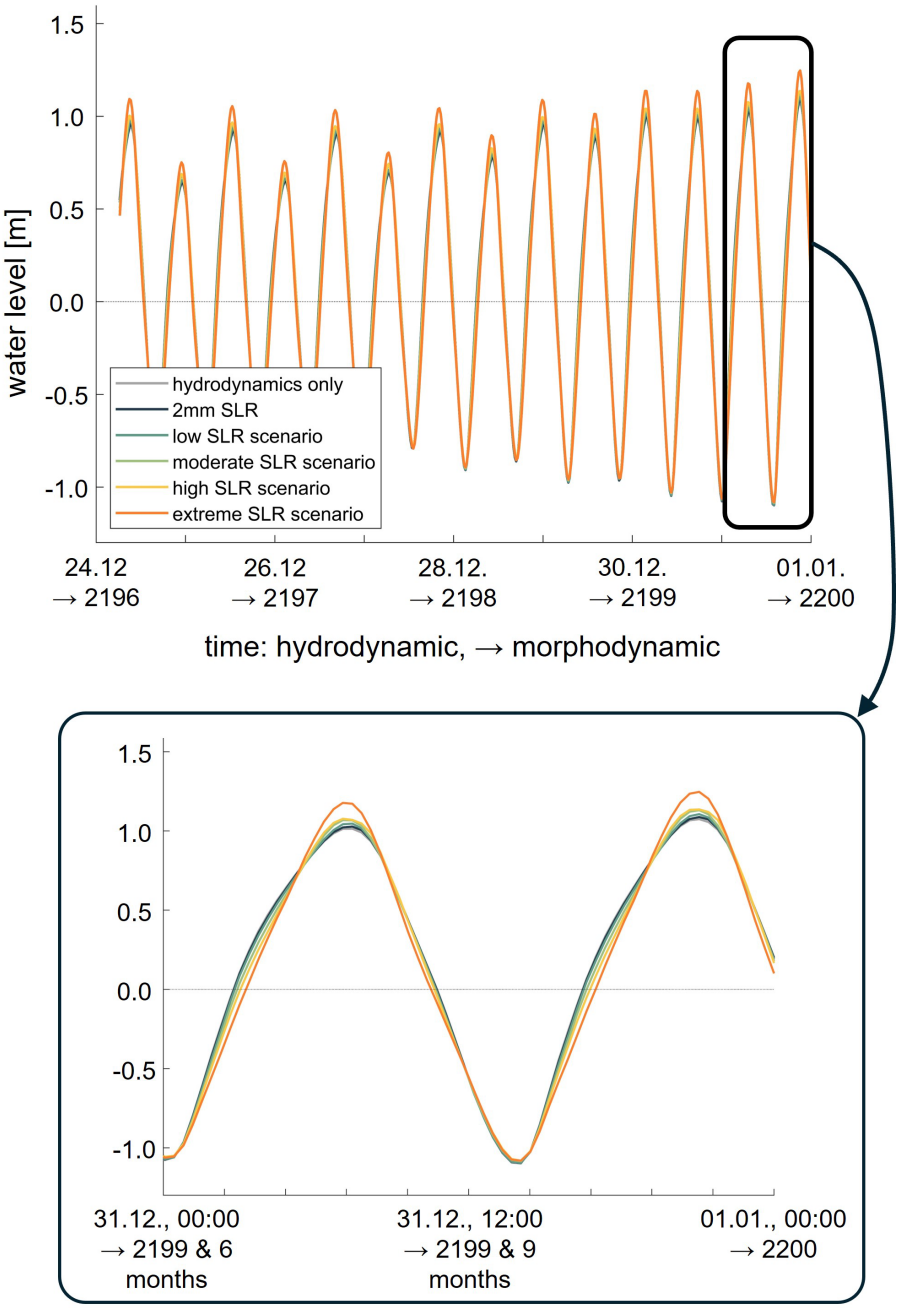

Figure 4.10. Water levels for different SLR scenarios at a water level station in the Ameland basin (for the location of the station, see Figure 4.3), plotted for the last week of the hydrodynamic simulation time, i.e. the last four years for the morphodynamic simulation period, where the changes in water level due to the imposed SLR will be most noticeable. As base line, we plot the water levels of a purely hydrodynamic simulation as a grey line, see the legend in the upper panel. The lower panel is a zoom-in on the last two tidal cycles.

4.5 Overview of changes in intertidal characteristics for all basins

To present the results for all individual basins of the MIS Wadden Sea model in a compact overview, we summarize the intertidal characteristics at the end of the 200-year simulation period for all the considered SLR scenarios in Table 4.6. Additionally, this table offers a

comprehensive way to compare the new Delft3D-ASMITA model results with regular ASMITA model results obtained in the past (e.g., Huismans et al. (2022)). However, such a comparison must be done with care, taking into account our assumptions (e.g. the current bathymetry is the equilibrium bathymetry, the omission of the residual sediment transport between neighbouring tidal basins, and the considered SLR scenarios).

The results presented in Table 4.6 should not be analysed alone, but in the context of the figures shown in Appendix B to get the full picture. A significant change in intertidal volume or area after the 200-year period does not necessarily indicate that the basin is not able to keep up with the imposed SLR, and vice versa. The clearest example is the Eierland basin, which loses 46% (2 mm/year SLR) and 56% (low SLR scenario) of intertidal area for the two mildest SLR scenarios after 200 years. However, consulting the figures which show the changes in intertidal characteristics over time (Figure B.2.1.), and the cumulative cross-throat sediment transport import and sediment transport rate (Figure B.2.3.), we see that the curves tend towards a plateau at the end of the simulation. We assume that Eierland is therefore approaching a dynamic equilibrium for the two mildest SLR scenarios. Pinkegat is another small basin which shows a trend towards a dynamic equilibrium for the two mildest SLR scenarios at the end of the simulation period. Its loss in intertidal area and volume is relatively minor compared to the Eierland basin. The difference between these basins lies in their hypsometric curves (Figures B.2.2 and B.5.2, respectively). The hypsometry of the intertidal flats in Pinkegat is steeper than in Eierland, which leads to smaller losses in intertidal characteristics for the same SLR.

For larger basins (e.g. Marsdiep and Vlie), it is more difficult to keep-up with SLR since they need to import much more sediment and over longer distances than the smaller basins. This is visible especially in the cumulative sediment/erosion maps, which show more sedimentation in intertidal flats closer to the inlet for large basins (see Figure B.1.4., Figure B.3.4., and Figure B.4.4), compared to basins such as Pinkegat and Eierland, which show a more even sedimentation in all intertidal flats in the basin (see Figure B.2.4. and Figure B.5.4).

For the three most extreme SLR scenarios, there is a considerable loss of intertidal characteristics for all basins. For the most extreme SLR scenario, the intertidal flats in all basins are all about to drown, as their area and volume suffer dramatic losses of over 90% in four of the six considered basins.

At the end of Table 4.6 we also present the summed-up values for the entire Wadden Sea basin (i.e. all six considered basins together). The numbers reflect the overall trend of the individual basins, with the intertidal volume and area reducing drastically, and the mean height also decreasing, but to a lesser degree.

Table 4.6. Changes in intertidal characteristics for all basins in the Wadden Sea at the end of the 200-year simulation period for all SLR scenarios

Basin	*SLR scenario*	*Volume change (in million m^3)*	*Area change (in km^2)*	*Height change (in cm)*	*relative volume change*	*relative area change*	*relative height change*
Marsdiep	2 mm constant	- 4.8	- 11.7	0.6	- 10 %	- 11 %	1 %
	low	- 7.6	- 24.9	4.8	- 16 %	- 24 %	10 %
	moderate	- 26.8	- 53.1	- 4.5	- 55 %	- 50 %	- 10 %
	high	- 41.6	- 84.3	- 12.9	- 86 %	- 80 %	- 28 %
	extreme	- 47.0	- 102.0	- 2.7	- 97 %	- 97 %	- 6 %
Eierland	2 mm constant	- 8.7	- 56.4	- 3.8	- 12 %	- 46 %	- 6 %
	low	- 21.2	- 68.9	- 8.2	- 28 %	- 56 %	- 13 %
	moderate	- 44.0	- 91.6	- 13.6	- 58 %	- 75 %	- 22 %
	high	- 56.9	- 104.6	- 17.8	- 76 %	- 85 %	- 29 %
	extreme	- 68.2	- 115.9	- 26.5	- 91 %	- 94 %	- 43 %
Vlie	2 mm constant	- 20.8	- 27.4	- 2.2	- 13 %	- 9 %	- 4 %
	low	- 51.1	- 71.7	- 5.6	- 32 %	- 24 %	- 10 %
	moderate	- 115.9	- 178.0	- 17.0	- 73 %	- 60 %	- 32 %
	high	- 142.2	- 245.2	- 20.5	- 89 %	- 82 %	- 38 %
	extreme	- 155.1	- 283.1	- 22.5	- 97 %	- 95 %	- 42 %
Ameland	2 mm constant	13.6	5.4	4.9	9 %	3 %	6 %
	low	14.7	2.8	6.7	10 %	1 %	8 %
	moderate	- 53.6	- 41.6	- 14.0	- 36 %	- 22 %	- 17 %
	high	- 106.6	- 85.8	- 37.8	- 72 %	- 46 %	- 47 %
	extreme	- 142.8	- 166.0	- 47.6	- 96 %	- 90 %	- 59 %
Pinkegat	2 mm constant	- 2.8	- 1.0	- 4.8	- 8 %	- 2 %	- 6 %
	low	- 5.0	- 1.9	- 8.8	- 15 %	- 4 %	- 11 %
	moderate	- 16.9	- 9.7	- 28.7	- 51 %	- 23 %	- 37 %
	high	- 25.0	- 24.5	- 33.8	- 76 %	- 58 %	- 43 %
	extreme	- 31.1	- 36.7	- 46.9	- 95 %	- 87 %	- 60 %
Zoutkamper-laag	2 mm constant	- 0.1	0.8	- 0.9	0 %	1 %	- 1 %
	low	- 8.9	- 0.3	- 8.5	- 8 %	0 %	- 8 %
	moderate	- 45.6	- 16.4	- 33.1	- 42 %	- 16 %	- 31 %
	high	- 75.9	- 37.9	- 55.8	- 70 %	- 37 %	- 52 %
	extreme	- 101.4	- 85.1	- 65.1	- 94 %	- 84 %	- 61 %
Entire Dutch Wadden Sea basin area	2 mm constant	- 23.6	- 90.3	- 6.2	- 4 %	- 11 %	7 %
	low	- 79.5	- 164.9	- 19.6	- 14 %	- 19 %	7 %
	moderate	- 302.8	- 390.4	- 110.9	- 53 %	- 46 %	- 13 %
	high	- 448.2	- 582.3	- 178.6	- 78 %	- 68 %	- 31 %
	extreme	- 545.6	- 788.8	- 211.4	- 95 %	- 92 %	- 37 %

4.6 Changes in channel hypsometry for all basins

In the previous sections, the hypsometric analysis focuses on the intertidal area (y-axis limitation). In contrast, in this section we show results focusing on the *channels*. For clarity, we present the results for the most extreme SLR scenario only, as they represent the most extreme end of a consistent trend through the different SLR scenarios.

For context we first show an example of a full hypsometric curve (in this case of the Marsdiep / Texel basin) in Figure 4.11. In Figure 4.11 we highlight the differences in the deeper areas of the basin (i.e. the channels) between the initial and the final curve. Contrary to the intertidal region, where the final hypsometric curve lies above the initial curve (i.e. sedimentation takes place during the simulation period), the final hypsometric curve crosses the initial curve around an elevation of -8 m NAP, to lie below the initial curve for the channel regions. The channels are therefore not accreting during the simulation but eroding and deepening. This trend, shown in Figure 4.11 for the Marsdiep / Texel basin, can be found for other basins as well (see Figure 4.12). Note that the axes scale differently in all six panels. For the larger basins, like the Vlie, Ameland, and Texel basins, the channel deepening is more pronounced, while the smaller basins like Pinkegat and Eierland show only minor channel deepening.

This observation is consistent with the cumulative sedimentation/erosion maps for the Wadden Sea model. For example, in Figure 4.8 for the Ameland basin, we see erosion in the deepest parts of the tidal inlet system, i.e. the channels, while the rest of the basin and the ebb-tidal delta exhibit sedimentation.

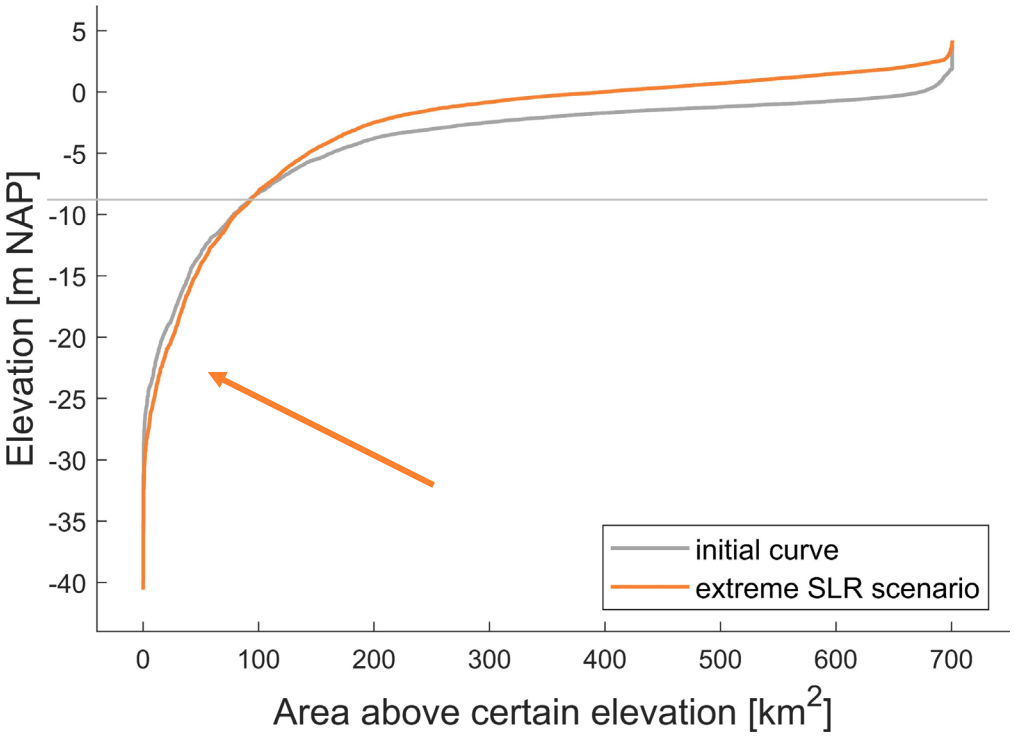

Figure 4.11. Hypsometric curves of the Marsdiep / Texel basin, results derived from the MIS Wadden Sea model. We show the initial curve as a grey line, and the final curve of the extreme SLR scenario in orange. Note the shift between the curves not only in the shallow, intertidal regions around 0 m NAP (highlighted in the other hypsometric curve figures of this report), but also in deeper areas (i.e. the channels) around -20 m, marked with the arrow.

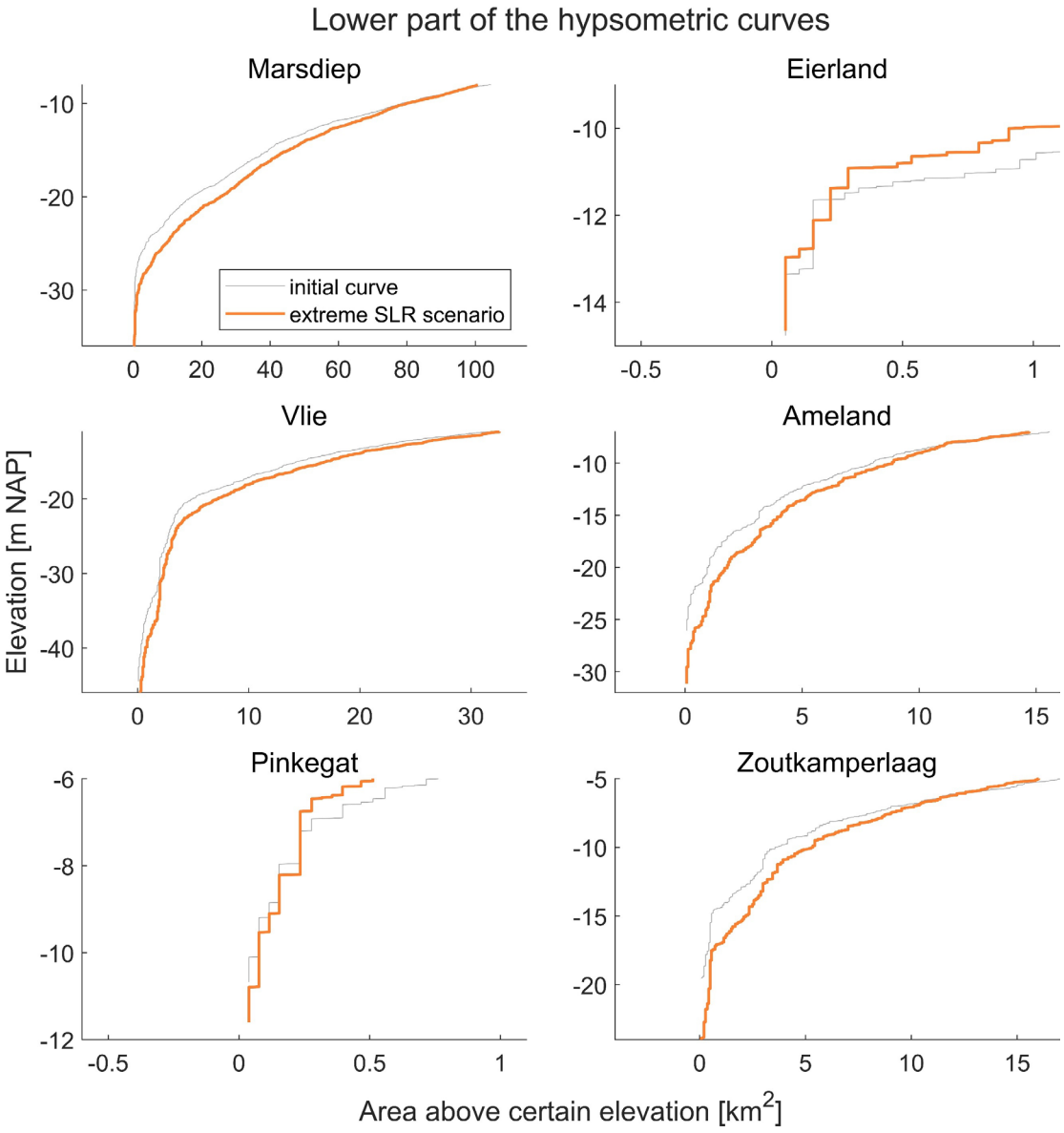

Figure 4.12. Comparison of the deeper parts of the hypsometric curves between the different Wadden Sea basins, results derived from the MIS Wadden Sea model. Each panel shows the initial hypsometric curve as a thin, grey line, and the final hypsometric curve after 200 years of the extreme SLR scenario in orange. Note the different axis scalings in the six panels. The deepening of the channels occurs in all six basins, but more noticeable in the larger basins like the Marsdiep / Texel basin, the Vlie basin or the Ameland basin, compared to the smallest basins of Pinkegat and Eierland.

5 Discussion, conclusions and recommendations

5.1 Discussion of results and current model limitations

The results presented in Chapter 3 and 4 highlight several factors that currently limit the model feasibility. We list the three most relevant points in the following:

5.1.1 Sediment source and supply

The representation of sediment sources and supply in the Delft3D-ASMITA model needs improvement. Currently, sediment supply is restricted to the open boundary import, and the sediment characteristics are limited to an artificial, slowly settling, non-cohesive sand fraction. In reality, sand and mud are both crucial for the sediment budgets of the Wadden Sea tidal inlet systems and come from different sources. Mud is supplied via the North Sea Continental Flow (Colina Alonso et al., 2024) and can be correctly reproduced by prescribing a mud concentration at the open boundaries. This requires a realistic reproduction of the residual flow in the coastal zone. Sand is supplied through erosion along the North Sea coast and subsequent longshore transport.

5.1.2 Residual flow pattern

Accurate reproduction of the residual flow patterns in the Wadden Sea is essential for understanding the morphological response to accelerated sea-level rise (SLR). In a regular model configuration without wind or wave dynamics, the residual flow pattern of the tidal signal leads to a circular residual sediment transport pattern with a large sediment import through the Vlie inlet throat and a large sediment export through the Marsdiep inlet throat. However, this does not match reality, where the Marsdiep / Texel basin heavily imports sediment, especially since it is still adapting to the closure of the Zuiderzee with the Afsluitdijk in 1936. Including relevant physical processes such as wind, wave dynamics, and storm surges is vital for accurately reproducing residual sediment transport. The MIS model results in this report use a model configuration with thin dams on all the tidal divides between individual basins to achieve residual sediment import into all basins. This approach is temporary until the relevant physical processes are sufficiently validated in the Delft3D-ASMITA model.

5.1.3 Consistency between single-inlet-system (SIS) and multi-inlet-system (MIS) models

The results between SIS and MIS modelling (Chapters 3 and 4, respectively) are currently not fully consistent with each other, even though the residual flow between individual inlet systems is blocked by the thin dams in the MIS Wadden Sea model. This thin dam configuration should render the individual inlet system in the MIS model similar to a SIS model. In our simulations, the results for the intertidal characteristics and the cross-throat sediment transports match qualitatively but are quantitatively different. Furthermore, there are clear, qualitative discrepancies between the sedimentation/erosion maps and the water level analyses. We identify two main factors for the differences: bathymetry resolution and sediment supply. ‘

- **Bathymetry resolution:** The resolution of the bathymetry is crucial when it comes to inundation of supratidal regions and tidal amplification. The grid resolution (and by design therefore also the resolution of the bathymetry) is different between the SIS and the MIS models, with the SIS model having a much higher spatial resolution than the MIS Wadden Sea model, see *Figure 5.1* for comparison. This not only influences the computational performance, but also directly links to the two models delivering different initial hypsometric curves (compare Figure 3.4 and Figure 4.6). Specifically, supratidal areas are represented differently in the two models. We compare Figure 3.3 with Figure 4.5, where distinct upticks in intertidal flat characteristics (area, volume and mean

height) for the SIS model are attributed to the inundation of the supratidal regions (step features of the hypsometric curve(s) in Figure 3.4). In the MIS Wadden Sea model, the hypsometric curve of the Ameland inlet system does not exhibit these distinct step features in the (initial) supratidal region. Therefore, the intertidal characteristics follow a more monotonous decline over time in Figure 4.5.

Regarding tidal amplification we point out the differences in water level signals in Figure 3.9 and Figure 4.10. While the SIS model predicts a dampening of the tidal range with increasing severity of SLR scenarios, the MIS Wadden Sea shows the opposite behaviour: the tidal range increases with more extreme SLR. In the MIS Wadden Sea model, the high-water level rises, and the low-water level stays quasi-constant. In the SIS model, the low-water level rises, while the high-water level stays quasi-constant. We can also interpret these results from a physical perspective: accelerated SLR causes the tidal prism to increase. For a larger tidal prism to be accompanied by an increase in the tidal range, the channel flow carrying capacity needs to grow more than the tidal basin storage capacity. This is the case in the MIS Wadden Sea model results, where the channels erode (see Figure 4.8 and Figure 4.9) and the low resolution of supratidal areas (artificially) prevents a large growth of tidal basin storage capacity. In contrast, in the SIS model the larger tidal prism due to accelerated SLR can be accommodated by a larger tidal basin storage capacity (by inundation of the supratidal areas), while the channels show accretion instead of erosion. Note that, even though the channels do not erode, their flow carrying capacity still increases. The sedimentation height in the channels is smaller than in the flats, and more importantly smaller than the projected SLR. The channel flow carrying capacity is however growing less than the tidal basin storage capacity, as indicated by the decrease in tidal range.

- **Sediment supply:** Sediment supply is implemented in the same way in the SIS and MIS model: sediment is imported through the open offshore boundaries and then transported through the model domain by the hydrodynamics, based on the imposed forcing conditions. We prescribe the same sediment concentration on the open boundaries in both models. However, the SIS model includes a much smaller offshore North Sea area than the MIS Wadden Sea model, leading to the open boundaries being much closer to the inlet system zone. This has implications for the sediment supply to the Ameland inlet system. Following the southwest-northeast longshore transport, the available sediment in the MIS model domain passes three other inlet systems before reaching the Ameland inlet system. In contrast, in the SIS model, the same equilibrium sediment concentration is immediately available for the single inlet system only.

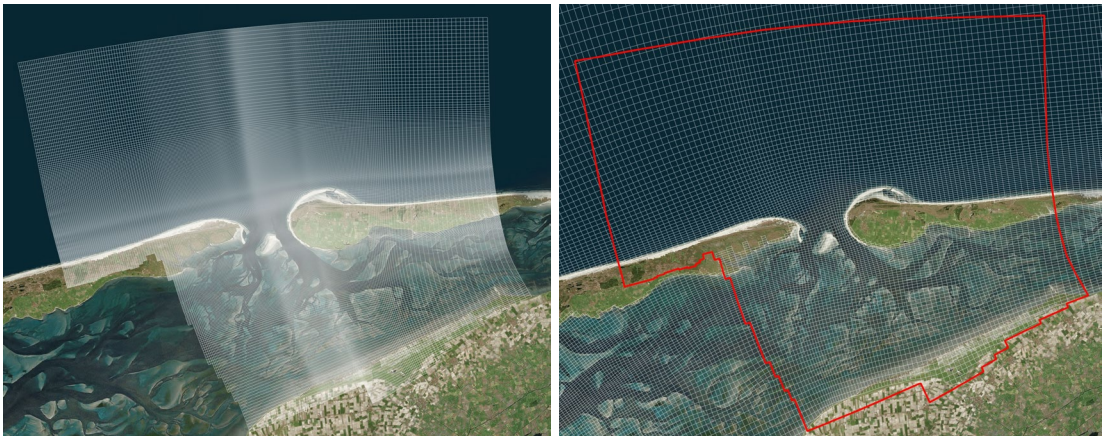

Figure 5.1. Comparison of the grid between the two models. The grid of the Ameland standalone model plotted on the left panel, and the regular grid of the Wadden Sea model in the right panel. For reference, the red contour on the right panel shows the edges of the grid of the Ameland standalone model. Note the difference in grid resolution.

5.2 Comparison with ASMITA

The Delft3D-ASMITA model is a novel approach and needs to be validated against previously reported results. The most logical choice for such a validation is to use regular ASMITA model results (e.g., Huismans et al., 2022; Wang et al., 2024). We show in this report, that the results of the Delft3D-ASMITA model are qualitatively similar to ASMITA results regarding the response of the Wadden Sea tidal inlet systems to various SLR scenarios (see for an overview Table 4.6).

The different basins show different responses to the imposed SLR scenarios, with the larger basins (Marsdiep / Texel, Vlie, and Ameland) showing higher losses in intertidal flats, as well as stronger channel erosion. They also suffer from more pronounced drowning effects (the difference between averaged sedimentation height in the basin and the imposed change in water depth due to SLR). The smaller basins (Eierland and Pinkegat, and to a lesser extent Zoutkamperlaag) seem more robust and able to keep up with the milder SLR scenarios. None of the basins can sustain their intertidal flats at initial levels during the simulations of the two highest SLR scenarios. These results are in line with previous ASMITA calculations.

Just like in ASMITA model results, the sediment import into the basins increases with SLR severity in Delft3D-ASMITA model results, because the sediment demand in the basins also increases faster with accelerated SLR. In none of the basins does the averaged sedimentation height balance the imposed SLR (increase in water depth). This drowning effect does not, however, take into account, that channel areas and intertidal zones react differently to SLR. The averaged sedimentation height is calculated as cumulative sediment import over the total basin area (flats and channels). This methodology therefore overestimates the drowning effects, especially in the flats. As the channels are constantly below MLW at any rate, this methodology can still be improved.

More surprising than the cumulative sediment transport is the sediment transport rate, which is less sensitive to the SLR rate than expected. Assuming that the yearly imported sediment into the basin gets distributed relatively evenly to keep up with SLR, the final import rate over the basin area gives an averaged sedimentation rate, which can be compared directly to the SLR rate. For example, the final SLR rate for the most extreme scenario is 20 times larger than for the mildest scenario (40 mm per year vs. 2 mm per year). In contrast, the factor between the averaged sedimentation rates for the mildest and most extreme scenarios is smaller than

9 for all of the basins, and even as small as 4.4 for the Zoutkamperlaag basin. This large discrepancy is a sign that the individual basins cannot counterbalance the imposed SLR; a fact emphasized by the (dramatic) decline of intertidal characteristics in all basins for higher SLR scenarios. However, the averaged sedimentation rate suffers from the same simplification as the averaged sedimentation height, i.e. that they are based on the entire basin area. Therefore, the different behaviour of flats and channels is not taken into account, and the sedimentation rates are underestimated in the flats, and overestimated in the channels.

Comparing the results of the Delft3D-ASMITA model quantitatively with the previous ASMITA results is challenging and should only be done with great care. Overall, the Delft3D-ASMITA model results of the intertidal characteristics are less sensitive to basin size than the ASMITA results. While in this report the smaller basins are shown to be more resilient than larger basins, the differences are not as pronounced as for the ASMITA results. In the following we list possible reasons for the quantitative differences between the two model approaches.

1. **Handling of sediment supply:** The Delft3D-ASMITA model uses an artificial sediment fraction, which is neither sand nor mud, in line with previous ASMITA calculations. While this approach was reasonable for the spatially aggregated model, which is independent of spatially varying hydrodynamics, it could lead to misrepresentations in the Delft3D-ASMITA model. If the sediment supply and transport through the model is simulated incorrectly, it will lead to diminished flat growth and enhanced channel erosion, causing differences in intertidal characteristics compared to previous results.

2. **ASMITA parameter settings:** Overall, the Delft3D-ASMITA model is based on the ASMITA parameters (see also Chapter 2). However, in the ASMITA model, the settling velocity for the intertidal flat element differs from the one used for the other two elements (ebb-tidal delta and channel). Meanwhile, the Delft3D-ASMITA model employs the same settling velocity everywhere in the tidal inlet system.

3. **Implementation of supratidal regions:** The original ASMITA model is based on fixed areas of its morphological elements. Therefore, the intertidal flats have a prescribed area extent, which does not change throughout the simulation period, and does not include any supratidal zones. The Delft3D-ASMITA model is based on spatially resolved, measured bathymetry and therefore can include supratidal zones. With SLR, and likewise rising MLW and MHW levels, inundation of supratidal areas takes place and causes an increase in intertidal area over time (or at least a slower net decrease). This also leads to a delay in their drowning (which occurs beyond our simulation period of 200 years), contrary to other reports based on ASMITA calculations, where intertidal flats in some Wadden Sea basins were reported to drown for the two most extreme SLR scenarios within the 200-year simulation period (e.g. Wang et al., 2024). Conceptually, the inundation of supratidal zones and consequent adaptation of the intertidal area is more realistic than the constant intertidal area of the ASMITA model. However, the implementation of supratidal zones in the Delft3D-ASMITA model is not correct yet, as the model does not include any vegetation and extreme weather events, like storms which periodically flood supratidal areas and can potentially cause drastic height changes over a short period of time. In reality, supratidal zones such as salt marshes exhibit sedimentation especially during storm surges on a shorter timeframe, but also on a longer time scale through vegetational sediment entrapment. These processes are not yet included in the simulations we report on here. For predictions of supratidal development under SLR, it is currently debated how salt marshes will react to SLR and in how far storms and waves influence the critical SLR that salt marshes will be able to compensate (Willemsen et al., 2022, Schuerch et al., 2013). We plan on investigating supratidal development further with the Delft3D-ASMITA model in the future.

5.3 Concluding evaluation of the model implementation & application

In this report we show that the Delft3D-ASMITA model can be successfully applied to both SIS and MIS models. The model results presented in this report are consistent with our expectations:

1. We achieve stable and robust simulations of long-term morphodynamic developments, with a comparatively high MorFac of 200. This reduces the computational time to hours instead of days or weeks[9].
2. The simulation results for different SLR scenarios are similar to previously reported results, such as regular ASMITA calculations (e.g., Huismans et al., 2022; Wang et al., 2024). As expected with a different modelling approach, the quantitative results do not match exactly.
3. The results of the Delft3D-ASMITA model provide information on the spatial variation in the long-term morphological development. This is an advantage of the Delft3D-ASMITA model compared to a regular ASMITA model, which is not designed to deliver this type of output, and a regular Delft3D model, which can arrive at these results under larger strain and uncertainty.

We want to emphasize that the Delft3D-ASMITA model has clear use cases and limitations, which need to be considered when setting up a new simulation. For example, (relative) SLR cases are the designated use case, but the ASMITA-based model formulations are only valid in tidal inlet systems. This leads to the implementation of SLR as subsidence in the ASMITA-governed zone of the domain only (see Figure 2.3), as the equilibrium concept at the heart of the model formulation is not applicable for the North Sea area (including barrier island coasts, foreshores, as well as offshore regions). Note, however, that the North Sea part of the model domain is crucial for the correct development of the hydrodynamic conditions. The artificially lowered bed levels (via subsidence) in the ASMITA-governed zone have to be corrected (i.e. raised) in the postprocessing stage of the results.

5.4 Recommendations

Following up on the previous sections of this chapter, there are three main improvements the Delft3D-ASMITA model needs to undergo to be further validated and provide valuable and more realistic insights in the future:

1. **Handling of several sediment fractions:** Implement separate sand and mud fractions with the respective sediment source (mud being prescribed on the open boundaries, and sand originating from coastal erosion).

2. **Correct representation of supratidal zones:** Accurately represent supratidal zones in the basins and their inundation over time. This development requires the implementation of vegetation (including their sediment entrapment capabilities) and extreme weather events. Additionally, the grid needs to be fine enough to properly represent the hypsometric curve (e.g., to better capture the supratidal zones).

3. **Further improvement of the hydrodynamics prescription:** Enhance the hydrodynamics prescription (e.g. tidal forcing, especially for the SIS Ameland model, wind and wave dynamics, as well as storm surges). Correctly implemented and validated, this

[9] Still, the computational time is heavily dependent on the grid resolution for both models: the SIS model of the Ameland system, with a much higher grid cell number than the MIS Wadden Sea model, runs in about a day and half on 16 cores of the cluster, while the Wadden Sea model runs within 4 hours on 16 cores of the cluster.

development will achieve a faithful reproduction of the residual flow pattern and, consequently, improved residual sediment transports throughout the model, especially in the MIS Wadden Sea model.

Once these main developments have taken place, it will be possible to improve predictions of SLR response throughout the entire Wadden Sea with the Delft3D-ASMITA model. Furthermore, we will be able to simulate sediment exchange between several tidal inlets across the tidal divides in one model run (with the MIS Wadden Sea model).

Additionally, we suggest the following improvements, which focus more on postprocessing and model input than on fundamental model development:

a) **Improve the methodology to derive sedimentation height and rate:** Specifically target the intertidal flats, instead of using an average over the whole tidal basin. This postprocessing step falls outside of the scope of this technically oriented report but seems to be a valuable step to investigate intertidal flat development further.

b) **Develop a methodology to estimate the equilibrium bathymetry:** Create a methodology for basins currently known to be out of morphological equilibrium. Except for the Ameland basin, all other basins are still adjusting to the closure of the Zuiderzee and the Lauwerszee. One option would be to use the measured bathymetry, and compensate for it to be out of equilibrium by prescribing additional sediment import through the inlet throat. This is the additional sediment import required by the basins to restore equilibrium due to anthropomorphic changes (e.g., building of dams), leaving the sediment import that happens from offshore into the basins as the one required to restore SLR-only.

c) **Improve the model implementation with respect to Delft3D options:** Enhance the model by adding a vertical spatial resolution (3D effects) or switching from structured curvilinear grids to unstructured grids in Delft3D flexible mesh. An unstructured grid is more computationally efficient since refinement can be focused on areas where it is needed most (to represent relevant local spatial scales more accurately). Additionally, an unstructured grid can be built to better follow flow directions. When this is well implemented, estimating the sedimentation/erosion patterns is expected to improve.

Finally, we want to highlight two possible use cases of the Delft3D-ASMITA model, which are currently not yet achievable but for which the model approach is uniquely suited:

I. **Application to fundamental research:** Answer questions about how the model input parameters of the regular ASMITA model should be related to those in standard process-based Delft3D models.

II. **Application to relative SLR (rSLR) cases:** When long-term rising sea levels coincide with anthropogenic subsidence, e.g. due to resource extraction like salt or gas mining, rSLR can lead to intricate morphological responses, especially because time- and length-scales can vary significantly for the two different drivers of water depth increase (rising water levels and bed level subsidence). Since the Delft3D-ASMITA model has proven to be stable with high MorFac's and therefore allows for modelling long-term developments, rSLR cases can be a suitable challenge to tackle next.

6 References

Becherer, J., Hofstede, J., Gräwe, U., Purkiani, K., Schulz, E. & Burchard, H. (2018). The Wadden Sea in transition – consequences of sea level rise. *Ocean Dynamics,* 68, pp. 131–151. https://doi.org/10.1007/s10236-017-1117-5

Chen, X. (2021). A new approach to simulate the Ameland inlet's response to sea-level rise and subsidence. MSc thesis. Delft University of Technology. https://resolver.tudelft.nl/uuid:1ea30c74-bfa4-4e69-99a7-10e1a0a2a234

Cleveringa, J. & Grasmeijer, B. (2010). Meegroeivermogen en gebruiksruimte in de getijbekkens Vlie en Marsdiep; Grootschalige morfologische ontwikkelingen westelijke Waddenzee. *Report A2062R3r5*, Arcadis (Zwolle).

Colina Alonso, A., van Maren, D. S., Oost, A. P., Esselink, P., Lepper, R., Kösters, F., Bartholdy, J., Bijleveld, A. I., & Wang, Z. B. (2024). A mud budget of the Wadden Sea and its implications for sediment management. *Communications Earth & Environment*, 5(1), pp. 1–9. https://doi.org/10.1038/s43247-024-01315-9

Dastgheib, A., Roelvink, J.A. & Wang, Z.B. (2008). Long-term process-based morphological modeling of the Marsdiep tidal basin. *Marine Geology*, 256, pp. 90–100. https://doi.org/10.1016/j.margeo.2008.10.003

de Fockert, A., 2008. Impact of relative sea level rise on the Amelander inlet morphology. MSc thesis. Delft University of Technology. https://resolver.tudelft.nl/uuid:5fd29cd3-8673-4319-89b1-a758703a8d36

Deltares, *3D/2D modelling suite for integral water solutions: Delft3D-FLOW Hydro-Morphodynamics*, Version 4.05 (February 2025). https://content.oss.deltares.nl/delft3d4/Delft3D-FLOW_User_Manual.pdf

de Swart, H.E. & Zimmerman, J.T.F. (2009). Morphodynamics of tidal inlet systems. *Annual Review of Fluid Mechanics*, 41, pp. 203–229. https://doi.org/10.1146/annurev.fluid.010908.165159

Dissanayake, D.M.P.K., Ranasinghe, R. & Roelvink, J.A. (2012). The morphological response of large tidal inlet/basin systems to relative sea level rise. *Climate Change*, 113, pp. 253–276. https://doi.org/10.1007/s10584-012-0402-z

Duran-Matute, M., Gerkema, T., De Boer, G. J., Nauw, J. J., & Gräwe, U. (2014). Residual circulation and freshwater transport in the Dutch Wadden Sea: A numerical modelling study. *Ocean Science*, 10(4), pp. 611–632. https://doi.org/10.5194/os-10-611-2014

Elias, E.P.L. (2006). Morphodynamics of Texel Inlet. PhD Thesis. Delft University of Technology. https://resolver.tudelft.nl/uuid:92ad4ac0-9d54-4f5f-8536-80b7782a6aa6

Elias, E.P.L., Van der Spek, A.J.F., Wang, Z.B. & De Ronde, J.G. (2012). Morphodynamic development and sediment budget of the Dutch Wadden Sea over the last century. *Netherlands Journal of Geosciences / Geologie en Mijnbouw*, 91, pp. 293–310. https://doi.org/10.1017/S0016774600000457

Galappatti, R. (1983). *A depth integrated model for suspended transport*. https://www.semanticscholar.org/paper/A-depth-integrated-model-for-suspended-transport-Galappatti/f742b12b307ce5980d754b8d4f495d26cd0b0fea

Galappatti, G., & Vreugdenhil, C. B. (1985). A depth-integrated model for suspended sediment transport. *Journal of Hydraulic Research*, *23*(4), pp. 359–377. https://doi.org/10.1080/00221688509499345

de Graaf, R. (2009). SBW Wadden Sea, water level modelling. Calibration hydrodynamic model. *Deltares project 1200114-005*. Deltares, Delft.

Hibma, A., De Vriend, H.J. & Stive, M.J.F. (2003). Numerical modelling of shoal pattern formation in well-mixed elongated estuaries. *Estuarine Coastal Shelf Science,* 57, pp. 981–991. https://doi.org/10.1016/S0272-7714(03)00004-0

Hibma, A., Schuttelaars, H.M. & Wang, Z.B. (2003). Comparison of longitudinal equilibrium profiles of estuaries in idealized and process-based models. *Ocean Dynamics,* 53, pp. 252–269. https://doi.org/10.1007/s10236-003-0046-7

Hibma, A., Schuttelaars, H.M. & De Vriend, H.J. (2004). Initial formation and long-term evolution of channel-shoal patterns. *Continental Shelf Research*, 24, pp. 1637–1650. https://doi.org/10.1016/j.csr.2004.05.003

Hofstede, J.L.A., Becherer, J. & Burchard, H. (2018). Are Wadden Sea tidal systems with a higher tidal range more resilient against sea level rise? *Journal of Coastal Conservation*, 22, pp. 71–78. http://www.jstor.org/stable/45047126

Huismans, Y., Van Der Spek, A., Lodder, Q., Zijlstra, R., Elias, E., & Wang, Z. B. (2022). Development of intertidal flats in the Dutch Wadden Sea in response to a rising sea level: Spatial differentiation and sensitivity to the rate of sea level rise. *Ocean & Coastal Management*, *216*, article 105969. https://doi.org/10.1016/j.ocecoaman.2021.105969

Jiao, J. (2014). Morphodynamics of Ameland Inlet – Medium-term Delft3D Modelling. MSc thesis. Delft University of Technology. http://resolver.tudelft.nl/uuid:e3d05254-1291-4334-b044-033e367b81fe

Kragtwijk, N.G., Zitman, T.J., Stive, M.J.F. & Wang, Z.B. (2004). Morphological response of tidal basins to human interventions. *Coastal Engineering,* 51, pp. 207–221. https://doi.org/10.1016/j.coastaleng.2003.12.008

Lesser, G.R., Roelvink, J.A., Van Kester, J.A.T.M. & Stelling, G.S. (2004). Development and validation of a three-dimensional model. *Coastal Engineering*, 51, pp. 883–915. https://doi.org/10.1016/j.coastaleng.2004.07.014

Lodder, Q. J., Wang, Z. B., Elias, E. P. L., Van Der Spek, A. J. F., De Looff, H., & Townend, I. H. (2019). Future Response of the Wadden Sea Tidal Basins to Relative Sea-Level rise—An Aggregated Modelling Approach. *Water*, 11(10), article 2198. https://doi.org/10.3390/w11102198

Lodder, Q., Huismans, Y., Elias, E., de Looff, H., & Wang, Z. B. (2022). Future sediment exchange between the Dutch Wadden Sea and North Sea Coast - Insights based on ASMITA modelling. *Ocean and Coastal Management*, 219, article 106067. https://doi.org/10.1016/j.ocecoaman.2022.106067

Marciano, R., Wang, Z.B., Hibma, A. & De Vriend, H.J. (2005). Modeling of channel patterns in short tidal basins. *Journal of Geophysical Research,* 110, article F01001. https://doi.org/10.1029/2003JF000092

Postma, H. (1961). Transport and accumulation of suspended matter in the Dutch Wadden Sea. *Netherlands Journal of Sea Research,* 1, pp. 148–190. https://doi.org/10.1016/0077-7579(61)90004-7

van Rijn, L. C. (1984). Sediment transport, Part II: suspended load transport. *Journal of Hydraulic Engineering*, 110 (11), pp. 1613–1640. https://doi.org/10.1061/(ASCE)0733-9429(1984)110:11(1613)

Schuerch, M., Vafeidis, A., Slawig, T., & Temmerman, S. (2013). Modeling the influence of changing storm patterns on the ability of a salt marsh to keep pace with sea level rise. *Journal of Geophysical Research: Earth Surface,* 118, pp. 84–96. https://doi.org/10.1029/2012JF002471

Stive, M.J.F., Wang, Z.B., Ruol, P. & Buijsman, M.C. (1998). Morphodynamics of a tidal lagoon and adjacent coast. *8th International Biennial Conference on Physics of Estuaries and Coastal Seas*, The Hague, pp. 397–407. Conference proceedings.

Stive, M.J.F. & Wang, Z.B. (2003). Morphodynamic modeling of tidal basins and coastal inlets. In: Lakhan, C. (ed.): *Advances in coastal modeling*. Elsevier Science (Amsterdam): pp. 367–392. https://doi.org/10.1016/S0422-9894(03)80130-7

Townend, I., Wang, Z.B., Stive, M. & Zhou, Z. (2016). Development and extension of an aggregated scale model: part 1. Background to ASMITA. *China Ocean Engineering,* 30, pp. 483–504. https://doi.org/10.1007/s13344-016-0030-x

Townend, I., Wang, Z.B., Stive, M. & Zhou, Z. (2016). Development and extension of an aggregated scale model: part 2. Extensions to ASMITA. *China Ocean Engineering*, 30, pp. 651–670. https://doi.org/10.1007/s13344-016-0042-6

van der Wegen, M., Wang, Z.B., Savenije, H.H.G. & Roelvink, J.A. (2008). Long-term morphodynamic evolution and energy dissipation in a coastal plain, tidal embayment. *Journal of Geophysical Research: Erath Surface,* 113(F3), article F03001. https://doi.org/10.1029/2007JF000898

van Goor, M.A., Zitman, T.J., Wang, Z.B. & Stive, M.J.F. (2003). Impact of sea level rise on the morphological equilibrium state of tidal inlets. *Marine Geology,* 202, pp. 211–227. https://doi.org/10.1016/S0025-3227(03)00262-7

van Koningsveld, M. & Mulder, J.P.M. (2004). Sustainable coastal policy developments in the Netherlands. A systematic approach revealed. *Journal of Coastal Research,* 20, pp. 375–385. https://research.utwente.nl/en/publications/sustainable-coastal-policy-developments-in-the-netherlands-a-syst

Vermeersen, L.L.A., Slangen, A.B.A., Gerkema, T., Baart, F., Cohen, K.M., Dangendorf, S., Duran-Matute, M., Frederikse, T., Grinsted, A., Hijma, M.P., Jevrejeva, S., Kiden, P., Kleinherenbrink, M., Meijles, E.W., Palmer, M.D., Rietbroek, R., Riva, R.E.M., Schulz, E., Slobbe, D.C., Simpson, M.J.R., Sterlini, P., Stocchi, P., van de Wal, R.S.W. & van der Wegen, M. (2018). Sea level change in the Dutch Wadden Sea. *Netherlands Journal of Geosciences / Geologie en Mijnbouw,* 97(3), pp. 79-127. https://research.rug.nl/nl/publications/sea-level-change-in-the-dutch-wadden-sea

Wang, Z. B. (1989). *Mathematical modelling of morphological processes in estuaries*.

Wang, Z. B. (1992). Theoretical analysis on depth-integrated modelling of suspended sediment transport. *Journal of Hydraulic Research*, 30(3), pp. 403–421. https://doi.org/10.1080/00221689209498927

Wang, Z.B., Louters, T. & De Vriend, H.J. (1995). Morphodynamic modelling for a tidal inlet in the Wadden Sea. *Marine Geology*, 126, pp. 289–300. https://doi.org/10.1016/0025-3227(95)00083-B

Wang, Z.B. & Eysink, W.D. (2005). Abiotische effecten van bodemdaling in de Waddenzee door gaswinning. *Report Z3995*, WL|Delft Hydraulics (Delft).

Wang, Z.B., Cleveringa, J. & Oost, A. (2017). Morfologische effecten bodemdaling in relatie tot gebruiksruimte. *Report 1230937-000*. Deltares (Delft). https://www.commissiemer.nl/projectdocumenten/00002808.pdf

Wang, Z. B., Elias, E. P. L., Van Der Spek, A. J. F., & Lodder, Q. J. (2018). Sediment budget and morphological development of the Dutch Wadden Sea: Impact of accelerated sea-level rise and subsidence until 2100. *Netherlands Journal of Geosciences*, 97(3), pp. 183–214. https://doi.org/10.1017/njg.2018.8

Wang, Z. B., & Lodder, Q. J. (2019). *Sediment exchange between the Wadden Sea and North* Sea Coast. *Deltares project 1220339–008*, Deltares, Delft. https://open.rijkswaterstaat.nl/open-overheid/onderzoeksrapporten/@131773/sediment-exchange-between-the-wadden-sea/

Wang, Z. B., Townend, I., & Stive, M. (2020). Aggregated morphodynamic modelling of tidal inlets and estuaries. *Water Science and Engineering*, 13(1), pp. 1–13. https://doi.org/10.1016/j.wse.2020.03.004

Wang, Z. B., Lodder, Q. J., Townend, I. H., & Zhu, Y. (2024). Future sediment transport to the Dutch Wadden Sea under severe sea level rise and tidal range change. *Anthropocene Coasts*, 7(1), article 12. https://doi.org/10.1007/s44218-024-00044-y

Willemsen, P.W.J.M., Smits, B.P., Borsje, B.W., Herman, P.M.J., Dijkstra, J.T., Bouma, T.J., & Hulscher, S.J.M.H. (2022). Modeling Decadal Salt Marsh Development: Variability of the Salt Marsh Edge Under Influence of Waves and Sediment Availability. *Water Resources Research*, 58, article e2020WR028962. https://doi.org/10.1029/2020WR028962

A Spin-up in morphodynamic modelling

A.1 Introduction

In various applications of morphodynamic modelling we encounter the problem of spin-up. The problem is that at the beginning of the model simulation, the model results show unrealistic morphological changes. Only after a certain spin-up period the model starts to give meaningful results.

A recent example is the application of the Delft3D-NeVla model to evaluate extreme but realistic strategies for disposing dredged material (Schrijvershof & Vroom, 2016). The authors concluded that only after about 7 years the model reproduces the total dredging volume well. An extreme example is the study by Dam et al. (2016), who simulated the morphological developments of the Western Scheldt for periods ranging from decades to more than a century. They concluded that the performance of the model, expressed in the Brier Skill Score (BSS), first decreases and then increases. The model results are "good" only after many decades. This issue raises questions such as, how best to handle morphological spin-up. And does it even make sense to model morphodynamics for periods of a decade?

In this appendix, we try to provide more insight into the problem. We do this using a simple example in the field of river morphology. We try to answer the following questions:

- What are the causes of the problem?
- Can a morphodynamic model be “span up”?
- If so, what is the time scale of the spin-up?
- Can we avoid or minimize the problem?

A.2 The problem with spin-up: does it really matter?

The spin-up phenomenon in numerical modelling is not strange. People encounter the problem in any hydrodynamic model (note that we are not mentioning *morphodynamics* yet), simulating for example tidal flow. As the initial conditions, i.e. the entire flow field (water level and flow velocity) at time 0 (start of simulation) are unknown, one often gives an arbitrary flow field as initial conditions. Although almost certainly incorrect, the initial conditions fortunately affect the results only within a limited period of time at the beginning of a simulation. Over time it does not matter anymore what was specified as initial hydrodynamic conditions. This means that the model results within the spin-up period, during which the initial conditions still have influence, are not reliable. For hydrodynamic models the spin-up period is usually short, in the order of a few tidal periods. Compared to the simulation period, the spin-up is therefore usually not a problem in hydrodynamic simulations.

Unsurprisingly, the same spin-up phenomenon occurs in *morphodynamic* modelling. Here, however, it is a more severe problem because of the following possible reasons: (1) we have less insight into the spin-up process; (2) the morphological spin-up takes a relatively long time, so that it becomes impossible to distinguish the effects of spin-up from the real morphological developments in the model results. The initial bed level (and composition) in a morphodynamic model may therefore be a crucial initial condition, influencing the entire model result.

A.3 Causes of the problem

We explain the spin-up of morphodynamic models using the example of 1D morphodynamic river modelling. Let's start with the simplest case: a river with a given, constant width *B*, a constant upstream discharge *Q,* and a constant upstream sediment transport *S*. For this case there is a morphological equilibrium in which the river with the given discharge can transport exactly the supplied sediment to the downstream sea. The equilibrium is expressed by two state variables: the depth *h* and the slope *i*, and they can be calculated from the data on the basis of the following two equations:

$$Q = BhC\sqrt{hi} = BCh^{\frac{3}{2}}i^{\frac{1}{2}} \tag{A-1}$$

$$S = Bmu^{n} = BmC^{n}h^{\frac{n}{2}}i^{\frac{n}{2}} \tag{A-2}$$

Equation (1) is the water movement equation for stationary, uniform flow and equation (2) is a simple sediment transport formula. For the sediment transport formula a power law is used here, but replacing the formula by any other, common sediment transport formula would not affect the following reasoning. Suppose that we want to implement interventions in this river, which is in a natural equilibrium for a long time, and we would like to evaluate the effects of the interventions with a 1D morphodynamic model. Then, one would like the model to simulate no morphological changes, if no intervention is implemented. In this simple case, this is easily achieved. The initial conditions must correspond to a stationary, uniform flow, of which the depth and slope exactly satisfy the two equations above, such that *S* is constant along the river. This can be achieved by adjustments to the model parameters, e.g. *C*, *m* and *n,* as the depth and slope are known from measurements.

The problem becomes more complex when we look at a real river, where the width, depth and slope are not constant but vary along the river, and the discharge and sediment transport at the upstream boundary vary over time. It is then more likely that we have to deal with the phenomenon of spin-up in the morphodynamic modelling. The problem occurs if the morphological equilibrium according to the model deviates from the initial bed level which is in morphodynamic equilibrium in reality. There are several reasons for such a deviation:

- Errors in the initial bed level (and bed composition). If the river is in morphodynamic equilibrium and the model is good, then errors in the bed level at the beginning of the simulation cause disturbances in the model results in a similar way as in hydrodynamic modelling. Such errors may be introduced during the measurements or the data processing in order to arrive at the model schematization. Note that the timescale of the spin-up is dependent on the length scale of the errors. The largest length scale of the errors is most important, because it corresponds to the longest time for damping out the error.
- Errors in the boundary conditions of the model. The discharge and sediment transport at the upstream boundary are also prone to errors. Especially the sediment transport is not easy to measure and, moreover, a certain schematization is always necessary in order to derive the model input. A systematic error in the averaged values of the discharge and the sediment transport can lead to length scale errors in the order of the entire model domain. The timescale of the spin up may then be long.
- Errors in the model parameters. In this simple example, the values of *C*, *m* and *n* are relevant, and in particular *n* has an influence on the morphological equilibrium. In practice, a wrong choice in the sediment transport formulas has the same effect as a wrong value of *n*.
- Errors of the model, such as missing or incorrectly modelled physics. The limitations of the model itself can also cause problems. In this simple example the model has for example the constraint that it does not take into account the spatial and temporal

variation of the sediment properties, because of the use of the simple power-law for the sediment transport formula. In reality, the sediment becomes finer in the downstream direction. The downstream refinement is accompanied by the decreasing slope of rivers (Blom, 2016). The consequence of this limitation is thus that the morphological equilibrium is not properly reproduced by the model.
- Another important potential source of error is the numerical solver.

For an intertidal system, the problem is much more complicated, especially because there is little insight into the morphological equilibrium according to the model. But in principle, these various causes of possible problems also apply.

A.4 How can the problem be avoided / limited?

In practice, the various causes of the problem can occur at the same time. It is important that the modeler solves the problem by eliminating the correct error(s) during the set-up and calibration of the model. Therefore, sufficient understanding of how different aspects affect the morphological equilibrium is required. For this simple river example, the problem is not serious because sufficient knowledge is available about the morphological equilibrium. The knowledge helps the modeler to identify the causes of the possible problems. One can then solve the problem by eliminating the errors in the data (and the schematisation thereof), or by adaptations of the model parameters via calibration. Note that some causes of the problem cannot be avoided. Errors / limitations of the model itself are and will always there. As a result, it is sometimes not sufficient to get all the model input data perfect (100% corresponding to reality).

For an intertidal system such as the Wadden Sea our knowledge of the morphological equilibrium is much more limited, compared to a 1D river application. The influence of the tide, and also considering it as a 2D / 3D problem instead of 1D, make the problem much more complicated. Moreover, an intertidal system such as the Wadden Sea is influenced by the ongoing human intervention on top of the changes in forcings such as sea level rise. The intertidal system is then never in equilibrium and always subject to morphological changes. Theoretically, it is not even known whether there is a morphological equilibrium according to the model, let alone how it looks and what influences the different forcings and model parameters have on it. This makes a similar solution as for the river cases often impossible. Therefore often practical solutions are used, such as:

- Let the model spin-up first. One can let the model spin-up first before the "real" simulations are performed. The results at the end the spin-up simulation are then used as the initial conditions. All the errors due to the different causes are then considered as errors in the initial bed level. As this is not always justified, it can lead to a poor model. For example, if the problem is actually caused by an error in the boundary conditions, the error will continue to influence the model results even after the spin-up of the model. Furthermore, it is still the question if the model spin-up can be well executed. It is not known beforehand what the required spin-up time will be, and it is difficult to assess when the spin up of a model is accomplished because it is hard to distinguish the real morphological developments and the spin-up errors. Morphodynamic modelling with 2D / 3D model for an intertidal system such as the Wadden Sea is time consuming, making the sufficient spin-up more difficult.
- Consider the model results in a relative way. Another way to deal with the problem is considering the model results only relatively, by comparing the different simulations with and without particular interventions with each other. In essence, one then accepts the errors in the model results of an individual simulation, for any reason whatsoever, and hopes that the errors cancel each other in the difference between the results of two simulations. Theoretically, this “solution” only works for a linear model, which

certainly does not describe a morphodynamic model. The errors may, depending on their sources, influence the difference between the results of two simulations.

- Forcing equilibrium. The adaptation of model input can bring the morphological equilibrium close to the initial bed level. For an aggregate model such as ASMITA this can be done by simply adjusting the coefficients in the relationships for the morphological equilibrium in such a way that the morphology at the beginning of the simulation is the same as the morphological equilibrium. For Delft3D modelling, similar attempts are sometimes made by e.g. spinning up the sediment composition of the bed first without adjustment of the bed level. This is meant to limit the morphological changes at the beginning of the model simulation. This method works to a limited degree.

At present, there are no easy solutions for the problem. The main obstacle is the lack of understanding of the morphological equilibrium according to the model. Improving this understanding will require extensive fundamental research and is therefore not feasible in the short term. We can and must use the understanding we have in the morphological system for setting up and calibrating a morphodynamic model. In addition, we should also use our insights in particular regarding the limitations of our model. With the insights into the morphological system and the model we should try to understand the various aspects of the unrealistic behaviour of a model. Then we can decide how we should deal with the various problems. It is not absolutely necessary to solve every problem. A model will never be perfect. It is important that we have sufficient understanding of the possibilities and limitations of our models. Morphological modelling can certainly be useful for studies despite the limitations of the models.

B Results for individual Wadden Sea basins

In this appendix we list, from west to east, all individual tidal inlet systems of the (Dutch) Wadden Sea and present the following results for each inlet: intertidal flat characteristics, hypsometric curves, cross-throat sediment transport, cumulative sedimentation/erosion maps and water level analysis. Additionally, we present for each inlet a table with averaged basin sedimentation heights and rates, compared to SLR (rates). For the methodology of all the listed results, we refer the reader to Section 2.5 of this report.

All the results shown in this appendix are derived from six Wadden Sea model simulations run for the five different SLR scenarios (plus an additional hydrodynamic simulation without morphodynamic changes, used for comparison in the water level analysis).

B.1 Marsdiep / Texel inlet

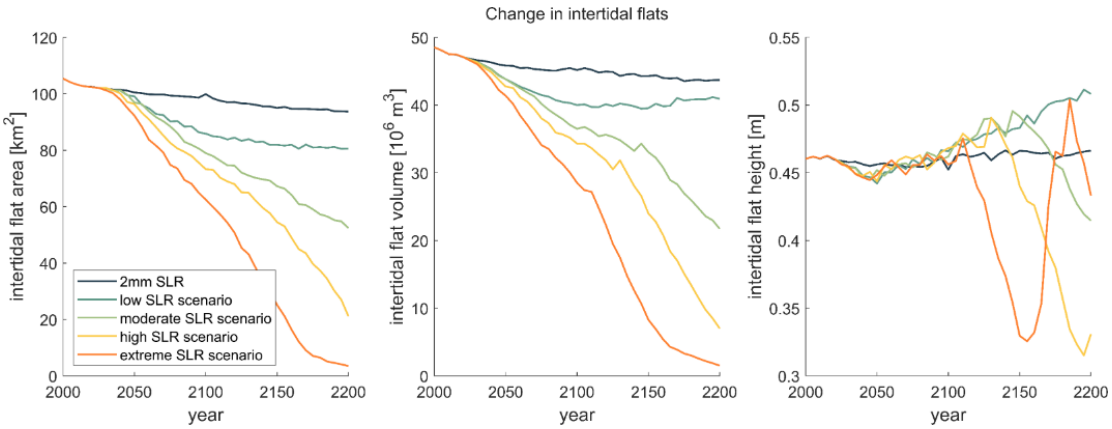

*Figure B.1.1. Intertidal area, volume and flat height over time for five different SLR scenarios, for the **Marsdiep/Texel** basin.*

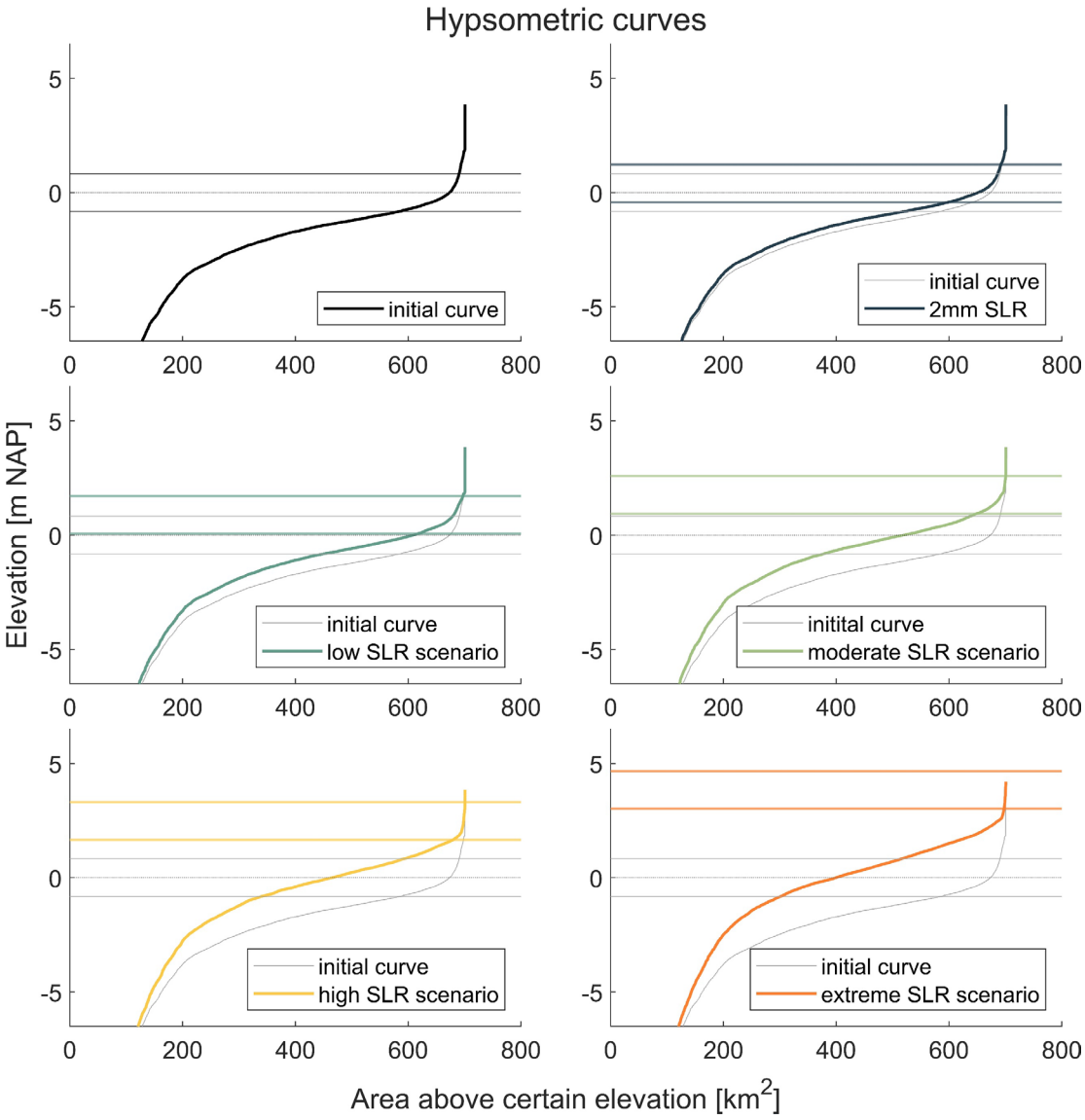

*Figure B.1.2. Hypsometric curves for the **Texel** basin, for different SLR scenarios. In the top left panel we show the initial curve, calculated from the input bathymetry. The two horizontal lines indicate the initial mean low and highwater levels. In all other panels, we plot the initial hypsometric curve, together with the respective water levels, as gray, thin lines for comparison. The mean low and highwater levels shift upwards with SLR, as indicated by the coloured horizontal lines in each panel. The legends in each panel specify the considered SLR scenario. The colour scheme for the SLR scenarios follows the rest of this report.*

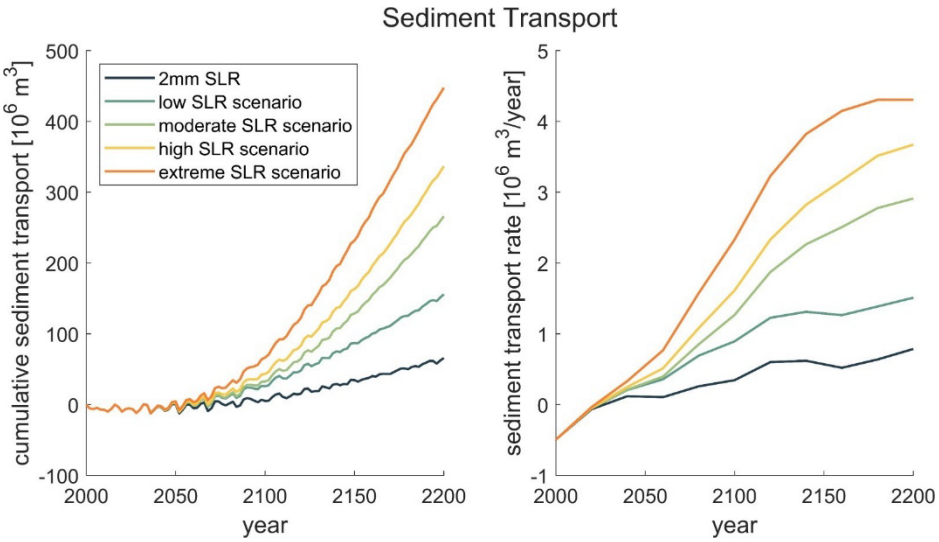

*Figure B.1.3. Cumulative sediment transport and yearly sediment transport rate through the inlet throat over time for five different SLR scenarios for the **Marsdiep/Texel** basin.*

Table B.1.1. Indication of drowning effect in the Marsdiep / Texel basin for different SLR scenarios. The basin area is 700.6 km^2 (derived from hypsometric curve).

SLR scenario	2 mm linear	low SLR	moderate SLR	high SLR	extreme SLR
$SLR_{cum,final}$ [m]	0.40	0.89	1.76	2.48	3.84
$\dot{d}_{SLR}$ [mm/year]	2	5	13.8	25	40
$t_{sed,final}$ [10^6 m^3]	65.7	155.8	266.0	336.0	447.6
$\dot{t}_{sed,final}$ [10^6 m^3/year]	0.79	1.51	2.91	3.67	4.30
$\overline{h}_{sed}$ [m]	0.09	0.22	0.38	0.48	0.64
$\dot{h}_{sed}$ [mm/year]	1.13	2.16	4.15	5.24	6.14
$\Delta h_{wd} = (SLR_{cum,final} - \overline{h}_{sed})$ [m]	0.31	0.67	1.38	2.0	3.20
$\frac{\dot{h}_{sed}}{\dot{d}_{SLR}}$	0.57	0.43	0.30	0.21	0.15

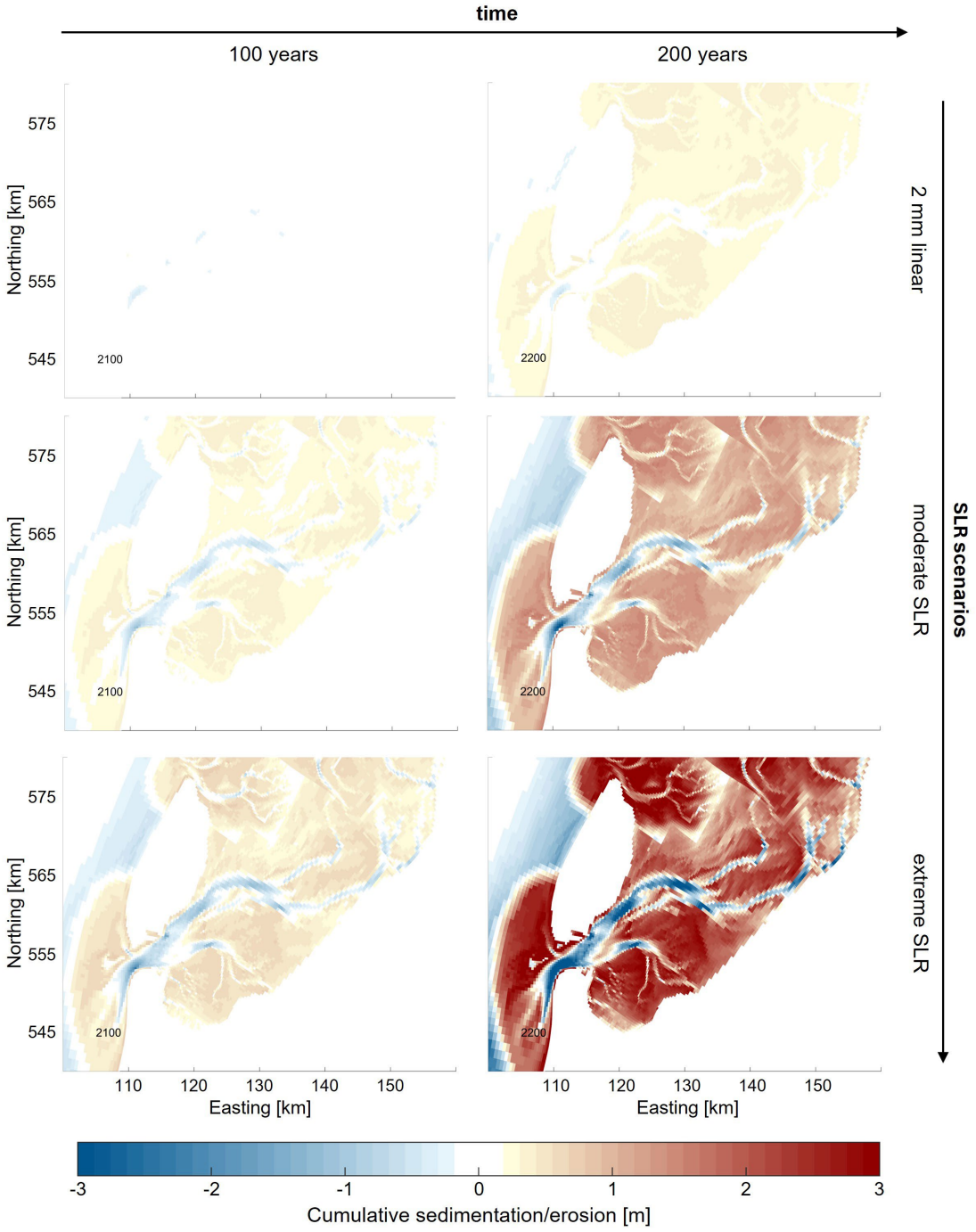

Figure B.1.4. Cumulative sedimentation / erosion patterns in the Marsdiep / Texel basin for two timesteps (after 100 years, left column, and 200 years, right column), as well as for three different SLR scenarios (respective rows). The years of the simulation period are printed as small, black numbers in the lower left corners of the maps. The colourbar shown at the bottom is valid for all panels. Note that the thin dams on the tidal divides between the basins cause disruptions in the pattern.

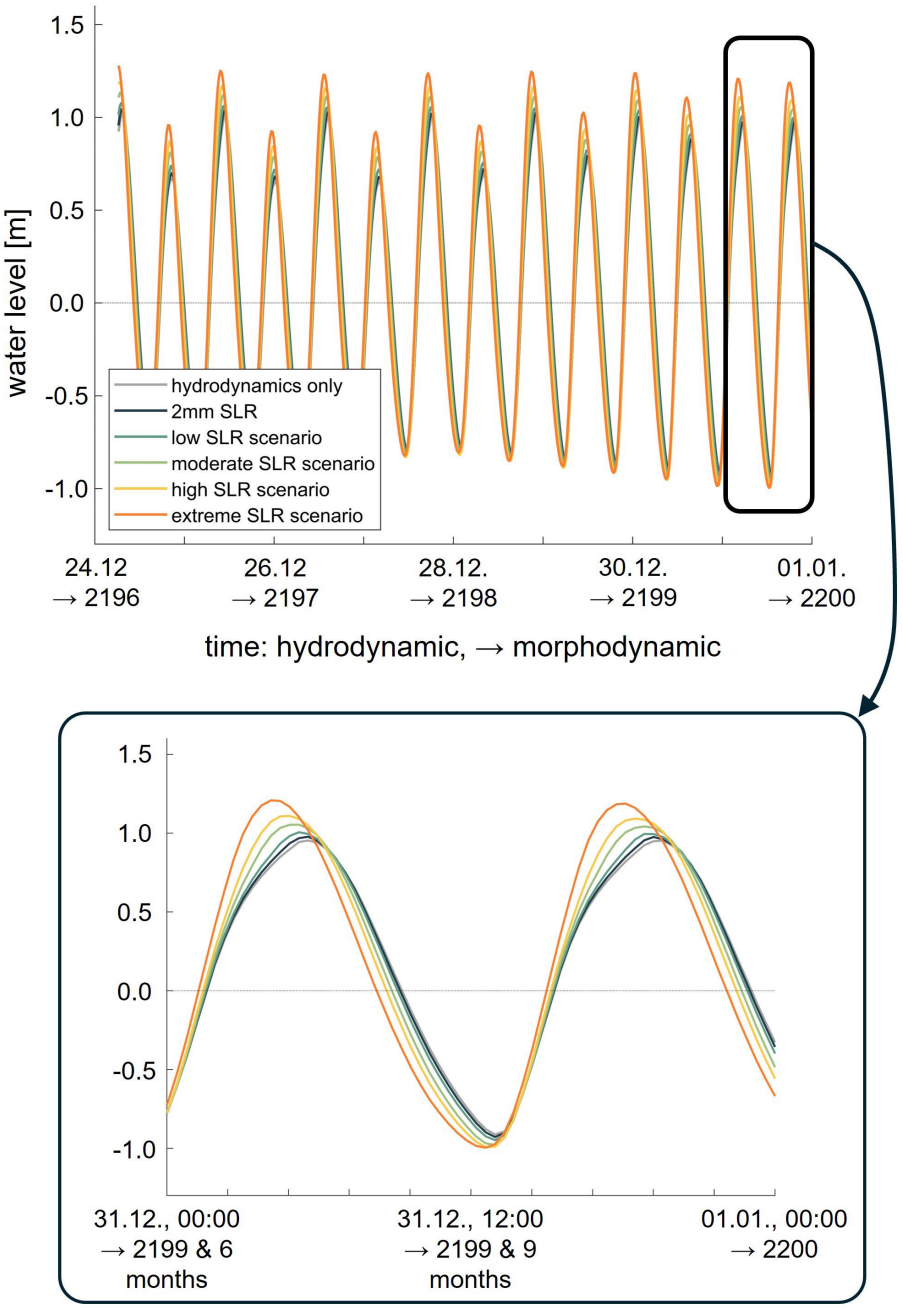

Figure B.1.5. Water levels for different SLR scenarios at a water level station in the Marsdiep / Texel basin (for the location of the station, see Figure 4.3), plotted for the last week of the hydrodynamic simulation time, i.e. the last four years for the morphodynamic simulation period, where the changes in water level due to the imposed SLR will be most noticeable. As base line, we plot the water levels of a purely hydrodynamic simulation as a grey line, see the legend in the upper panel. The lower panel is a zoom-in on the last two tidal cycles.

B.2 Eierland inlet

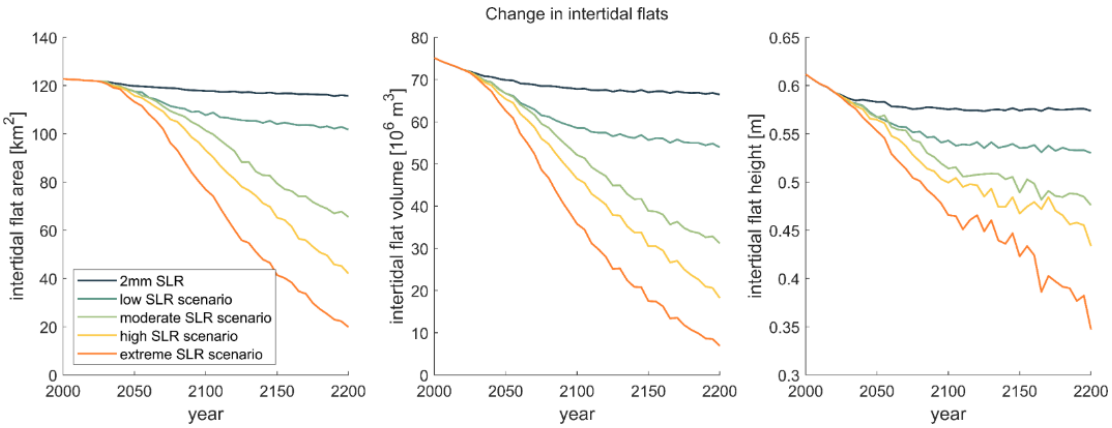

*Figure B.2.1. Intertidal area, volume, and flat height over time for five different SLR scenarios for the **Eierland** basin.*

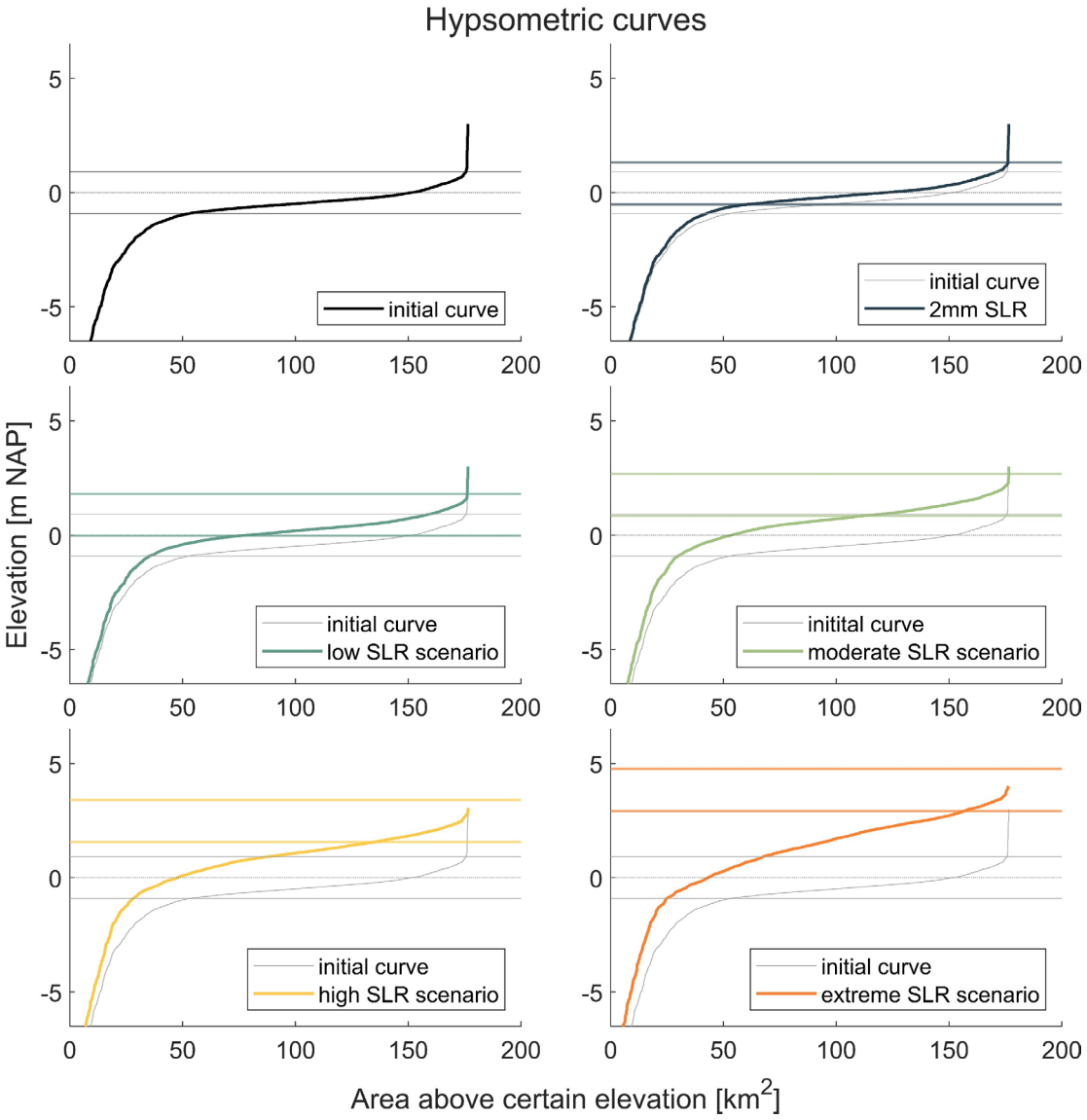

*Figure B.2.2. Hypsometric curves for the **Eierland** basin, for different SLR scenarios. In the top left panel we show the initial curve, calculated from the input bathymetry. The two horizontal lines indicate the mean low and highwater levels. In all other panels, we plot the initial hypsometric curve, together with the respective water levels, as gray, thin lines for comparison. The mean low and highwater levels shift upwards with SLR, as indicated by the coloured horizontal lines in each panel. The legends in each panel specify the considered SLR scenario. The colour scheme for the SLR scenarios follows the rest of this report.*

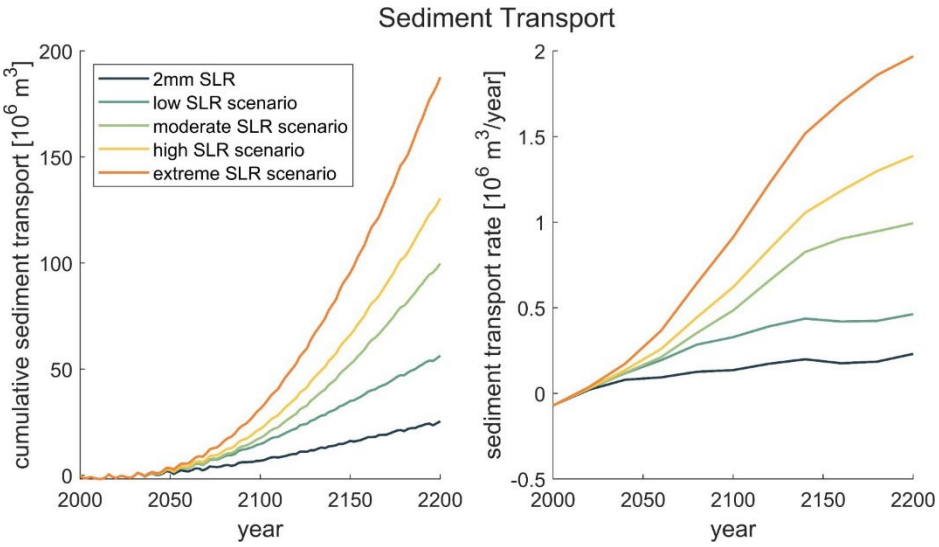

*Figure B.2.3. Cumulative sediment transport and yearly sediment transport rate through the inlet throat over time for five different SLR scenarios for the **Eierland** basin.*

Table B.2.1. Indication of drowning effect in the Eierland basin for different SLR scenarios. The basin area is 176.5 km² (derived from hypsometric curve).

SLR scenario	2 mm linear	low SLR	moderate SLR	high SLR	extreme SLR
$SLR_{cum,final}$ [m]	0.40	0.89	1.76	2.48	3.84
$\dot{d}_{SLR}$ [mm/year]	2	5	13.8	25	40
$t_{sed,final}$ [10^6 m^3]	24.5	56.3	99.8	130.5	187.6
$\dot{t}_{sed,final}$ [10^6 m^3/year]	0.23	0.46	0.99	1.39	1.97
$\overline{h}_{sed}$ [m]	0.14	0.32	0.57	0.74	1.06
$\dot{h}_{sed}$ [mm/year]	1.30	2.61	5.61	7.88	11.16
$\Delta h_{wd} = (SLR_{cum,final} - \overline{h}_{sed})$ [m]	0.26	0.57	1.19	1.74	2.78
$\frac{\dot{h}_{sed}}{\dot{d}_{SLR}}$	0.65	0.52	0.41	0.32	0.28

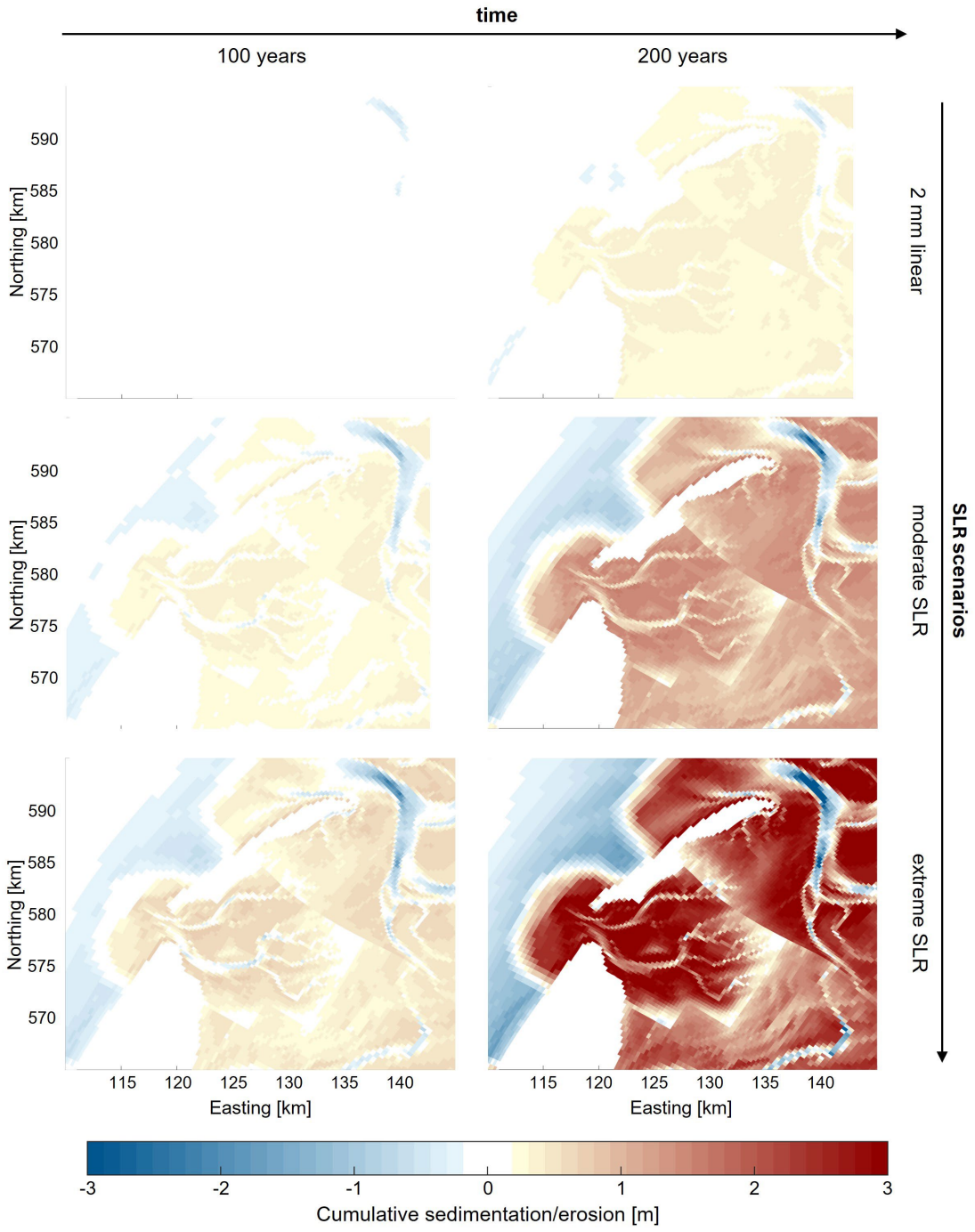

Figure B.2.4. Cumulative sedimentation / erosion patterns in the Eierland basin for two timesteps (after 100 years, left column, and 200 years, right column), as well as for three different SLR scenarios (respective rows). The years of the simulation period are printed as small, black numbers in the lower left corners of the maps. The colourbar shown at the bottom is valid for all panels. Note that the thin dams on the tidal divides between the basins cause disruptions in the pattern.

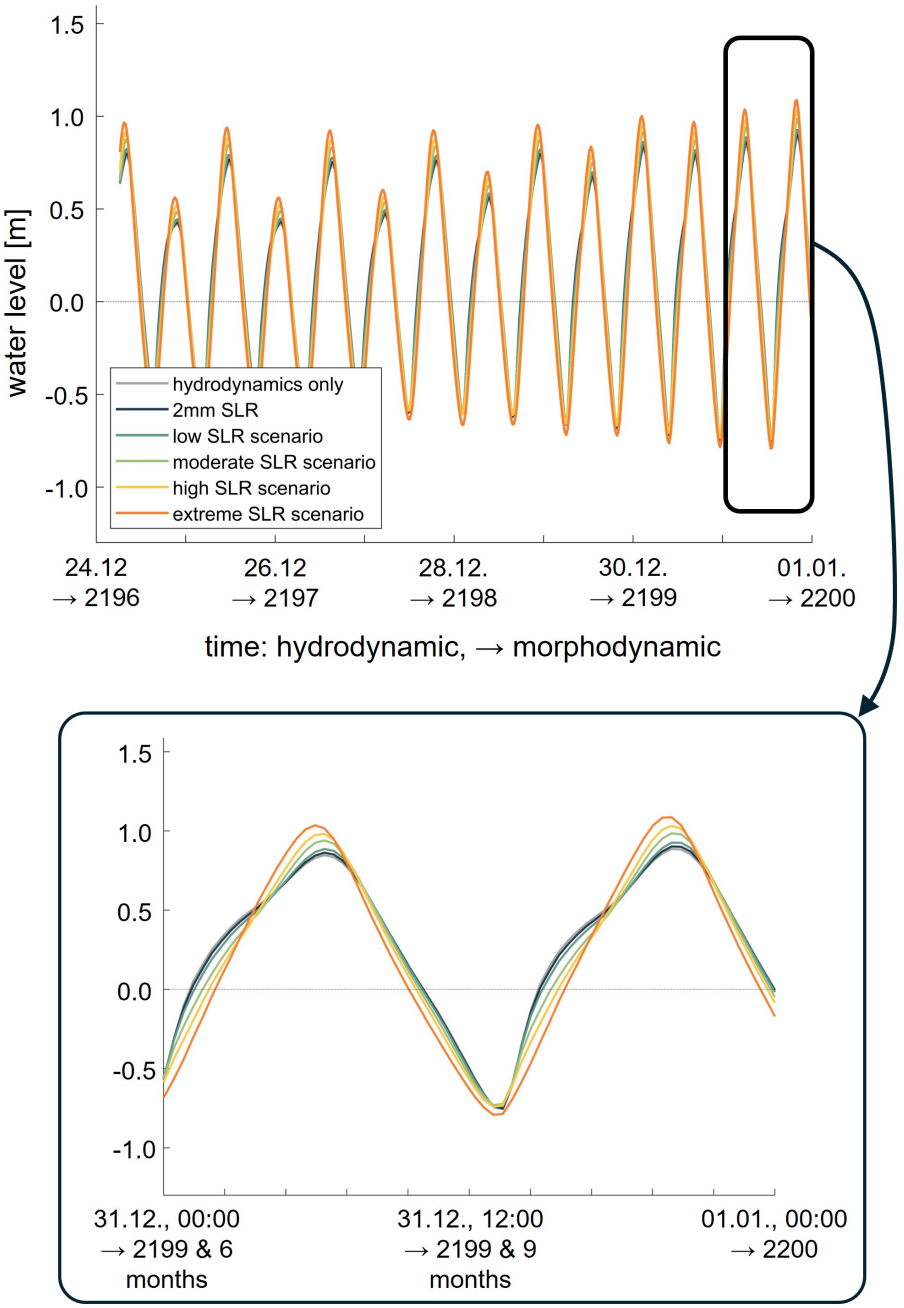

Figure B.2.5. Water levels for different SLR scenarios at a water level station in the Eierland basin (for the location of the station, see Figure 4.3), plotted for the last week of the hydrodynamic simulation time, i.e. the last four years for the morphodynamic simulation period, where the changes in water level due to the imposed SLR will be most noticeable. As base line, we plot the water levels of a purely hydrodynamic simulation as a grey line, see the legend in the upper panel. The lower panel is a zoom-in on the last two tidal cycles.

B.3 Vlie inlet

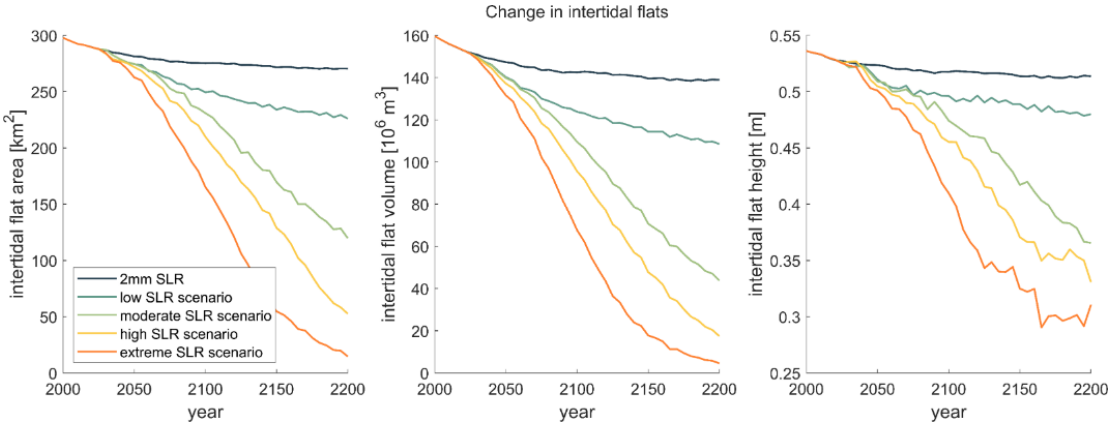

*Figure B.3.1. Intertidal area, volume, and flat height over time for five different SLR scenarios for the **Vlie** basin.*

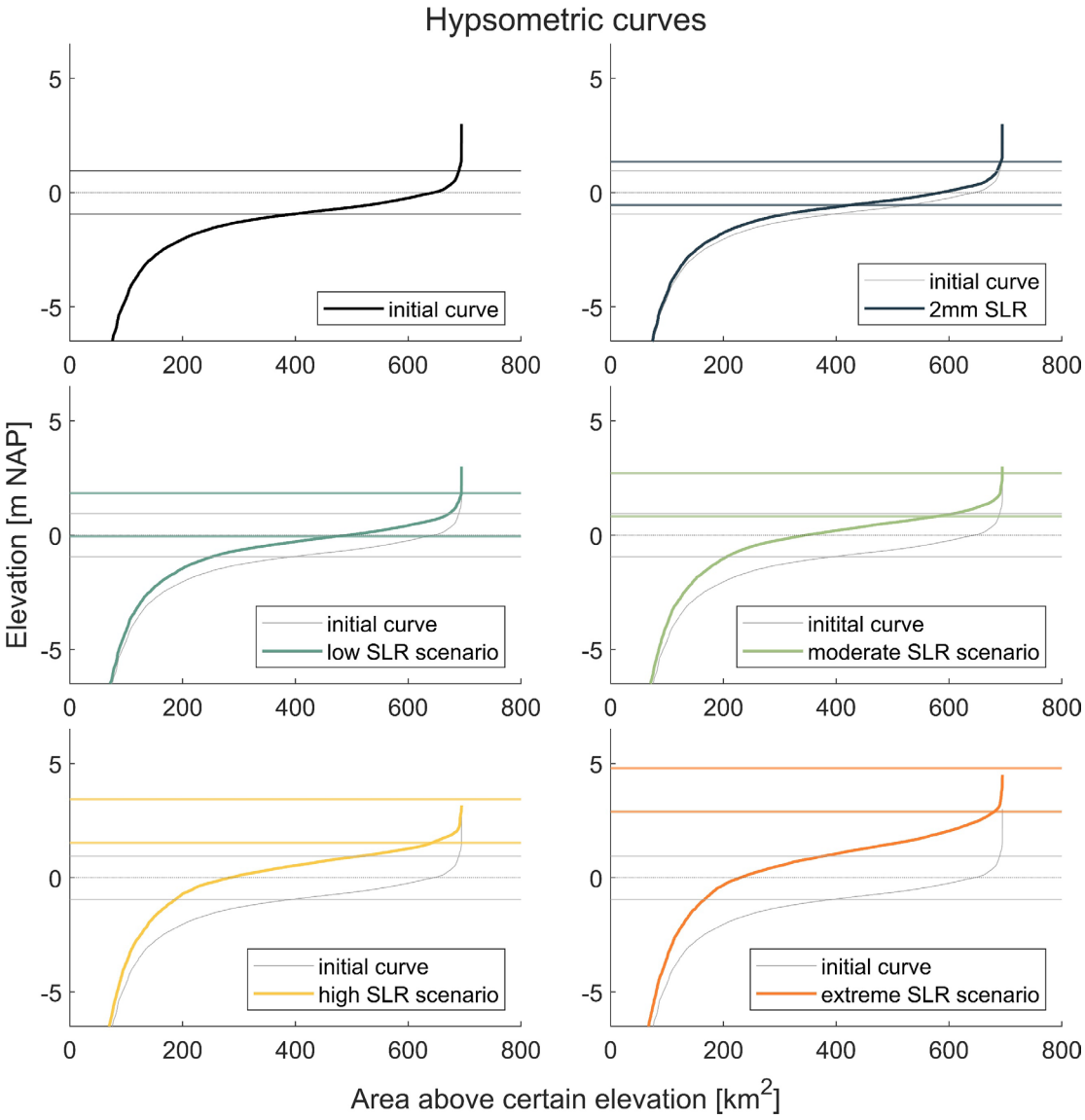

*Figure B.3.2. Hypsometric curves for the **Vlie** basin, for different SLR scenarios. In the top left panel we show the initial curve, calculated from the input bathymetry. The two horizontal lines indicate the mean low and highwater levels. In all other panels, we plot the initial hypsometric curve, together with the respective water levels, as gray, thin lines for comparison. The mean low and highwater levels shift upwards with SLR, as indicated by the coloured horizontal lines in each panel. The legends in each panel specify the considered SLR scenario. The colour scheme for the SLR scenarios follows the rest of this report.*

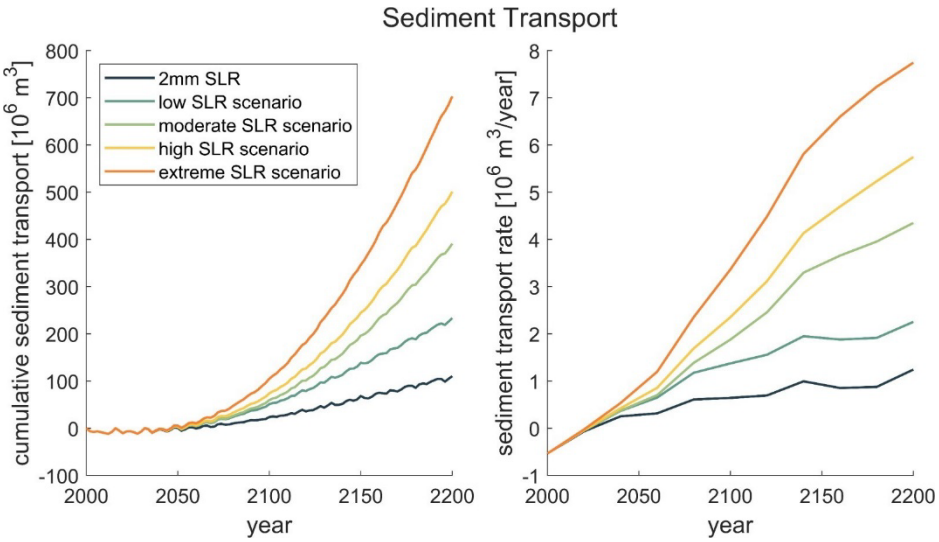

*Figure B.3.3. Cumulative sediment transport and yearly sediment transport rate through the inlet throat over time for five different SLR scenarios for the **Vlie** basin.*

Table B.3.1. Indication of drowning effect in the Vlie basin for different SLR scenarios. The basin area is 694.5 km² (derived from hypsometric curve).

SLR scenario	2 mm linear	low SLR	moderate SLR	high SLR	extreme SLR
$SLR_{cum,final}$ [m]	0.40	0.89	1.76	2.48	3.84
$\dot{d}_{SLR}$ [mm/year]	2	5	13.8	25	40
$t_{sed,final}$ [10^6 m^3]	110.4	233.4	391.1	501.2	703.1
$\dot{t}_{sed,final}$ [10^6 m^3/year]	1.24	2.25	4.35	5.75	7.74
$\overline{h}_{sed}$ [m]	0.16	0.34	0.56	0.72	1.01
$\dot{h}_{sed}$ [mm/year]	1.79	3.24	6.26	8.28	11.14
$\Delta h_{wd} = (SLR_{cum,final} - \overline{h}_{sed})$ [m]	0.24	0.55	1.20	1.76	2.83
$\frac{\dot{h}_{sed}}{\dot{d}_{SLR}}$	0.90	0.65	0.45	0.33	0.28

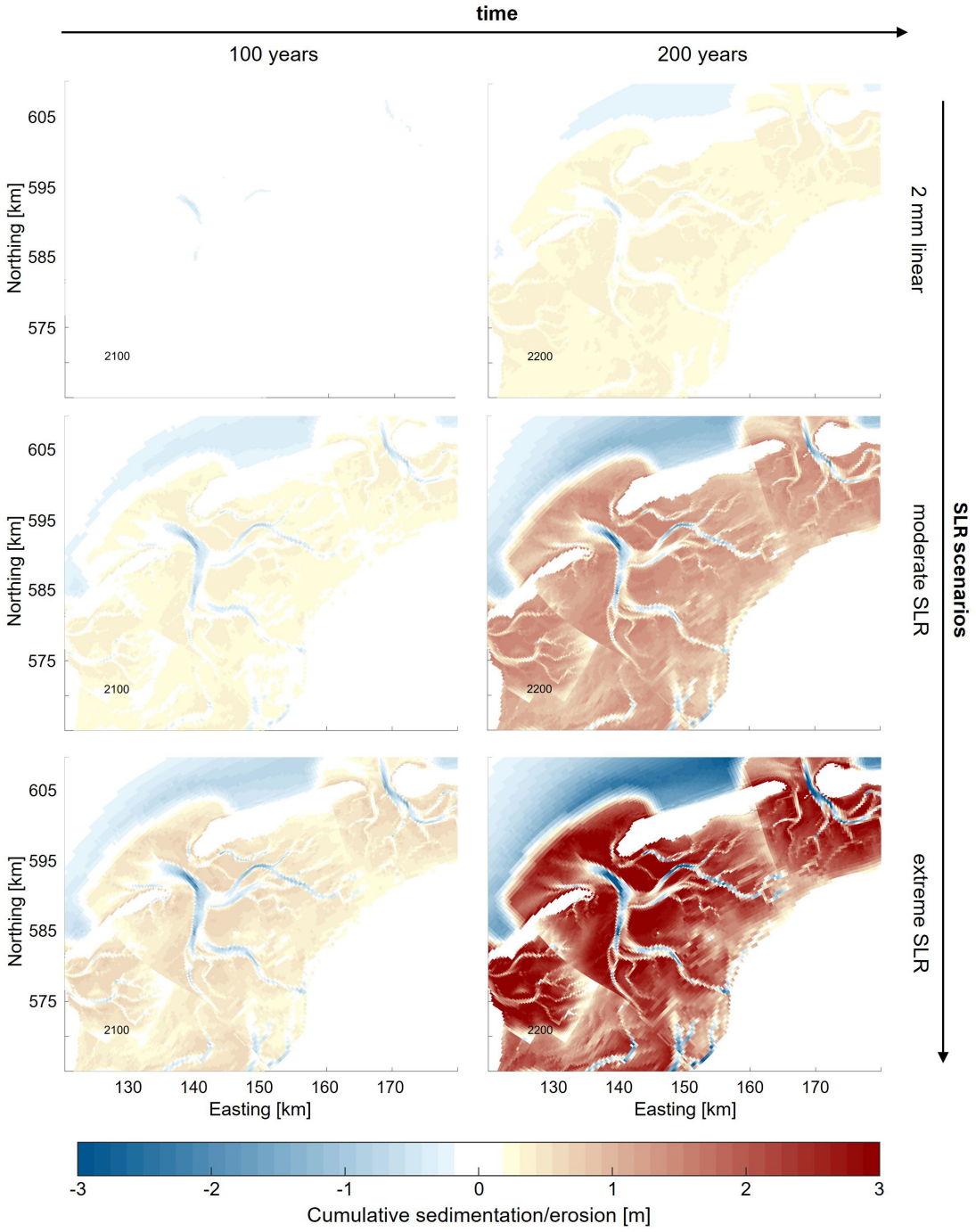

Figure B.3.4. Cumulative sedimentation / erosion patterns in the Vlie basin for two timesteps (after 100 years, left column, and 200 years, right column), as well as for three different SLR scenarios (respective rows). The years of the simulation period are printed as small, black numbers in the lower left corners of the maps. The colourbar shown at the bottom is valid for all panels. Note that the thin dams on the tidal divides between the basins cause disruptions in the pattern.

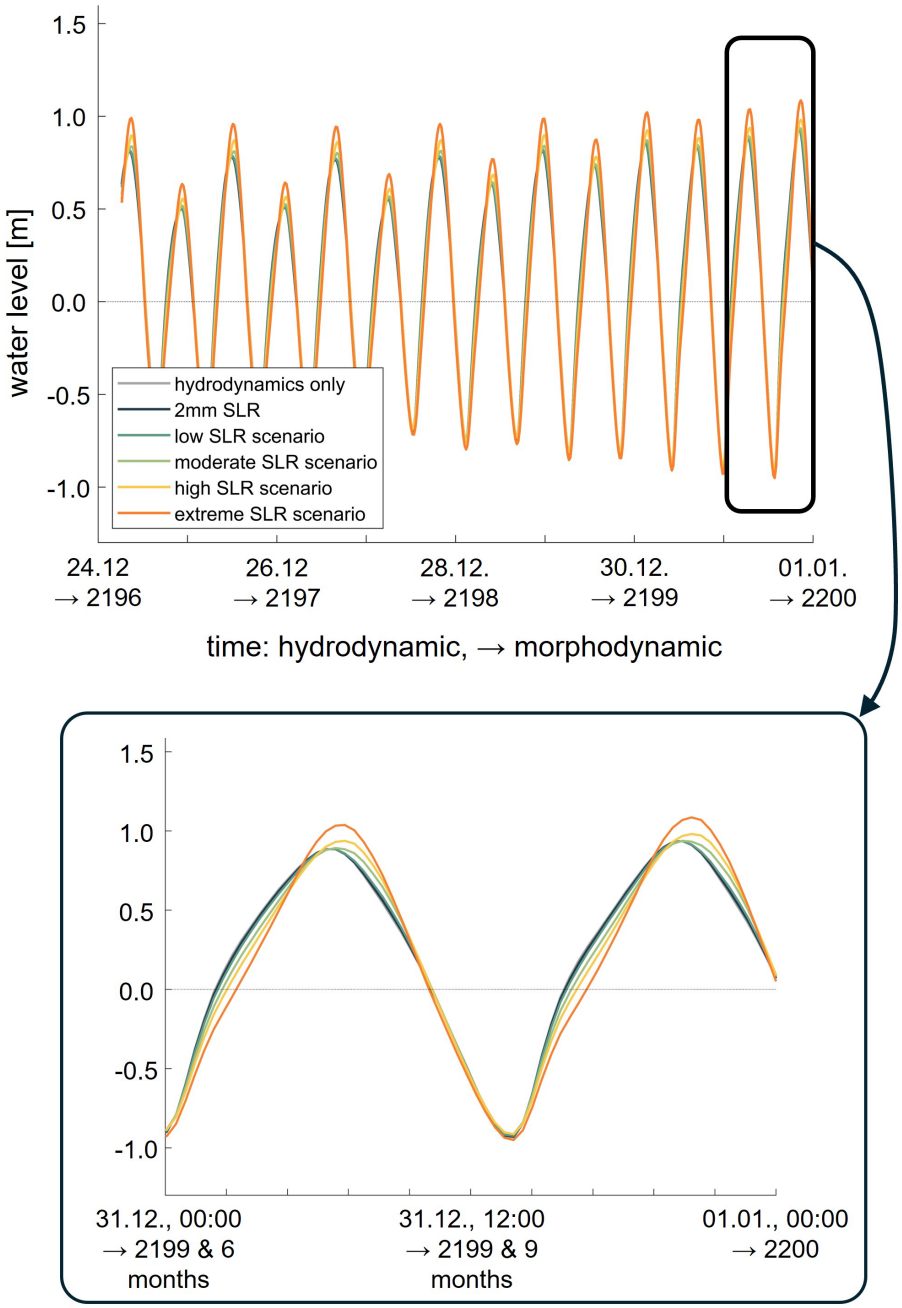

Figure B.3.5. Water levels for different SLR scenarios at a water level station in the Vlie basin (for the location of the station, see Figure 4.3), plotted for the last week of the hydrodynamic simulation time, i.e. the last four years for the morphodynamic simulation period, where the changes in water level due to the imposed SLR will be most noticeable. As base line, we plot the water levels of a purely hydrodynamic simulation as a grey line, see the legend in the upper panel. The lower panel is a zoom-in on the last two tidal cycles.

B.4 Borndiep inlet / Ameland basin

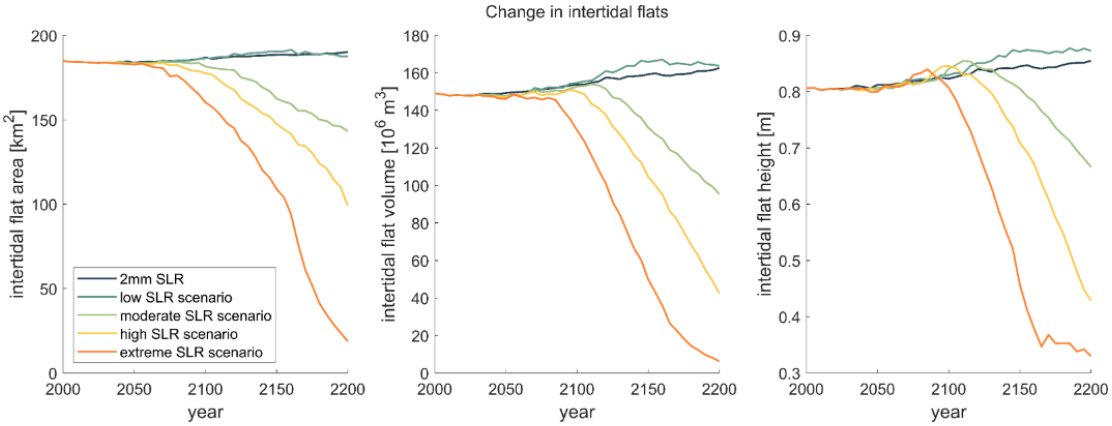

*Figure B.4.1. Intertidal area, volume, and flat height over time for five different SLR scenarios for the **Ameland** basin.*

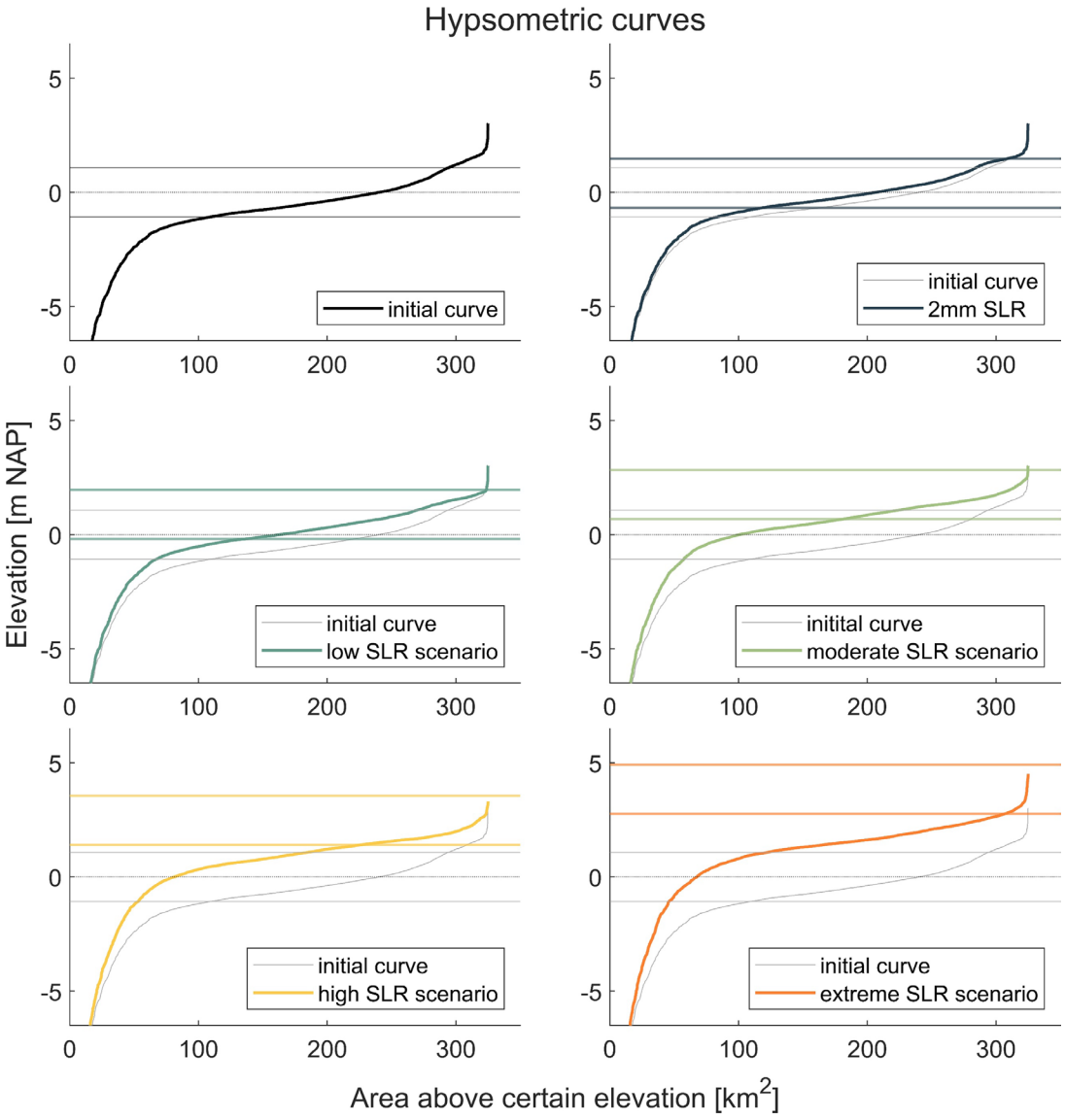

*Figure B.4.2. Hypsometric curves for the **Ameland** basin, for different SLR scenarios. In the top left panel we show the initial curve, calculated from the input bathymetry. The two horizontal lines indicate the mean low and highwater levels. In all other panels, we plot the initial hypsometric curve, together with the respective water levels, as gray, thin lines for comparison. The mean low and highwater levels shift upwards with SLR, as indicated by the coloured horizontal lines in each panel. The legends in each panel specify the considered SLR scenario. The colour scheme for the SLR scenarios follows the rest of this report.*

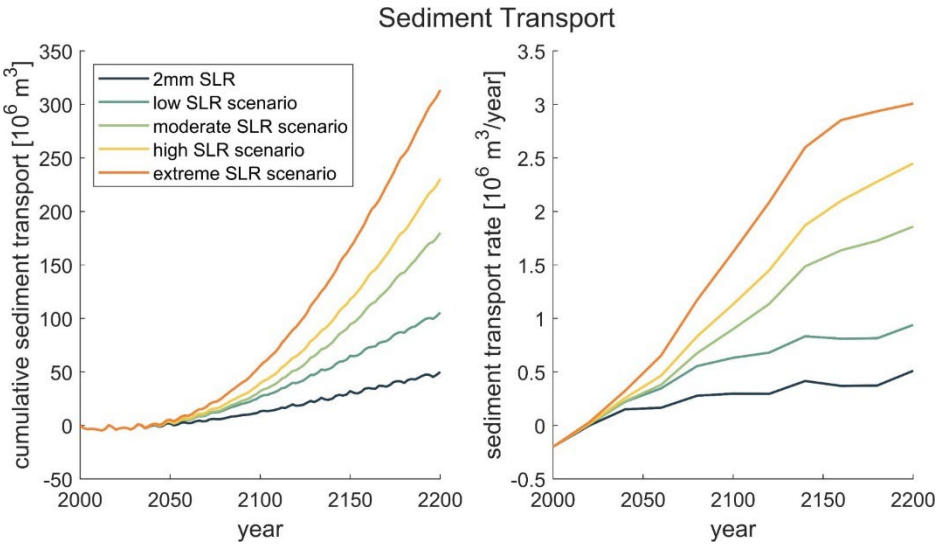

*Figure B.4.3. Cumulative sediment transport and yearly sediment transport rate through the inlet throat over time for five different SLR scenarios for the **Ameland** basin.*

Table B.4.1. Indication of drowning effect in the Ameland basin for different SLR scenarios. The basin area is 324.8 km² (derived from hypsometric curve).

SLR scenario	2 mm linear	low SLR	moderate SLR	high SLR	extreme SLR
$SLR_{cum,final}$ [m]	0.40	0.89	1.76	2.48	3.84
$\dot{d}_{SLR}$ [mm/year]	2	5	13.8	25	40
$t_{sed,final}$ [10^6 m^3]	50.0	105.4	180.1	230.4	313.5
$\dot{t}_{sed,final}$ [10^6 m^3/year]	0.51	0.94	1.86	2.45	3.01
$\overline{h}_{sed}$ [m]	0.15	0.32	0.55	0.71	0.97
$\dot{h}_{sed}$ [mm/year]	1.57	2.89	5.73	7.54	9.27
$\Delta h_{wd} = (SLR_{cum,final} - \overline{h}_{sed})$ [m]	0.25	0.57	1.21	1.77	2.87
$\frac{\dot{h}_{sed}}{\dot{d}_{SLR}}$	0.79	0.58	0.42	0.30	0.23

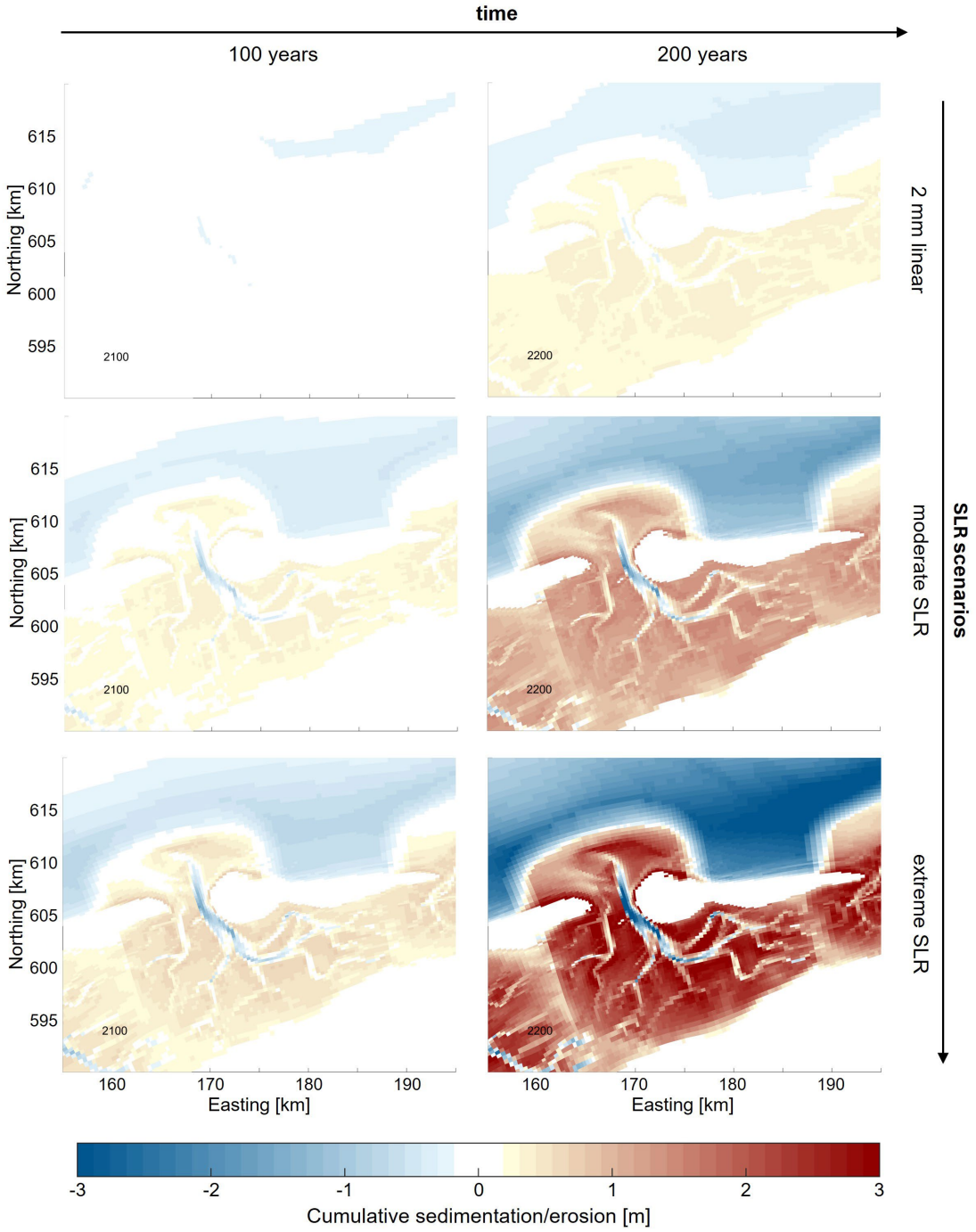

Figure B.4.4. Cumulative sedimentation / erosion patterns in the Ameland basin for two timesteps (after 100 years, left column, and 200 years, right column), as well as for three different SLR scenarios (respective rows). The years of the simulation period are printed as small, black numbers in the lower left corners of the maps. The colourbar shown at the bottom is valid for all panels. Note that the thin dams on the tidal divides between the basins cause disruptions in the pattern.

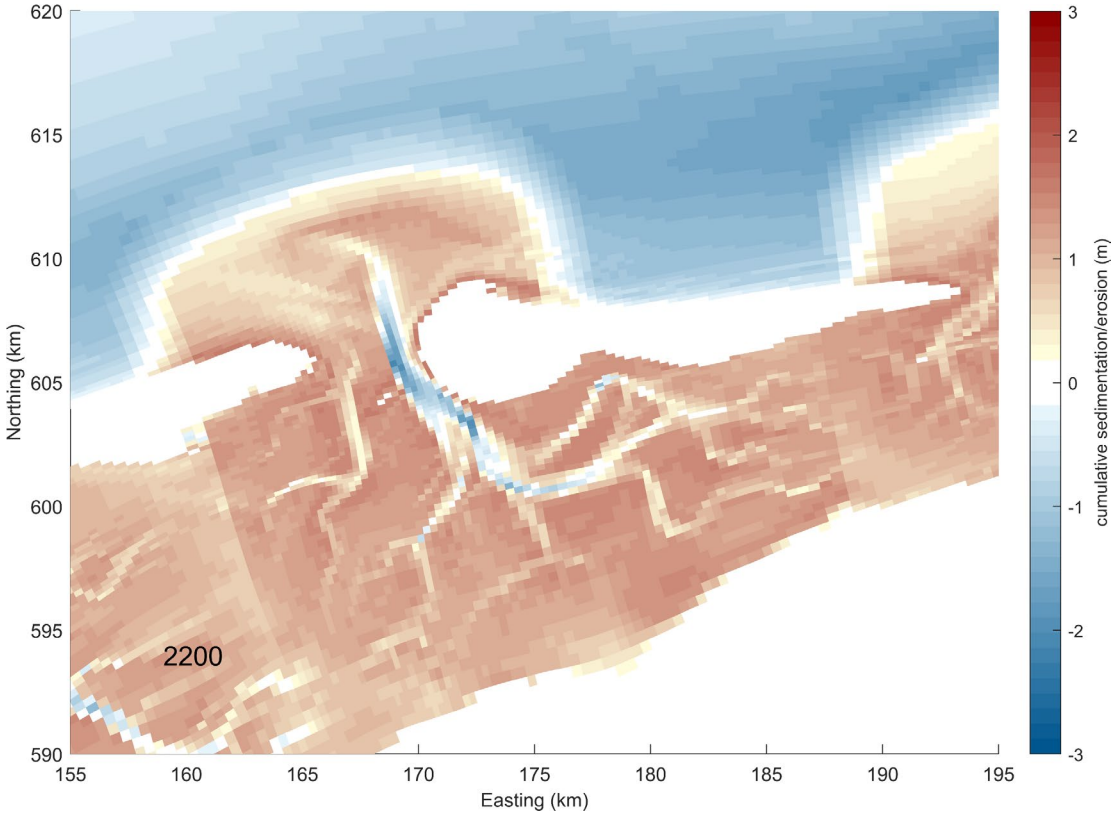

Figure B.4.5. Cumulative sedimentation/erosion map for a moderate SLR scenario at the end of the simulation period (2200, as indicated by the small number in the lower left corner of the plot). Note that the thin dams on the tidal divides cause disruptions in the pattern between the individual basins. The same figure is also presented in Figure B.4.4, in the centre right panel.

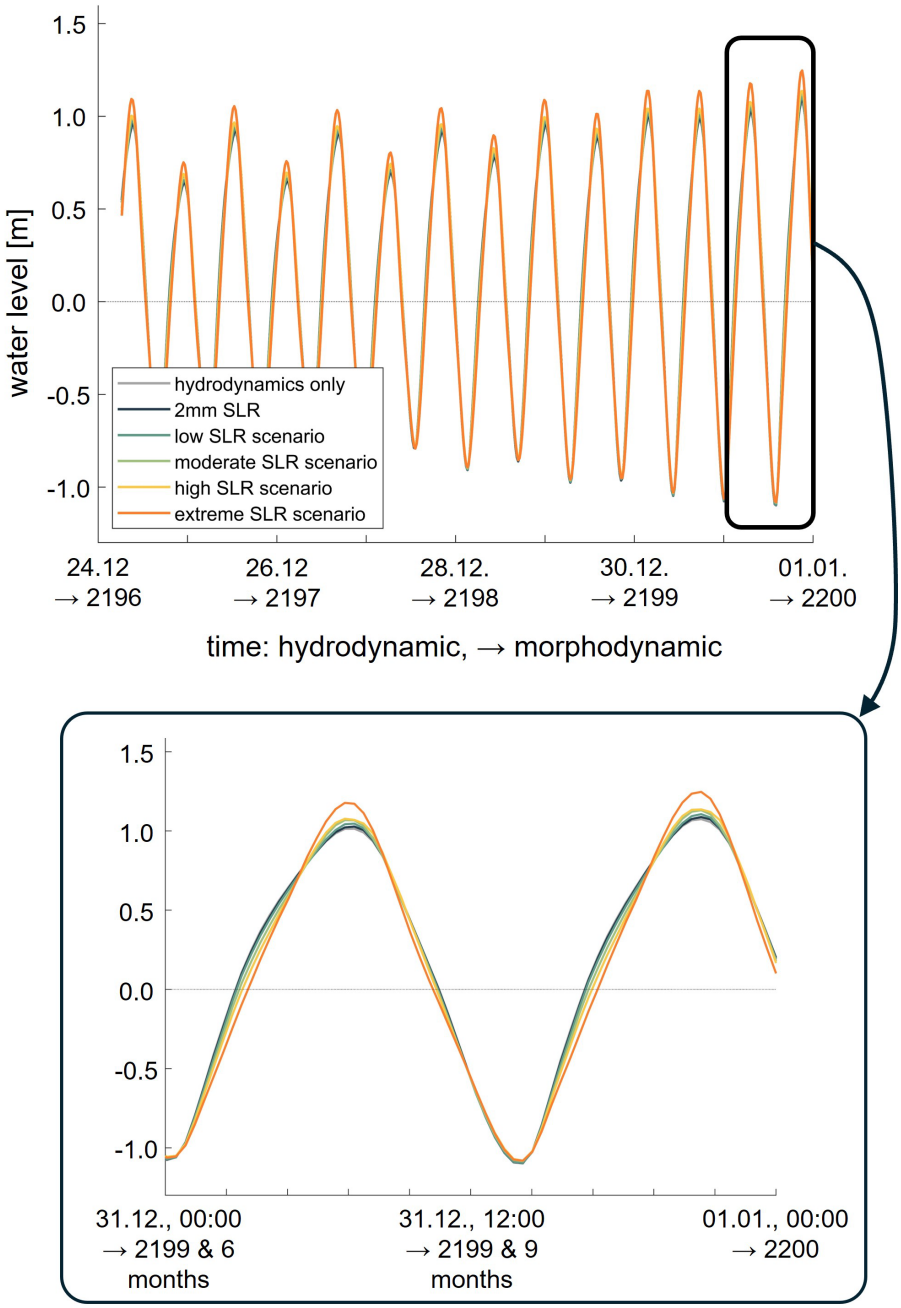

Figure B.4.6. Water levels for different SLR scenarios at a water level station in the Ameland basin (for the location of the station, see Figure 4.3), plotted for the last week of the hydrodynamic simulation time, i.e. the last four years for the morphodynamic simulation period, where the changes in water level due to the imposed SLR will be most noticeable. As base line, we plot the water levels of a purely hydrodynamic simulation as a grey line, see the legend in the upper panel. The lower panel is a zoom-in on the last two tidal cycles.

B.5 Pinkegat inlet

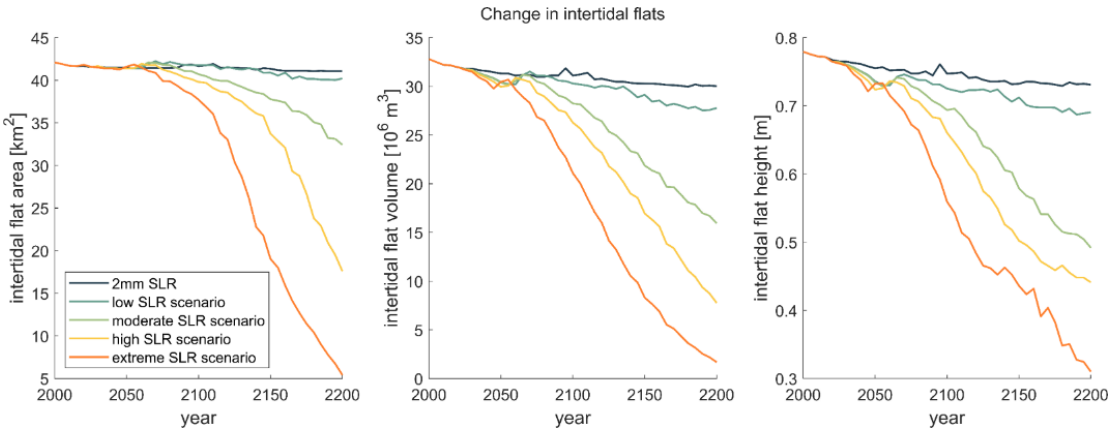

*Figure B.5.1. Intertidal area, volume, and flat height over time for five different SLR scenarios for the **Pinkegat** basin.*

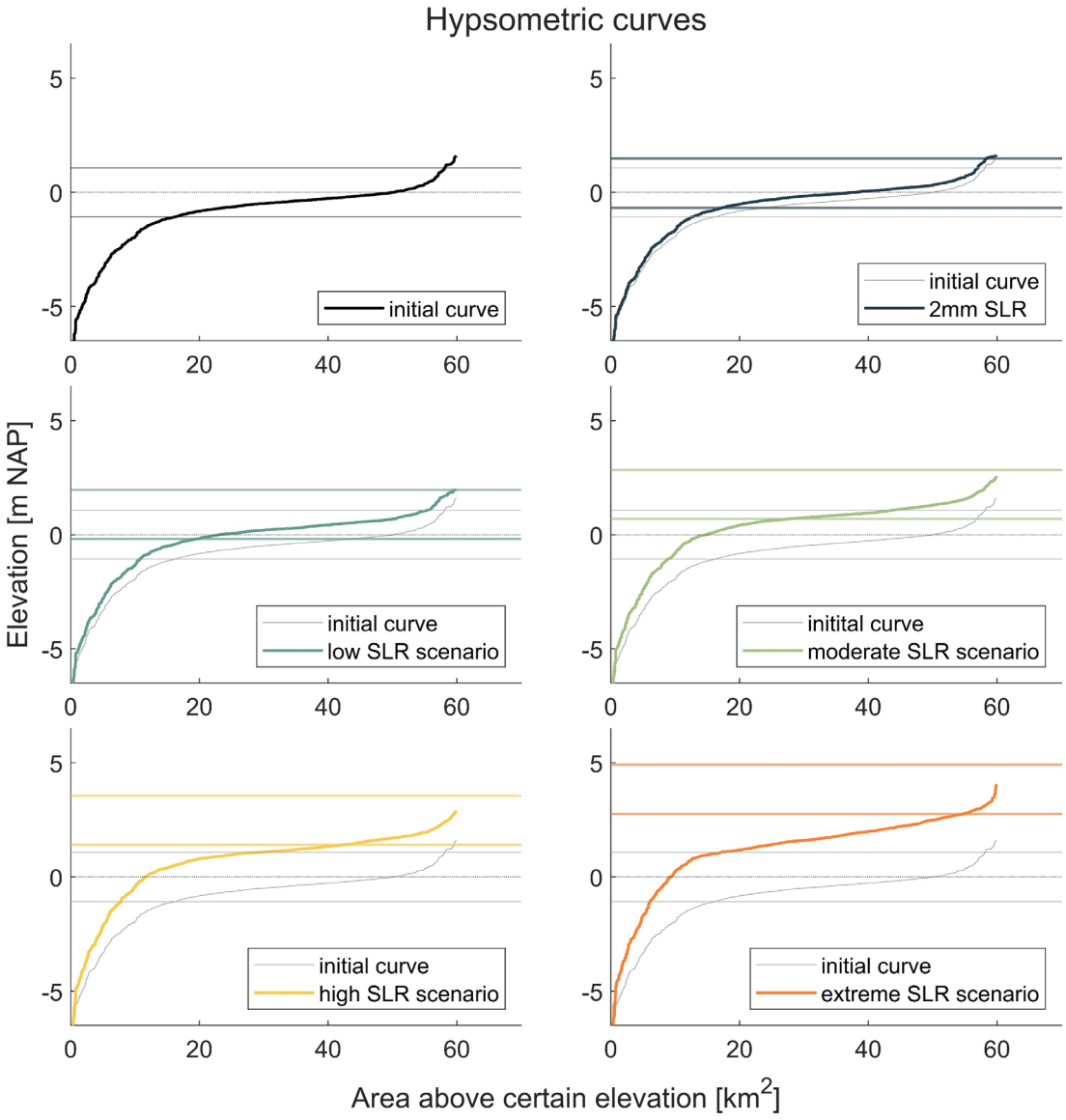

*Figure B.5.2. Hypsometric curves for the **Pinkegat** basin, for different SLR scenarios. In the top left panel we show the initial curve, calculated from the input bathymetry. The two horizontal lines indicate the mean low and highwater levels. In all other panels, we plot the initial hypsometric curve, together with the respective water levels, as gray, thin lines for comparison. The mean low and highwater levels shift upwards with SLR, as indicated by the coloured horizontal lines in each panel. The legends in each panel specify the considered SLR scenario. The colour scheme for the SLR scenarios follows the rest of this report.*

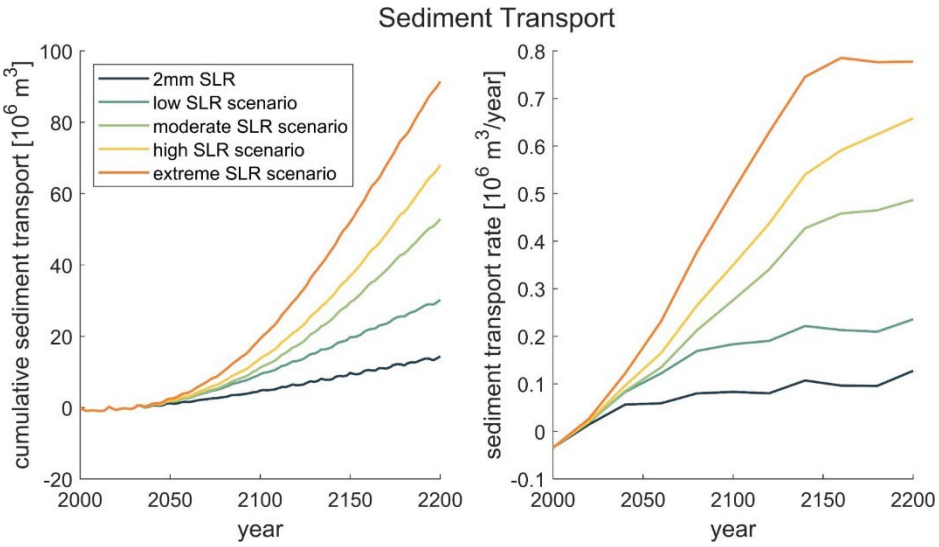

*Figure B.5.3. Cumulative sediment transport and yearly sediment transport rate through the inlet throat over time for five different SLR scenarios for the **Pinkegat** basin.*

Table B.5.1. Indication of drowning effect in the Pinkegat basin for different SLR scenarios. The basin area is 59.9 km² (derived from hypsometric curve).

SLR scenario	2 mm linear	low SLR	moderate SLR	high SLR	extreme SLR
$SLR_{cum,final}$ [m]	0.40	0.89	1.76	2.48	3.84
$\dot{d}_{SLR}$ [mm/year]	2	5	13.8	25	40
$t_{sed,final}$ [10^6 m^3]	14.4	30.2	52.9	68.0	91.4
$\dot{t}_{sed,final}$ [10^6 m^3/year]	0.13	0.24	0.49	0.66	0.78
$\overline{h}_{sed}$ [m]	0.24	0.50	0.88	1.14	1.53
$\dot{h}_{sed}$ [mm/year]	2.17	4.01	8.18	11.02	13.02
$\Delta h_{wd} = (SLR_{cum,final} - \overline{h}_{sed})$ [m]	0.16	0.39	0.88	1.34	2.31
$\frac{\dot{h}_{sed}}{\dot{d}_{SLR}}$	1.09	0.80	0.59	0.44	0.33

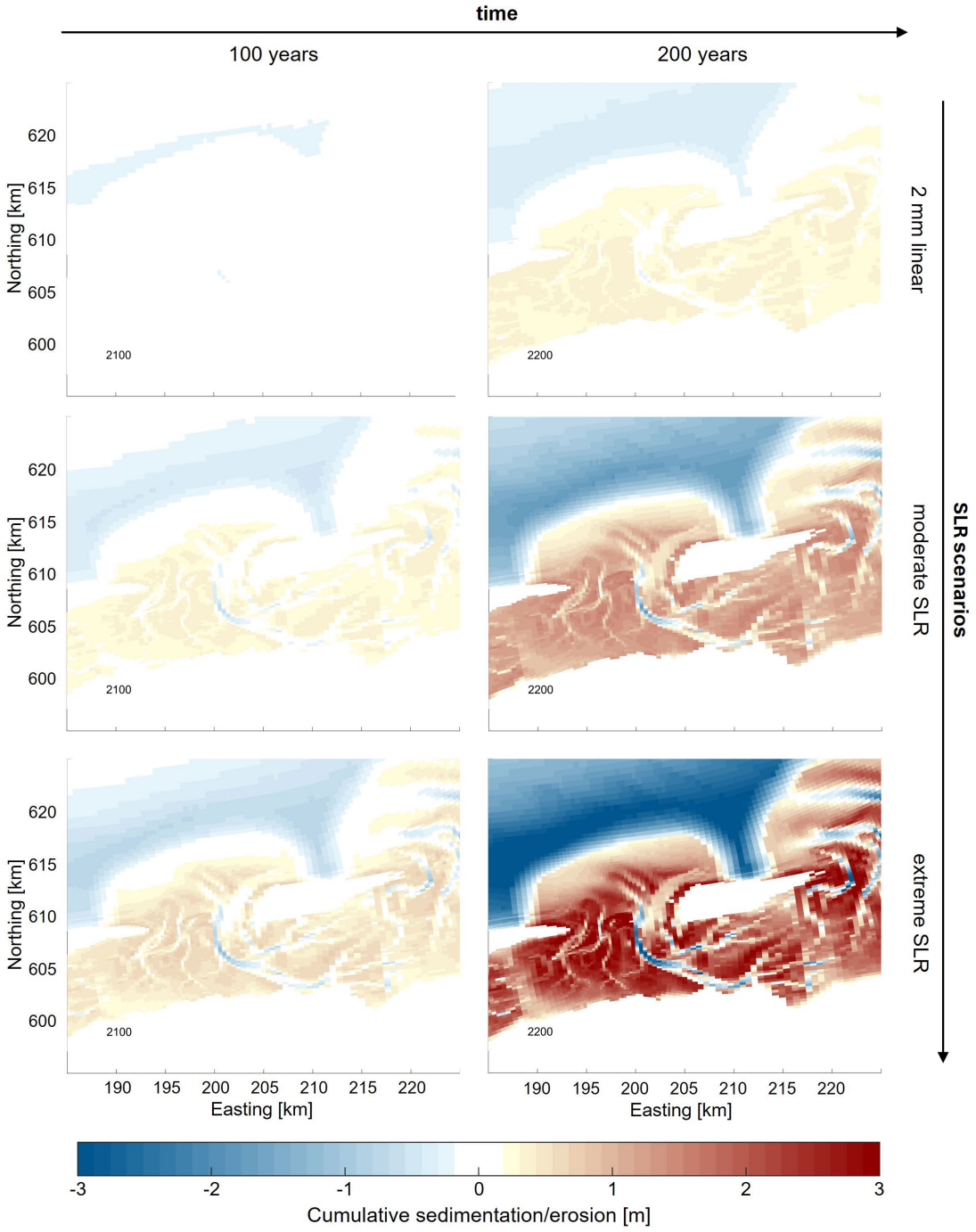

Figure B.5.4. Cumulative sedimentation / erosion patterns in the Frisian inlet (i.e. the Pinkegat basin and the Zoutkamperlaag basin) for two timesteps (after 100 years, left column, and 200 years, right column), as well as for three different SLR scenarios (respective rows). The years of the simulation period are printed as small, black numbers in the lower left corners of the maps. The colourbar shown at the bottom is valid for all panels. Note that the thin dams on the tidal divides between the basins cause disruptions in the pattern.

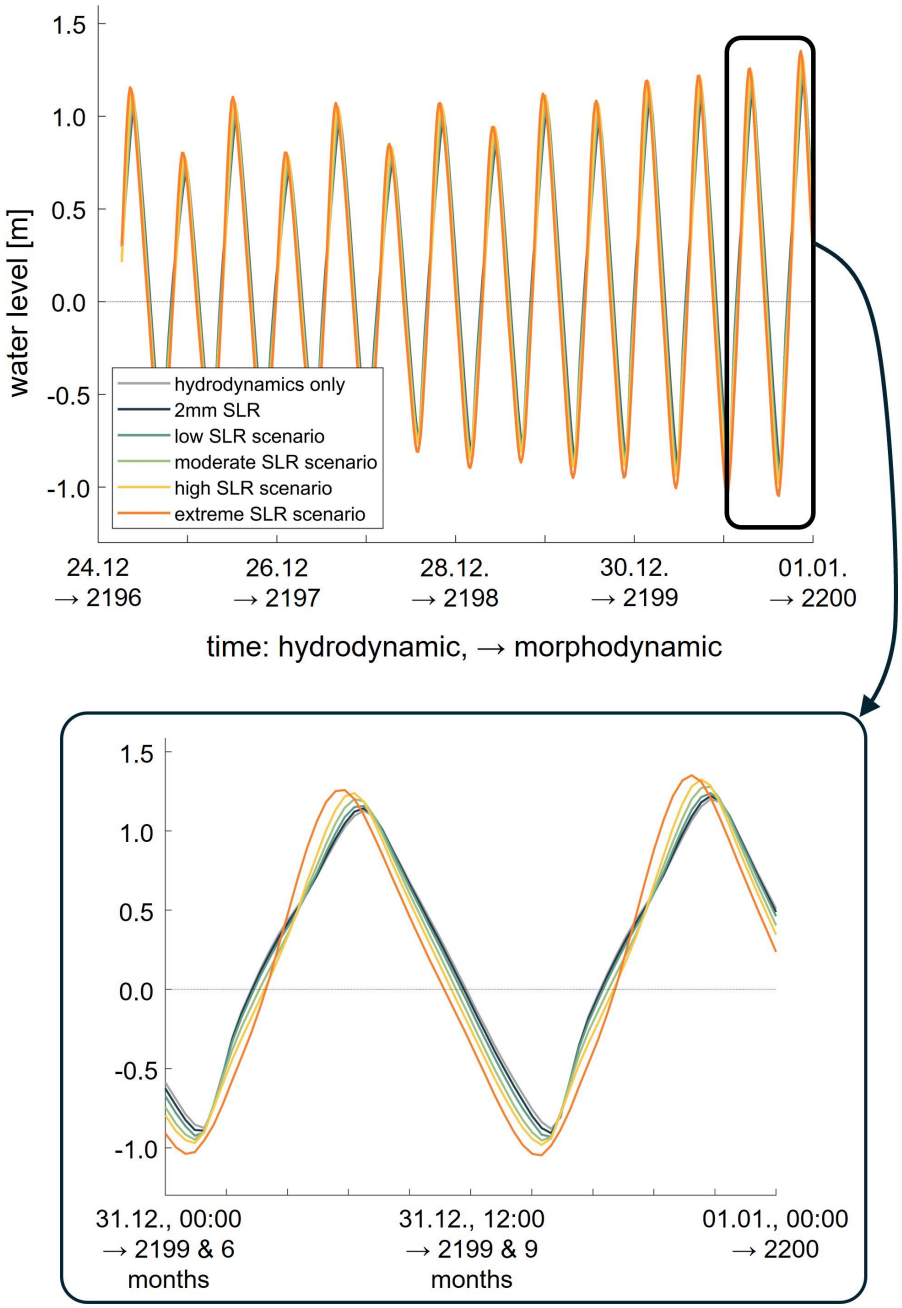

Figure B.5.5. Water levels for different SLR scenarios at a water level station in the Pinkegat basin (for the location of the station, see Figure 4.3), plotted for the last week of the hydrodynamic simulation time, i.e. the last four years for the morphodynamic simulation period, where the changes in water level due to the imposed SLR will be most noticeable. As base line, we plot the water levels of a purely hydrodynamic simulation as a gray line, see the legend in the upper panel. The lower panel is a zoom-in on the last two tidal cycles.

B.6 Zoutkamperlaag inlet

For the sedimentation/erosion pattern overview plot, see previous chapter, as Pinkegat and Zoutkamperlaag are plotted together as Frisian Inlet (Figure B.5.4.).

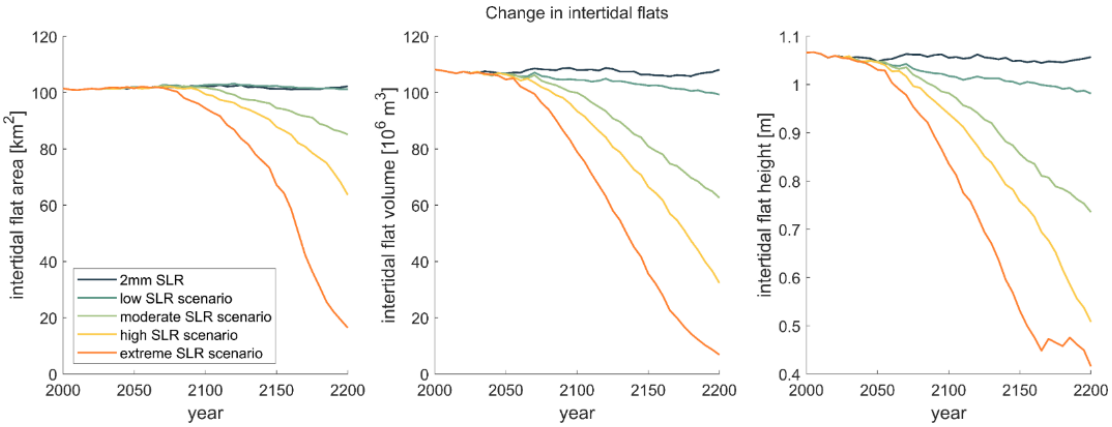

*Figure B.6.1. Intertidal area, volume, and flat height over time for five different SLR scenarios for the **Zoutkamperlaag** basin.*

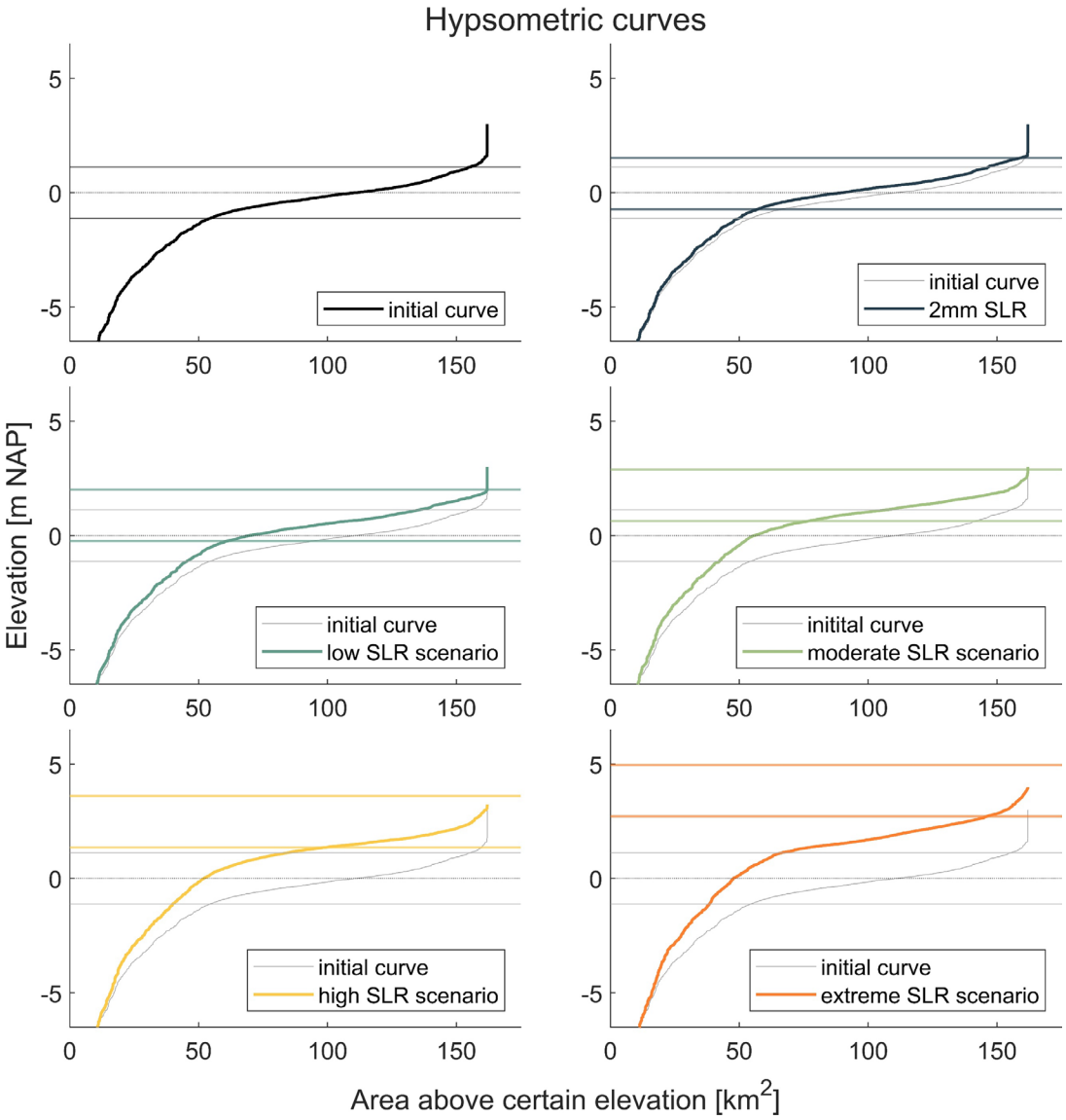

*Figure B.6.2. Hypsometric curves for the **Zoutkamperlaag** basin, for different SLR scenarios. In the top left panel we show the initial curve, calculated from the input bathymetry. The two horizontal lines indicate the mean low and highwater levels. In all other panels, we plot the initial hypsometric curve, together with the respective water levels, as gray, thin lines for comparison. The mean low- and highwater levels shift upwards with SLR, as indicated by the coloured horizontal lines in each panel. The legends in each panel specify the considered SLR scenario. The colour scheme for the SLR scenarios follows the rest of this report.*

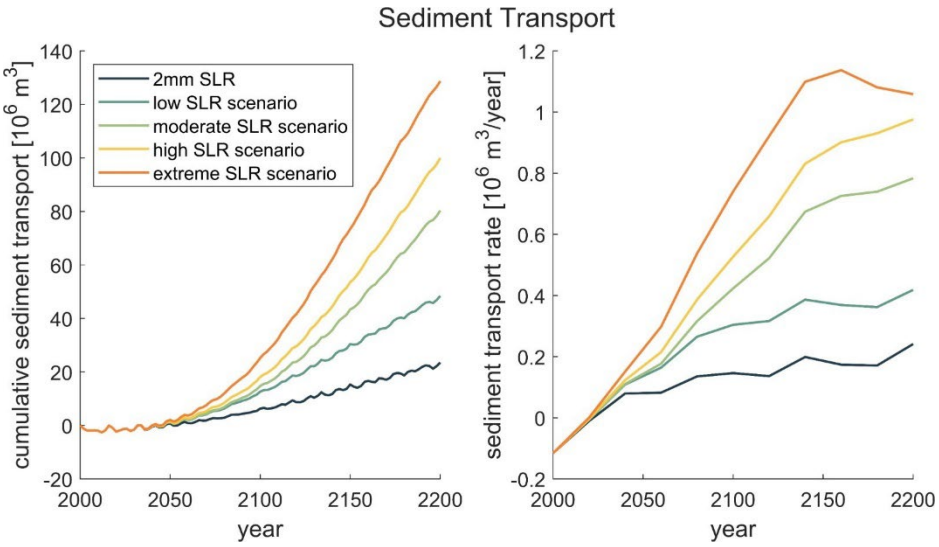

*Figure B.6.3. Cumulative sediment transport and yearly sediment transport rate through the inlet throat over time for five different SLR scenarios for the **Zoutkamperlaag** basin.*

Table B.6.1. Indication of drowning effect in the Zoutkamperlaag basin for different SLR scenarios. The basin area is 162.0 km² (derived from hypsometric curve).

SLR scenario	2 mm linear	low SLR	moderate SLR	high SLR	extreme SLR
$SLR_{cum,final}$ [m]	0.40	0.89	1.76	2.48	3.84
$\dot{d}_{SLR}$ [mm/year]	2	5	13.8	25	40
$t_{sed,final}$ [10^6 m^3]	23.5	48.4	80.3	100.0	128.7
$\dot{t}_{sed,final}$ [10^6 m^3/year]	0.24	0.42	0.78	0.98	1.06
$\overline{h}_{sed}$ [m]	0.15	0.30	0.50	0.62	0.79
$\dot{h}_{sed}$ [mm/year]	1.48	2.59	4.81	6.05	6.54
$\Delta h_{wd} = (SLR_{cum,final} - \overline{h}_{sed})$ [m]	0.25	0.59	1.26	1.86	3.05
$\frac{\dot{h}_{sed}}{\dot{d}_{SLR}}$	0.74	0.52	0.35	0.24	0.16

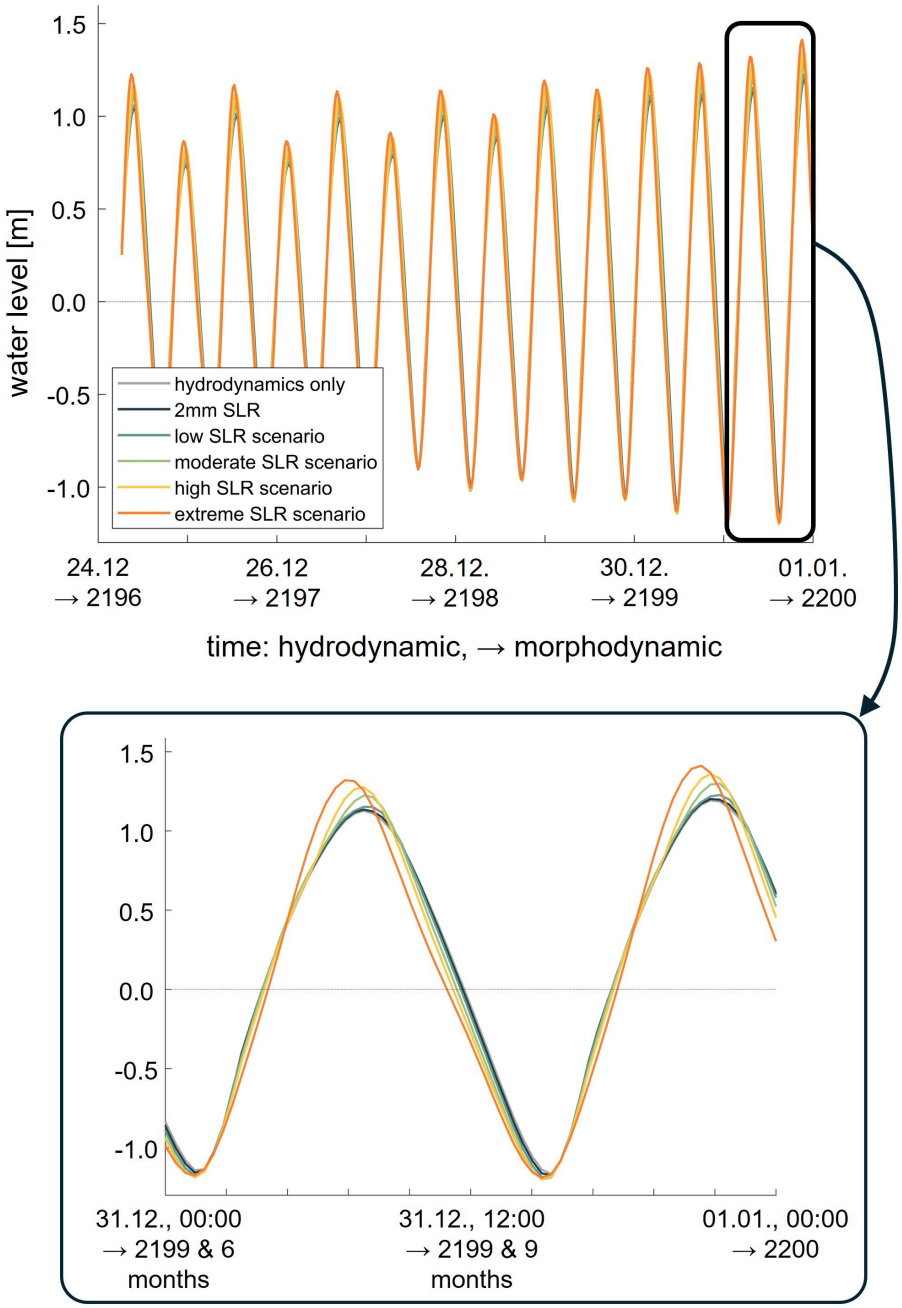

Figure B.6.4. Water levels for different SLR scenarios at a water level station in the Zoutkamperlaag basin (for the location of the station, see Figure 4.3 (?)), plotted for the last week of the hydrodynamic simulation time, i.e. the last four years for the morphodynamic simulation period, where the changes in water level due to the imposed SLR will be most noticeable. As base line, we plot the water levels of a purely hydrodynamic simulation as a gray line, see the legend in the upper panel. The lower panel is a zoom-in on the last two tidal cycles.

Deltares is an independent institute for applied research in the field of water and subsurface. Throughout the world, we work on smart solutions for people, environment and society.

Deltares

www.deltares.nl